Collectivity along the $N = Z$ line: Lifetime studies in self-conjugate even-even nuclei in the $0f_{7/2}$ shell

Inaugural-Dissertation

zur Erlangung des Doktorgrades
der Mathematisch-Naturwissenschaftlichen Fakultät
der Universität zu Köln

vorgelegt von

Konrad Arnswald
aus Oberhausen

Köln 2021

Berichterstatter:	Prof. Dr. Peter Reiter Prof. Dr. Jan Jolie
Tag der letzten mündlichen Prüfung:	23.12.2021

Abstract

Nuclear level lifetimes and corresponding reduced transition strengths are signatures for collective properties of atomic nuclei. They allow for stringent tests of modern shell-model interactions. Self-conjugate nuclei (with equal numbers of protons and neutrons) provide special access to nuclear-structure phenomena such as the isospin symmetry. Along the $N = Z$ line, these features can be studied for spherical nuclei in the vicinity of shell-closures and for well-deformed nuclei with various shapes.

Within this work lifetimes and reduced transition strengths are investigated in $^{44}_{22}$Ti, $^{48,50}_{24}$Cr, $^{52}_{26}$Fe, and $^{56}_{28}$Ni. These nuclei are located in the $0f_{7/2}$ orbital of the lower pf shell between the doubly-magic shell closures ^{40}Ca and ^{56}Ni. Lifetime measurements were performed at the FN tandem accelerator at the Institute for Nuclear Physics (University of Cologne, Germany) combining a setup of twelve high-purity germanium detectors and the Cologne coincidence-plunger device. Excited states in the nuclei of interest were populated via favorable fusion-evaporation reactions. Lifetimes in the range of several hundreds femtoseconds up to one hundred picoseconds were determined utilizing the Doppler-shift attenuation method and the recoil-distance Doppler-shift technique.

The deduced reduced transition probabilities expressed with $B(\sigma\lambda)$ values are compared within the systematics along their isotopic and isotonic chains. Within this comparison, the experimental findings show an enhanced collective behavior for the 2^+_1 states in ^{44}Ti, ^{48}Cr, and ^{52}Fe as well as for the 4^+_1 and 6^+_1 states in the doubly-magic nucleus ^{56}Ni. Further studies on ^{44}Ti address the impact of multi-particle multi-hole cross-shell configurations on the experimental spectrum. Lifetimes of the 3^-_1 and 4^-_1 states are determined and are confronted with previous, in part preliminary, values. Large deviations are found for the 4^-_1 state which lifetime appeared to be 28 times larger than originally measured. The finite $E1$ strength of the $3^-_1 \rightarrow 2^+_1$ transition gives indication of isospin-symmetry breaking in this nucleus.

All experimental values are confronted with results from shell-model calculations utilizing the established GXPF1A, FPD6, and KB3G effective interactions complemented by the novel PFSDG-U interaction. Moreover, valence ab-initio calculations are performed using modern Hamiltonians derived from chiral perturbation theory with and without contributions of three-body forces. For sake of completeness, the ZBM2M interaction within the pn-symmetric $1s_{1/2}0d_{3/2}0f_{7/2}1p_{3/2}$ model space is used to calculate negative-parity states and to investigate cross-shell excitations in ^{44}Ti.

The newly determined $B(E2)$ values in doubly-magic ^{56}Ni are used to compare with theoretical predictions in the $N = Z$ doubly-magic partner nucleus ^{100}Sn. For this purpose, a large-scale shell-model calculation using the gds valence space as well as results from a Hartree-Fock random-phase approximation are utilized. The combined results could indicate higher $B(E2; 6^+_1 \rightarrow 4^+_1)$ values for ^{100}Sn which would contradict the assumption of a 6^+_1 isomer in this nucleus.

Zusammenfassung

Nukleare Lebensdauern und entsprechende reduzierte Übergangsstärken sind Signaturen für kollektive Eigenschaften von Atomkernen. Sie ermöglichen strenge Tests moderner Schalenmodellinteraktionen. Selbstkonjugierte Atomkerne (mit gleicher Anzahl von Protonen und Neutronen) liefern einen besonderen Zugang zu Kernstrukturphänomenen wie zum Beispiel der Isospinsymmetrie. Entlang der $N = Z$-Kette können diese Eigenschaften von sphärische Kernen in der Nähe von Schalenabschlüssen ebenso wie von wohldeformierten Kernen unterschiedlicher Formen untersucht werden.

In dieser Arbeit werden Lebensdauern und reduzierte Übergangsstärken in $^{44}_{22}$Ti, $^{48,50}_{24}$Cr, $^{52}_{26}$Fe und $^{56}_{28}$Ni untersucht. Diese Kerne befinden sich in dem $0f_{7/2}$-Orbital der unteren pf-Schale zwischen den doppelt-magischen Schalenabschlüssen ^{40}Ca und ^{56}Ni. Lebensdauermessungen wurden am FN-Tandem-Beschleuniger am Institut für Kernphysik (Universität zu Köln, Deutschland) durchgeführt, wobei ein Aufbau von zwölf hochreinen Germaniumdetektoren mit dem Kölner Koinzidenzplunger kombiniert wurde. Angeregte Zustände in den Kernen von Interesse wurden über geeignete Fusionsverdampfungsreaktionen bevölkert. Lebensdauern im Bereich von einigen hundert Femtosekunden bis zu einhundert Pikosekunden wurden unter Verwendung der Doppler-shift attenuation Methode und der recoil-distance Doppler-shift Technik bestimmt.

Ermittelte reduzierte Übergangsstärken, ausgedrückt durch $B(\sigma\lambda)$-Werte, werden mit Systematiken entlang ihrer Isotopen- und Isotonenketten verglichen. Die experimentellen Ergebnisse zeigen innerhalb dieses Vergleichs ein erhöhtes kollektives Verhalten für die 2^+_1-Zustände in ^{44}Ti, ^{48}Cr und ^{52}Fe sowie für die 4^+_1- und 6^+_1-Zustände im doppelt-magischen Kern ^{56}Ni. Weitere Studien zu ^{44}Ti beziehen sich auf den Einfluss von schalenübergreifenden Mehr-Teilchen Mehr-Loch Konfigurationen auf das experimentelle Spektrum. Lebensdauern von den 3^-_1- und 4^-_1-Zuständen werden bestimmt und früheren, zum Teil vorläufigen, Werten gegenübergestellt. Große Abweichungen werden dabei für den 4^-_1-Zustand gefunden, dessen Lebensdauer sich um einen Faktor von 28 größer darstellt als ursprünglich gemessen. Die endliche $E1$-Stärke des $3^-_1 \rightarrow 2^+_1$-Übergangs gibt Hinweis auf eine Isospinsymmetriebrechung in diesem Kern.

Alle experimentellen Werte werden mit Ergebnissen von Schalenmodellrechnungen konfrontiert, unter Verwendung der etablierten GXPF1A, FPD6 und KB3G effektiven Wechselwirkungen, ergänzt um die neuartige PFSDG-U-Interaktion. Des Weiteren werden Valenz-Ab-initio-Rechnungen durchgeführt, welche einen modernen Hamiltonian benutzen, der aus chiraler Störungstheorie, mit und ohne Beiträge von Dreikörperkräften, hergeleitet wurde. Zur Vollständigkeit wird die ZBM2M-Wechselwirkung innerhalb des pn-symmetrischen $1s_{1/2}0d_{3/2}0f_{7/2}1p_{3/2}$-Modellraums genutzt, um Zustände negativer Parität zu berechnen und um schalenübergreifende Anregungen in ^{44}Ti zu untersuchen.

Die neu bestimmten $B(E2)$-Werte im doppelt-magischen ^{56}Ni werden mit theoretischen Vorhersagen im $N = Z$ doppelt-magischen Partnerkern ^{100}Sn verglichen. Hierfür werden eine großskalige Schalenmodellrechnung unter Verwendung des gds-Valenzraums sowie Ergebnisse von Hartree-Fock Random-Phase Approximationen genutzt. Die vereinigten Ergebnisse könnten Hinweise auf einen höheren $B(E2; 6^+_1 \rightarrow 4^+_1)$-Wert in ^{100}Sn geben, was der Vermutung eines 6^+_1-Isomers in diesem Kern entgegensteht.

Contents

Introduction

Recent advances in theoretical nuclear physics have been made with the consistent continuing development of existing microscopic and collective models. One major framework for the microscopic description of nuclear spectroscopy has been found in the nuclear shell model. Although it was originally conceived as a single-particle model [1, 2], with the inclusion of many valence particles, it turned out to successfully compute and predict nuclear states. However, with an increasing number of participating nucleons, the dimension of the full valence-nucleon Hilbert space increases rapidly and the direct diagonalization of the Hamiltonian matrix is limited due to the computing power [3]. Nowadays, complex many-body problems can be solved with the increasing computational infrastructures provided by supercomputers. A variety of phenomenological and realistic, i.e. microscopically derived, two-body nucleon-nucleon interactions are available [4]. Latter ones can be extended by three-body terms in order to provide more reliable shell-model Hamiltonians [5]. The theoretical predictions are benchmarked with available experimental data and the underlying shell-model interactions are continuously refined. Hence, precise measurements with sophisticated instruments are needed in order to optimize the fundamental models and, thus, to improve the understanding of the nuclear force.

In this work atomic nuclei with equal numbers of protons and neutrons are studied by means of excited states' lifetimes and reduced transition strengths which are confronted with theoretical predictions from the nuclear shell model. The following chapter provides a short overview of the nuclear shell model and the shell-model interactions used in this work. Furthermore, a theoretical background of the electromagnetic properties subject to this thesis is given followed by a summary of physical properties of adjacent nuclei in the investigated region of the Segrè chart. The chapter subsequently provides introductions to the concepts of isospin symmetry and α-clustering as well as a short comparison of the doubly-magic nuclei ^{56}Ni and ^{100}Sn. It closes with an outline of the included publications.

1.1 The nuclear shell model

The atomic nucleus is a many-body quantum system built by two types of particles, the positively charged protons and the neutrons which are electrically neutral. The interaction between these particles is characterized by a short-range strong attractive force, which acts in the range of femtometers and can surmount the Coulomb repulsion between the protons, and a very short-range repulsive core. In first order, this interaction can be considered as two-body like. In this case, the Hamiltonian for A

interacting nucleons is given by the sums of the kinetic energies $T_i = \mathbf{p}_i^2/2m_i$ and the nucleon-nucleon interaction V_{ij}:

$$H = T + V = \sum_{i=1}^{A} T_i + \sum_{i>j=1}^{A} V_{ij}(\mathbf{r}_i - \mathbf{r}_j) \tag{1.1}$$

For all A nucleons the Hamiltonian exhibits $3A$ position coordinates. These are translated into relative position coordinates in the nucleon-nucleon interaction V_{ij}. With an increasing number of nucleons, the dimension of the Hamiltonian increases rapidly, thus, it was originally only solved for the lightest nuclei. The Hamiltonian can be simplified by the introduction of a distance-dependent effective average potential $U_i(\mathbf{r})$ which replaces the nucleon-nucleon interaction in a rearranged Hamiltonian:

$$H = \sum_{i=1}^{A} [T_i + U_i(\mathbf{r})] + \sum_{i>j=1}^{A} V_{ij}(\mathbf{r}_i - \mathbf{r}_j) - \sum_{i=1}^{A} U_i(\mathbf{r}) \equiv H_0 + H_R \tag{1.2}$$

By this means, the Hamiltonian H considers an ensemble of A independent particles in a mean-field potential $U_i(\mathbf{r})$ described by H_0 which is (slightly) perturbed by the residual interaction H_R of all valence nucleons as independent particles outside an inert core [6, 7].

Within the whole nuclear landscape only few nuclei meet the requirements of such inert cores. The best candidates are so-called doubly-magic nuclei with proton and neutron numbers of:

2, 8, 20, 28, 50, 82, 126

These nuclei are more stable relative to adjacent nuclei which is expressed in a number of nuclear properties such as (i) increased excitation energies of the first excited state, (ii) decreased reduced transition probabilities between the first excited state and the ground state, (iii) higher proton- and neutron separation energies, and (iv) lower proton- and neutron-capture cross sections.

In analogy to the atomic shell model where electrons occupy shells within a central potential emanating from the atomic nucleus, the nuclear shell model is assumed with protons and neutrons filling up successive shells within a mean-field potential. Doubly-magic nuclei represent closed-shell nuclei analogous to the noble gases within the periodic table of elements. Contrary to the atomic shell model, the spin-orbit coupling term for the nucleon-nucleon interaction was found to be strong [1, 2]. This is expressed in a pronounced spin-orbit splitting which – in the case of the $0f$ orbitals – results in a shell closure at $N = Z = 28$. A schematic view of the first orbitals is illustrated in Fig. 1. This example shows the occupation of valence protons (open red circles) and valence neutrons (open blue circles) beyond a completely occupied $^{40}_{20}$Ca core (filled circles).

The residual nucleon-nucleon interaction can be given as a sum of local and non-local components which depend on the position, spin, and isospin[i] operators $\mathbf{r}$, $\boldsymbol{\sigma}$, and $\boldsymbol{\tau}$, respectively:

$$V_{1,2} = V_{1,2}(\mathbf{r}_1, \mathbf{r}_2, \boldsymbol{\sigma}_1, \boldsymbol{\sigma}_2, \boldsymbol{\tau}_1, \boldsymbol{\tau}_2) = V_{1,2}^C + V_{1,2}^T + V_{1,2}^{LS} + ... \tag{1.3}$$

[i]The isospin operator is in more details discussed in chapter 1.5.

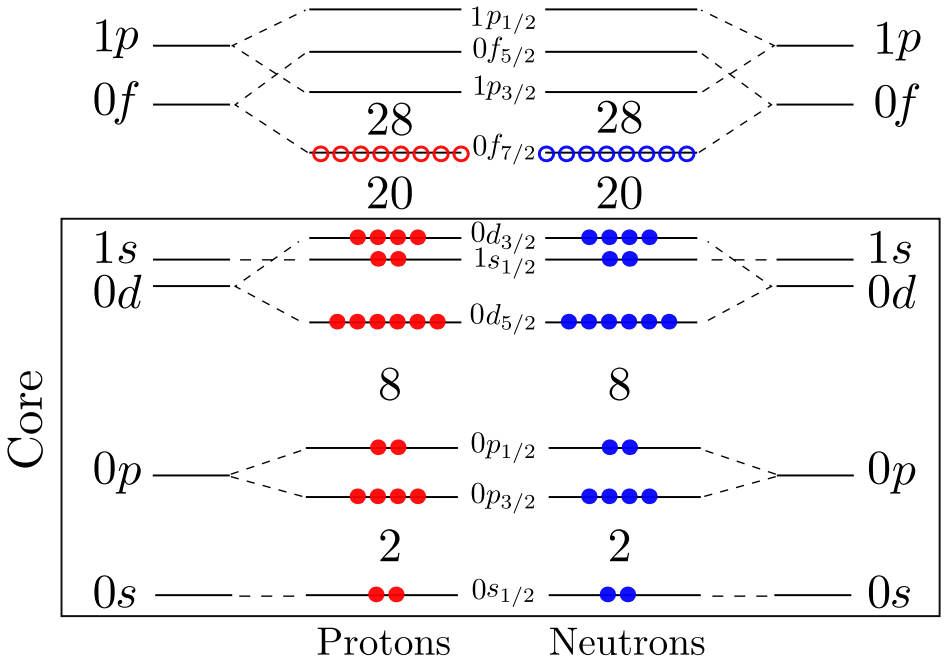

Figure 1: Schematic illustration of the first shell-model orbitals. Example shows eight proton (red) and eight neutron (blue) valence particles (open circles) outside a completely occupied (filled circles) $^{40}_{20}$Ca core. See text for details.

The local components are divided into a strong central component $V^C_{1,2}$ and a remaining tensor part $V^T_{1,2}$:

$$V^C_{1,2} = V_0(r) + V_\sigma(r)\boldsymbol{\sigma}_1\boldsymbol{\sigma}_2 + V_\tau(r)\boldsymbol{\tau}_1\boldsymbol{\tau}_2 + V_{\sigma\tau}(r)(\boldsymbol{\sigma}_1\cdot\boldsymbol{\sigma}_2)(\boldsymbol{\tau}_1\cdot\boldsymbol{\tau}_2) \tag{1.4}$$

and

$$V^T_{1,2}(r) = \left(V^{T_0}(r) + V^{T_\tau}(r)\boldsymbol{\tau}_1\boldsymbol{\tau}_2\right)\mathbf{S}_{12} \tag{1.5}$$

with $\mathbf{S}_{12} = 3/r^2(\boldsymbol{\sigma}_1\cdot\mathbf{r})(\boldsymbol{\sigma}_2\cdot\mathbf{r}) - \boldsymbol{\sigma}_1\cdot\boldsymbol{\sigma}_2$ and $r = |\mathbf{r}_2 - \mathbf{r}_1|$ the distance between both nucleons.

The strong spin-orbit term is of non-local character

$$V^{LS}_{1,2}(r) = V^{LS}(r)\boldsymbol{\ell}\cdot\mathbf{S} \tag{1.6}$$

with the total intrinsic spin $\mathbf{S} = \mathbf{s}_1 + \mathbf{s}_2 = 1/2(\boldsymbol{\sigma}_1 + \boldsymbol{\sigma}_2)$ and the relative orbital momentum $\boldsymbol{\ell}$ between both nucleons [8, 9].

Within the single-particle model, the solution of the Schrödinger equation in a central potential is given by the single-particle energies (SPE). These are observed in single-particle states or single-hole states, respectively, in the direct neighbors one particle outside a doubly-closed shell core.

Two-particle wavefunctions are characterized by the mutual interaction between the nucleons and holes, respectively. This is expressed in the two-body matrix elements (TBME) including the residual interaction. The effective nucleon-nucleon interaction of all valence nucleons in a given model space can be described by one SPE for each participating (proton and neutron) orbital in the valence space and a set of TBMEs (for more details see Ref. [8]). Additional, adjustments to the Hamiltonian have to be considered, as the interacting valence nucleons polarize the inert core. This polarization leads to effective reduced transition matrix elements which is corrected for by means of the so-called *effective charges* e_π for the proton and e_ν the neutron (cf. Refs. [10–12]).

1.2 Shell-model interactions for the pf shell

The pf shell comprising the four nuclear orbitals $0f_{7/2}$, $1p_{3/2}$, $1p_{1/2}$, and $0f_{5/2}$ is one of the most thoroughly studied regions within the table of isotopes both in experiment as well as in shell-model theory. It provides a fertile study ground for both single-particle and collective excitations as different signatures of nuclear structure. Due to the spin-orbit splitting of the $f_{7/2}$ orbital from the other three orbitals, a sizeable energy gap is created at $N, Z = 28$ (cf. Fig. 1). Thus, $^{56}_{28}$Ni is understood as a doubly-magic nucleus closing the $f_{7/2}$ shell. However, as the model space is symmetric for protons and neutrons, the proton-neutron interactions are relatively strong, increasing the *softness* of the shell closure at ^{56}Ni [13]. An excerpt of the Segrè chart showing the pf-shell nuclei between ^{40}Ca and ^{60}Zn is displayed in Fig. 2. In this region, the shell model is an indispensable framework for the computation of nuclear quantum states.

Within the last decades, several shell-model interactions were developed for a comprehensive microscopic description of pf-shell nuclei. Within this work seven interactions were utilized which will be introduced shortly:

The pioneering **FPD6** interaction [14] was derived by W. A. Richter *et al.* in 1990. It focuses on the lower mass region of the pf shell. The two-body interaction was obtained from a semi-empirical fit function of potentials and two-body matrix elements to a set of 61 excitation and binding energies in $^{41-46,48,49}$Ca, $^{42-44}$Sc, and ^{44}Ti. Later investigations of the single-particle energies showed that the $f_{5/2}$ orbital is too low in energy [13] which results in a distorted single-particle spectrum of the first three excited states in ^{57}Ni [15]. Nevertheless, the FPD6 interaction has been successful for lower pf-shell nuclei and it was employed for the calculations of excitation energies and $B(E2)$ values in the two publications given in chapters 2 [16] and 3 [17]. The experimental $B(E2)$ values of neutron-deficient chromium and iron isotopes (including the values determined in this work) are well described by this interaction.

The **GXPF1A** interaction [18] was developed by M. Honma *et al.* in 2005. It is a microscopic effective interaction on the basis of the Bonn-C potential [12]. The interaction was derived and modified by fitting 70 linear combinations of four SPEs as well as 195 TBMEs to a set of 699 binding- and excitation energies out of 87 nuclei in a region spanning from ^{47}Ca to ^{65}Ge. Furthermore, an empirical $A^{-0.3}$ mass dependence is assumed for the two-body matrix elements. The GXPF1A interaction is a

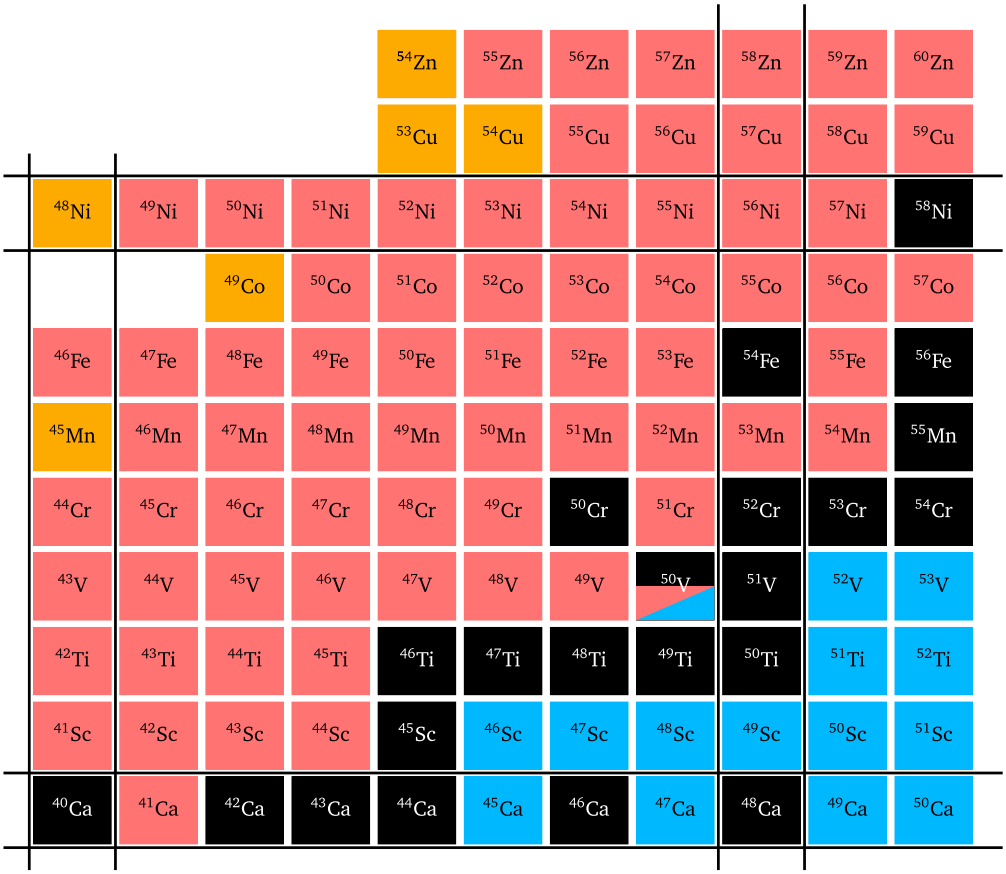

Figure 2: Partial Segrè chart between ^{40}Ca and ^{60}Zn. Black colored nuclei are stable. Red and blue colored isotopes are β^+ and β^- emitting radioactive isotopes, respectively. Orange colored nuclei are proton emitters. White boxes represent nuclei that have not been observed until now. The shell closures at $N, Z = 20$ and $N, Z = 28$ are marked with black frames.

modified version of the GXPF1 interaction [13], including adaptions to the quadrupole-quadrupole (QQ) term without changing the monopole centroid. Most recent developments on the GX1 family are carried out by Jha *et al.* who slightly modified the $1p_{3/2}$ single-particle energy as well as $0f$ two-body matrix elements in order to improve shell-model results in terms of the tensor-force monopole matrix elements [19]. Despite such minor adjustments, the GXPF1A interaction is well established and has proven to provide reliable predictions in the pf shell, especially in the vicinity of the $N = Z$ line. It is used to calculate nuclear level energies and reduced transition strengths in each of the publications included in this work. In particular, the calculation nearly perfectly resembles the excitation energies of the $N = 28$ isotones and the newly determined $B(E2)$ values in ^{56}Ni discussed in Publication III of this work [20].

The **KB3G** interaction [21], developed by A. Poves *et al.* in 2001, is a mass-dependent modification of the pioneering KB3 interaction [22] which is based on the Kuo-Brown G-matrix, starting from a Hamada-Johnston potential [23]. The modifications include adjustments of various monopole

shifts. However, at the shell-closure $N = Z = 28$ the excitation energy of the 2_1^+ state in ^{56}Ni is overestimated by the KB3G interaction [13]. The 2_1^+ excitation reflects the shell gap at $N = Z = 28$ and has main contributions stemming from the $(0f_{7/2})^7(1p_{3/2})^1$ configuration [13]. The authors furthermore emphasize that the corresponding $V(f_{7/2}p_{3/2}f_{7/2}p_{3/2}; J(T = 1))$ matrix elements have a dominant monopole character. Monopole modifications could improve the result for the KB3G interaction but still did not reproduce the experimental value [13]. These issues have been fixed within the pf part of the novel **PFSDG-U** interaction [24, 25] which is a monopole constrained realistic interaction in the spirit of the older KB3G interaction. The modern PFSDG-U interaction is utilized to calculate nuclear states and $B(E2)$ values in doubly-magic ^{56}Ni presented in Publication III of this thesis [20]. It reproduces the excitation energies along the chosen chain of $N = 28$ isotones well. Merely, the 4_1^+ energy in ^{56}Ni is slightly overestimated. In addition, it is also in good agreement with the trend of $B(E2)$ values [20]. The experimental values, which are discussed in Publication I and Publication II, are confronted with results from the KB3G interaction. Although the $B(E2; 2_1^+ \rightarrow 0_{\text{g.s.}}^+)$ values along the chain of titanium isotopes could not be reproduced, similar results agree well with the experimental values from neutron-deficient Cr isotopes and show the best overall agreement with the iron isotopes [16]. The calculated $B(E2)$ values along the yrast band in ^{44}Ti underestimate the experimental findings for the 2_1^+ and 4_1^+ decays but reproduce the feeding transitions well up to the 12_1^+ state [17].

Beside these interactions, a novel effective shell-model Hamiltonian starting from a **realistic** nucleon-nucleon (**2N**) potential was developed by Coraggio *et al.* [26]. The starting realistic nucleon-nucleon potential is a low-momentum potential derived from the CD-Bonn potential [27] within the $V_{\text{low-k}}$ approach. It is employed for the calculation of 2_1^+ states and $B(E2; 2_1^+ \rightarrow 0_{\text{g.s.}}^+)$ values in ^{44}Ti, ^{48}Cr, and ^{52}Fe presented in Publication I [16]. The calculated $B(E2; 2_1^+ \rightarrow 0_{\text{g.s.}}^+)$ values agree well with the measured values in ^{48}Cr and ^{52}Fe. Towards higher neutron numbers the calculations overestimate the evaluated data. Similar to the other three pf shell interactions, the realistic 2N interaction is not able to reproduce the trend of titanium isotopes [16]. Apart from this, pure nucleon-nucleon realistic interactions are unable to reproduce the spin-orbit shell closures at $Z, N = 14, 28, 50, 82$, and 126 [28]. As a consequence, the $f_{7/2}$-$p_{3/2}$ gap is too small in the present case of the shell closure at $Z = N = 28$. Therefore, the inclusion of three-body contributions (**2N+3N**) [5] were needed to properly describe ^{56}Ni within this approach which is demonstrated in the third publication of this thesis given in chapter 4 [20]. Distinct deviations are obtained for the 2N and 2N+3N calculations in this nucleus. While the 2N calculations cannot reproduce the energy spacings (e.g. the calculated 2_1^+ energy is 977 keV instead of 2701 keV), the inclusion of three-body contributions resembles the experimental values well; with the sole exception of the $B(E2; 6_1^+ \rightarrow 4_1^+)$ value in ^{56}Ni which is significantly overestimated [20].

To cope with multi-particle multi-hole cross-shell excitations from the *sd* shell, the **ZBM2** interaction was developed by Caurier *et al.* [29]. It uses an extended model space comprising the $1s_{1/2}$, $0d_{3/2}$, $0f_{7/2}$, and $1p_{3/2}$ orbitals [30] and enables cross-shell calculations. Most recent modifications of the interaction (**ZBM2M**) address the $d_{3/2}$-$d_{3/2}$ monopole matrix elements which improve the $T = 1$ versus $T = 0$ ordering in ^{38}K [31]. Due to the extended model space, unnatural-parity states can be

derived for pf- and sd-shell nuclei which cannot be obtained from pure pf- and sd-shell interactions, respectively. Thus, the ZBM2M interaction provides excellent features to study ^{44}Ti which exhibits low-lying negative-parity states and is assumed to be influenced by multi-particle multi-hole cross-shell excitations [16]. Results from this interaction are obtained in this thesis and are discussed in chapter 3 [17].

The above introduced shell-model interactions were used to calculate excitation energies and $B(E2)$ values for pf-shell nuclei. Three different shell-model codes were employed in this thesis: the (i) coupled jj scheme NUSHELLX@MSU code by B. A. Brown and W. D. M. Rae [32], the (ii) novel KSHELL code by Shimizu *et al.* [33, 34] as well as the (iii) shell-model code ANTOINE [4] based on the uncoupled m scheme. The m-scheme code KSHELL enables for massively parallel computation utilizing a hybrid of OpenMP and MPI (Message Passing Interface) [33]. This results in a calculation speed advantage of up to a factor of 30 with respect to NUSHELLX@MSU for the servers currently installed at the IKP Cologne [35]. On the other hand, within the jj scheme, the code NUSHELLX@MSU provides detailed information on shell-model configurations, couplings, and spin decompositions. Within the scope of this thesis, shell-model calculations employing the KSHELL and NUSHELLX@MSU codes with the GXPF1A, KB3G, FPD6, and ZBM2M interactions were carried out at the Institute for Nuclear Physics, University of Cologne. Calculations using the ANTOINE shell-model code utilizing the PFSDG-U as well as the 2N and 2N+3N realistic ab-initio calculations were provided by our collaboration partners F. Nowacki as well as by L. Coraggio, A. Gargano, and N. Itaco.

1.3 Excitation energies and $B(E2)$ values in even-even nuclei

Nuclei with even numbers of protons and neutrons are characterized by an energetically favored ground state where all nucleons couple to $J^\pi = 0^+$. In most cases, the first excited state arises from a break-up of one of these pairs coupling to $J^\pi = 2^+$. At shell-closure nuclei, such an excitation across a large shell-gap results in a high excitation energy of this state. With a rising number of possible states at mid-shell, multistate mixing significantly reduces the energy eigenvalues of first excited states [6].

In addition to the excitation energy, the reduced electric quadrupole transition probability is another signature for collectivity. These transition probabilities are expressed in terms of $B(E2)$ values. Within isotopic and isotonic chains, a decreased $B(E2;\ 2_1^+ \rightarrow 0_{\text{g.s.}}^+)$ value can indicate a (sub-)shell closure, while increased $B(E2)$ values are associated with collective excitations.

In general, the transition probability for a multipolarity λ and the electric or magnetic transition character σ is described by the inital and final wavefunctions $|\psi_i\rangle$ and $\langle\psi_f|$, respectively, connected by the electromagnetic multipole operator $M(\sigma\lambda)$ and normalized to the initial angular momentum J_i:

$$B(\sigma\lambda;\ J_i \rightarrow J_f) = \frac{1}{2J_i+1} \left| \left\langle \psi_f \| M(\sigma\lambda) \| \psi_i \right\rangle \right|^2 \tag{1.7}$$

Transition probabilities can be directly determined from the experimental lifetime τ of a state J_i which decays into various final states J_f. The lifetime of this initial state is

$$\tau(J_i) = \left(\sum_{J_f} \sum_{\lambda} T(\sigma\lambda;\ J_i \rightarrow J_f)[1+\alpha(\lambda)] \right)^{-1} \tag{1.8}$$

only depending on the multipole conversion coefficient $\alpha(\lambda)$ and the absolute transition probability $T(\sigma\lambda;\ J_i \rightarrow J_f)$ [36]:

$$T(\sigma\lambda;\ J_i \rightarrow J_f) = \frac{8\pi(\lambda+1)}{\hbar\lambda[(2\lambda+1)!!]^2} \left(\frac{E_\gamma}{\hbar c}\right)^{2\lambda+1} B(\sigma\lambda;\ J_i \rightarrow J_f) \tag{1.9}$$

For the case of a pure electric quadrupole transition with a branching ratio BR, the lifetime simplifies to

$$\tau(J_i) = \frac{816.2 \cdot E_\gamma^{-5} \cdot BR}{B(\mathrm{E2};\ J_i^+ \rightarrow (J_i-2)^+) \cdot [1+\alpha(\mathrm{E2})]}\ [\mathrm{ps}] \tag{1.10}$$

Here, the transition energy E_γ is given in units of MeV and the B(E2) value is given in units of $e^2\mathrm{fm}^4$ (cf. Ref. [37]). Often $B(E2)$ values are given in Weisskopf units (W.u.). These can be converted from the aforementioned units $e^2\mathrm{fm}^4$ by the following equation (cf. Ref. [6]):

$$1\ \mathrm{W.u.} = (4.94 \cdot 10^{-2})\, A^{4/3}\ e^2\mathrm{fm}^4 \tag{1.11}$$

1.4 Systematics of pf-shell nuclei

Excitation energies and $B(E2)$ values are sensitive signatures to describe the evolution of shell structures. The systematics of both observables along the titanium, chromium, iron, and nickel isotopic chains between $20 \leq N \leq 34$ is presented in Fig. 3.

The excitation energies (Figs. 3(a-d)) of the 2_1^+ states (red triangles) show similar courses with considerable increases at the shell closures $N = 20, 28$. Moreover, smaller yet significant increases are obtained for ^{54}Ti and ^{56}Cr at $N = 32$. These are referred to a subshell closure originating from a $1p_{3/2}$-$1p_{1/2}$ spin-orbit splitting (cf. Refs. [44, 45]). The impact of the $Z = 28$ shell closure is illustrated by the nickel energies which are higher than the ones in the neighboring isotones. With an increase of a factor of ~ 2, with respect to the adjacent even-even isotopes, the doubly-magic shell-closure at ^{56}Ni ($Z = N = 28$) stands out against its semi-magic neighbors. The 4_1^+ energies (blue squares) follow the trend of the 2_1^+ energies. Especially for ^{56}Cr, the signature of the $N = 32$ subshell closure is present in the 4_1^+ energies. The 6_1^+ energies (green circles) have their maximum values along the chain of isotopes at the $N = Z$ nuclei. With increasing neutron numbers the 6_1^+ energy stabilizes and it remains nearly constant.

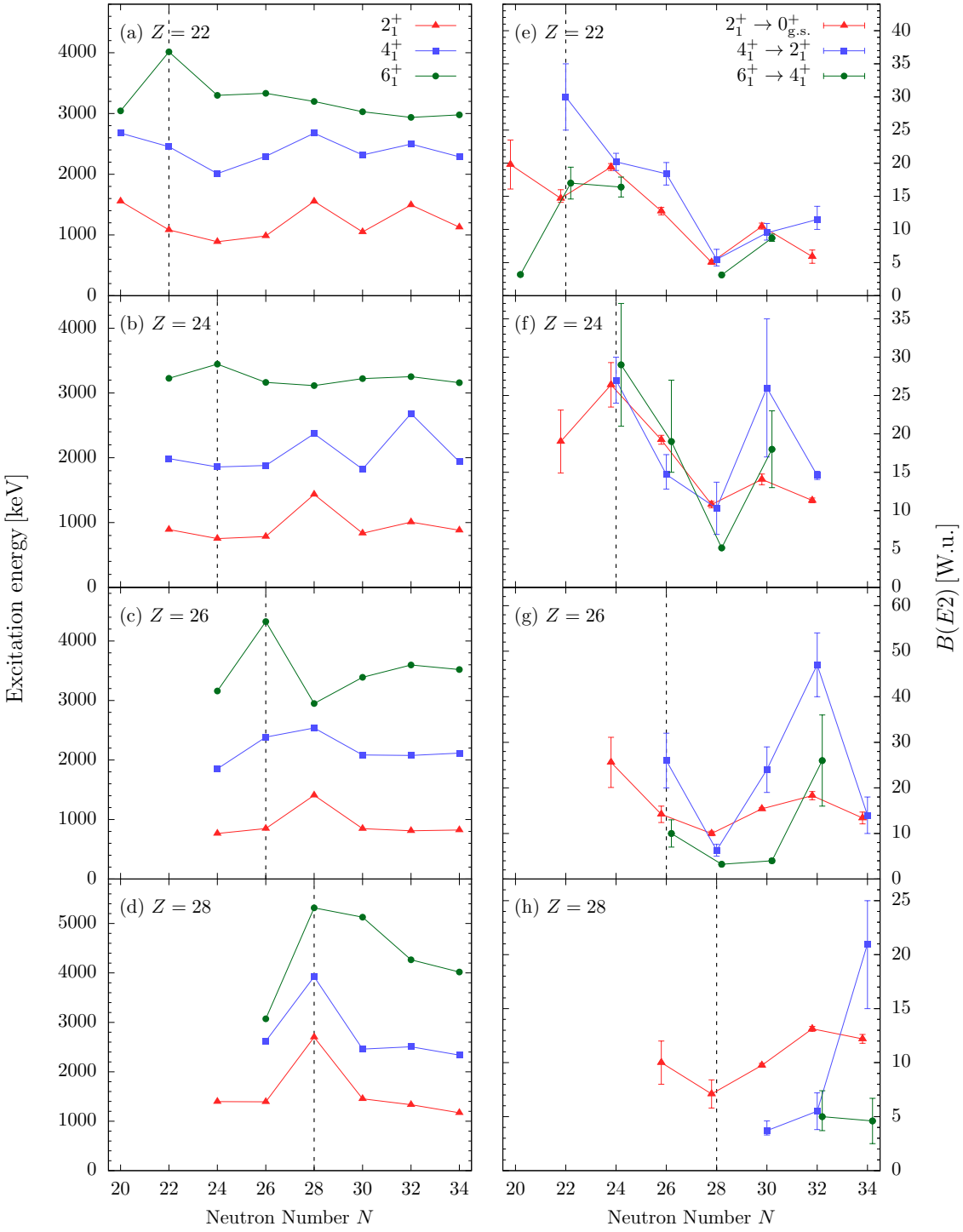

Figure 3: Systematics of (a,e) Ti, (b,f) Cr, (c,g) Fe, and (d,h) Ni even-even isotopes for (a-d) excitation energies and (e-h) $B(E2)$ values. Evaluated experimental values for 2_1^+ states (red triangles), 4_1^+ states (blue squares), 6_1^+ states (green circles) are obtained from Refs. [38, 39]. Recent results from Ref. [40–43] are additionally considered. To guide the eyes, the data points are connected with lines and the $B(E2)$ values are slightly shifted. $N = Z$ isotopes are marked with black dashed lines. See text for details.

The reduced transition strengths expressed with $B(E2)$ values (Figs. 3(e-h)) exhibit ambiguous systematics. For the $2_1^+ \rightarrow 0_{\text{g.s.}}^+$ transitions (red triangles), the isotopic Ti, Cr, and Fe chains have maximum values at $N = 24$ and minima at $N = 28$. However, in doubly-magic ^{56}Ni, only a minor dip in $E2$ strength has been observed for the $2_1^+ \rightarrow 0_{\text{g.s.}}^+$ transition [46]. This enhanced $B(E2)$ value (compared with harmonic oscillator shell closures, such as ^{40}Ca) originates from the 2_1^+ state which results from a direct quadrupole excitation of the doubly-magic core [20]. Within the titanium and chromium chains, minimum $B(E2; 2_1^+ \rightarrow 0_{\text{g.s.}}^+)$ values were measured at $N = 32$ with respect to the preceding even-even isotopes (cf. Refs. [40, 41]) giving further indication of a subshell closure at $N = 32$. For ^{44}Ti a minimum $B(E2)$ value was observed for the $2_1^+ \rightarrow 0_{\text{g.s.}}^+$ transition which is significantly smaller than the respective value in the semi-magic neighbor ^{42}Ti. This would question the robustness of the shell closure at $N = 20$ and motivated precise measurements discussed in the Publication I of this thesis [16]. The $B(E2)$ values for the $4_1^+ \rightarrow 2_1^+$ (blue squares) and $6_1^+ \rightarrow 4_1^+$ (green circles) transitions are predominantly only known with considerable uncertainties. Moreover, at doubly-magic ^{56}Ni, no concrete $B(E2)$ values for these transitions were previously available which motivated for further lifetime studies reported in Publication III [20].

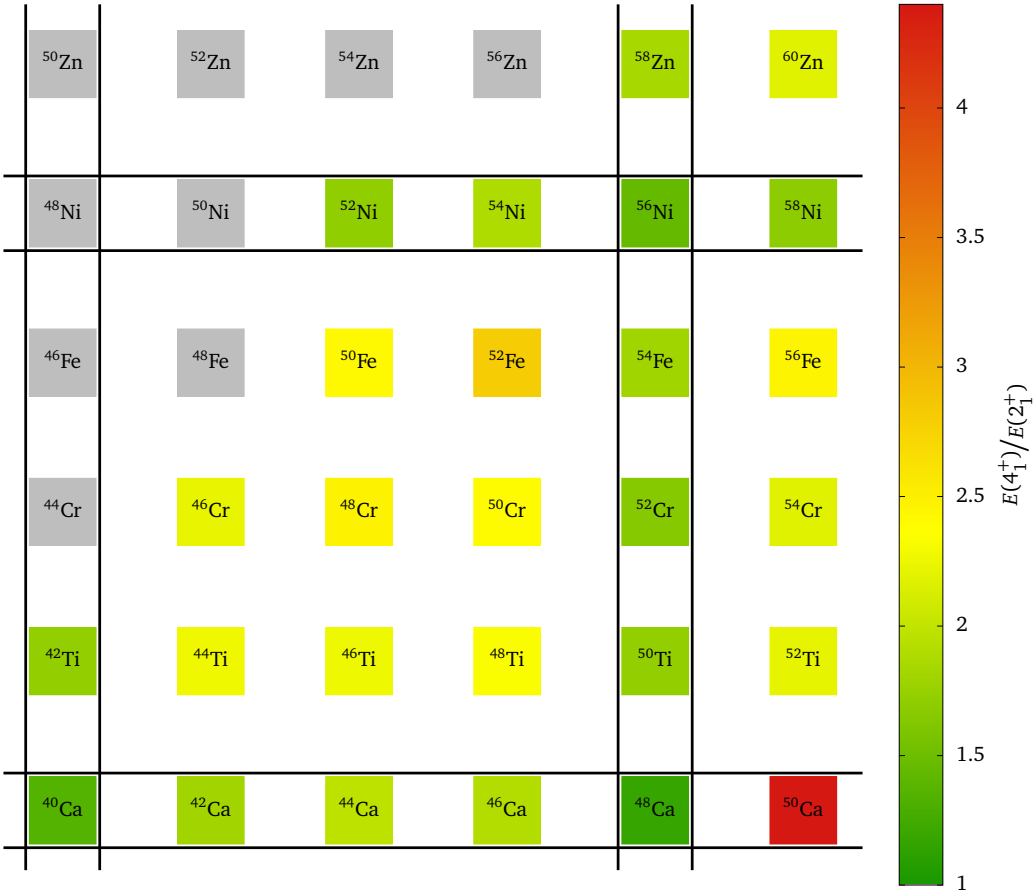

Figure 4: Evaluated ratios of excitation energies of the 4_1^+ and 2_1^+ states for even-even nuclei in the lower pf shell. For nuclides highlighted in gray, no information on at least one of the respective excitation energies is available. Data adopted from Ref. [39]

Apart from single excitation energies and $B(E2)$ values, signatures of collective excitations can also be deduced from the ratio of these quantities. Within the rotor model these ratios give $E_{4/2} = E(4_1^+)/E(2_1^+) = 3.33$ and $B_{4/2} = B(E2; 4_1^+ \rightarrow 2_1^+)/B(E2; 2_1^+ \rightarrow 0_{\text{g.s.}}^+) = 1.43$. In the harmonic vibrator model both ratios yield $E_{4/2} = B_{4/2} = 2$ [47]. $E_{4/2}$ values < 2 and $B_{4/2} \approx 1$ ratios are generally associated with shell-model nuclei in the vicinity of shell-closures [48].

The $E_{4/2} = {}^{E(4_1^+)}/_{E(2_1^+)}$ ratios of even-even nuclei in the lower pf shell are mapped in Fig. 4. Along the $N = Z$ line, the values evolve from spherical closed-shell ^{40}Ca with $E_{4/2} = 1.35$ over a vibrational-like ^{44}Ti ($E_{4/2} = 2.27$) to transitional $f_{7/2}$ mid-shell nuclei ^{48}Cr (2.47) and ^{52}Fe (2.81) until the $f_{7/2}$ shell is fully occupied at ^{56}Ni (1.45). The semi-magic nuclei along $N, Z = 20$ and $N, Z = 28$ have values between 1.6 and 1.9 except for ^{50}Ca (4.40). The latter high value results from a neutron particle-hole core excitation [49] ($\nu f_{7/2} - \nu p_{3/2}$) of the 4_1^+ state. Thus, the large value is understood as a single-particle excitation and is not of collective nature.

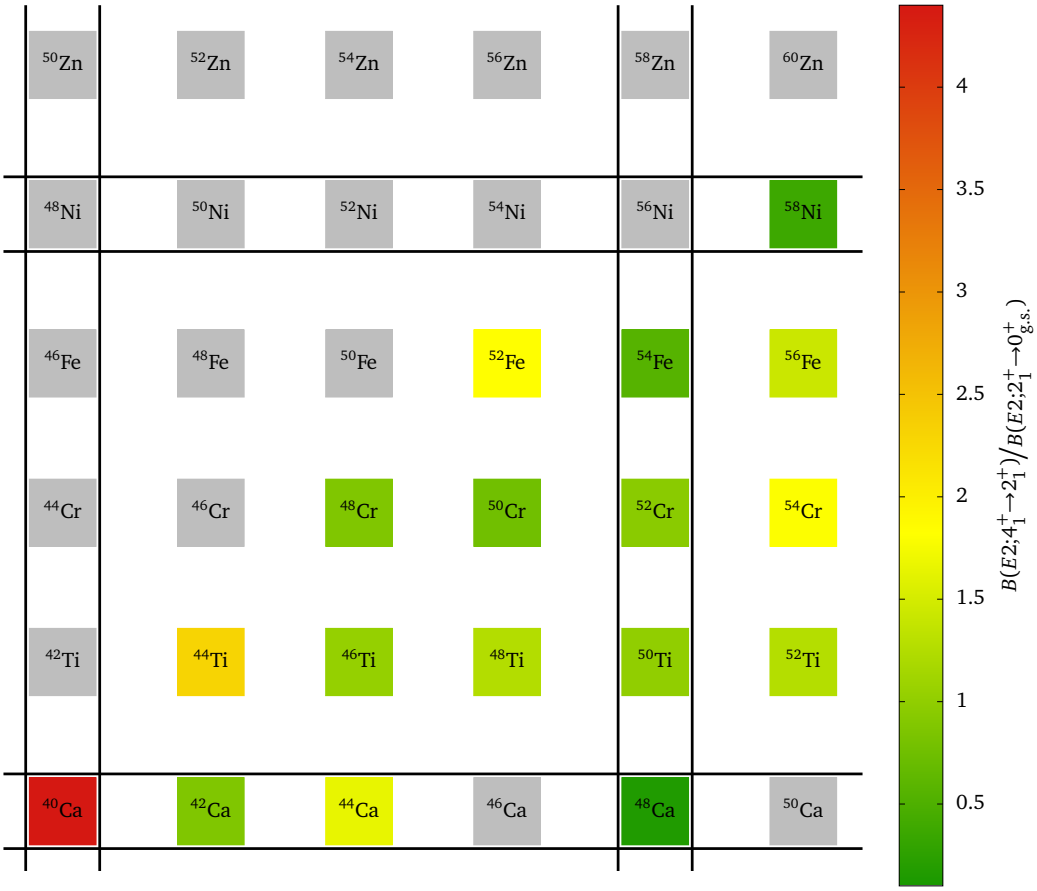

Figure 5: Evaluated ratios of $B(E2)$ values of the $4_1^+ \rightarrow 2_1^+$ and $2_1^+ \rightarrow 0_{\text{g.s.}}^+$ states for even-even nuclei in the lower pf shell. For nuclides highlighted in gray, no information on at least one of the respective $E2$ strengths is available. Data adopted from Ref. [39] as well as from Refs. [41, 42]

In addition to the ratio of excitation energies, the ratios of $B(E2)$ values, especially for the $4_1^+ \rightarrow 2_1^+$ and $2_1^+ \rightarrow 0_{\text{g.s.}}^+$ transitions, can give complementary information on nuclear structures in the lower pf shell. This ratio is mapped in Fig. 5 for the even-even nuclei between ^{40}Ca and ^{60}Zn. In contrast to the ratio of excitation energies, the existing experimental data on $B(E2; 4_1^+ \rightarrow 2_1^+)$ values and, thus, deduced $B_{4/2}$ ratios in this region is rather scarce. The available data shows an inconsistent picture of the evolution along $N = Z$: at ^{40}Ca, a high $B_{4/2}$ ratio of ≈ 30 is obtained as the yrast band exhibits a prolate quadrupole deformation with $\beta_2 = 0.27$ [50]. Towards the middle of the $0f_{7/2}$ shell, the $B_{4/2}$ ratios of ^{44}Ti (2.30) and ^{52}Fe (1.83) indicate a vibrator-like behavior. However, the mid-shell nucleus ^{48}Cr has a ratio of 0.87. Such anomalous $B_{4/2}$ ratios smaller than unity are hard to find in the table of isotopes and they predominantly occur when seniority is a good quantum number [48]. Within the pf shell, such an anomalous $B_{4/2}$ ratio is also obtained for the even-even neighbor ^{50}Cr (cf. Ref. [51]). Along the $N = Z$ line between ^{44}Ti and ^{52}Fe, the $B_{4/2}$ ratios fluctuate within a range of 2.3 and 0.8. This rapid change from vibrator-like over single-particle to vibrator-like contrasts with the smooth evolution of the excitation-energy ratios and is subject of this thesis. For that reason, the $B_{4/2}$ ratios are redetermined using the newly measured $B(E2)$ values from the present work and will be discussed in Publication I [16].

1.5 Isospin symmetry and $N = Z$ nuclei

Neglecting the contribution of the Coulomb term, the nuclear force can be considered as charge-symmetric and charge-independent. Within this isospin symmetry, the neutron (ν) and the proton (π) are described as two states of the same particle, the nucleon, with spatial wave functions:

$$\varphi_\nu(\mathbf{r}) = \varphi(\mathbf{r}) \begin{pmatrix} 1 \\ 0 \end{pmatrix}, \qquad \varphi_\pi(\mathbf{r}) = \varphi(\mathbf{r}) \begin{pmatrix} 0 \\ 1 \end{pmatrix} \tag{1.12}$$

Similar to the intrinsic spin, the canonical coordinates of the isospin are given by the Pauli isospin matrices $\boldsymbol{\tau}(\tau_x, \tau_y, \tau_z)$

$$\tau_x = \begin{pmatrix} 0 & 1 \\ 1 & 0 \end{pmatrix}, \qquad \tau_y = \begin{pmatrix} 0 & -i \\ i & 0 \end{pmatrix}, \qquad \tau_z = \begin{pmatrix} 1 & 0 \\ 0 & -1 \end{pmatrix} \tag{1.13}$$

and the isospin operator is defined as $\mathbf{t} = \tau/2$ [8].

Both types of nucleons differ in the third component of the isospin quantum number which are $t_z = +\frac{1}{2}$ and $t_z = -\frac{1}{2}$ for neutrons and protons, respectively [6]. For a nucleus combined of $A = N + Z$ nucleons, the isospin projection algebraically adds up to

$$T_z = \sum_{i=1}^{A} t_{z,i} = \frac{N - Z}{2} \tag{1.14}$$

The total isospin vector is defined as the vector sum over the number of all nucleons A

$$\mathbf{T} = \mathbf{t}_1 \oplus \mathbf{t}_2 \oplus ... \oplus \mathbf{t}_A \tag{1.15}$$

Thus, the total isospin quantum number can be considered as a coupling of all contributing nucleons

$$\frac{|N-Z|}{2} \leq T \leq \frac{N+Z}{2} \tag{1.16}$$

The possible isospin states in the simple case of two nucleons are schematically shown in Fig. 6.

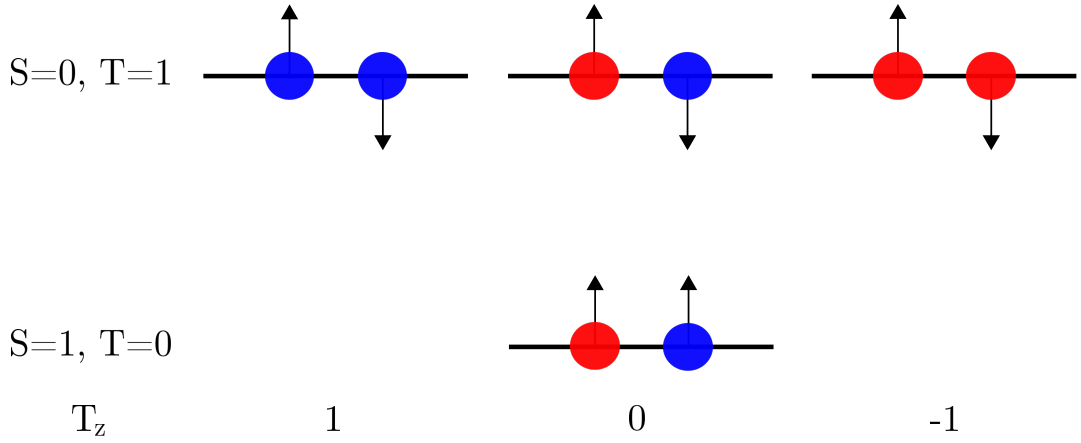

Figure 6: Possible isospin states for two nucleons (protons red, neutrons blue) for the $T = 0$ isospin singlet (bottom) and the $T = 1$ isospin triplet (top). Intrinsic spins are indicated with arrows.

The impact of isospin symmetry in nuclear systems can be observed in so-called mirror nuclei with interchanged proton- and neutron numbers. These nuclei show almost equal excitation schemes except for the Coulomb-energy differences caused by the different proton numbers.

The collectivity of excited states in $N = Z$ nuclei is subject of this thesis. For the even-even nuclei $^{44}_{22}$Ti, $^{48}_{24}$Cr, $^{52}_{26}$Fe, and $^{56}_{28}$Ni within the $0f_{7/2}$ orbital, $E2$ strengths from low-lying yrast states were obtained and compared with the relevant isotope and isotone chain systematics. In recent years, the determination of $B(E2)$ values in $N = Z$ nuclei were subject of several lifetime and Coulomb-excitation experiments (cf. [52, 53]). Highest $B(E2)$ values were determined for $^{76}_{38}$Sr, $^{78}_{39}$Y, and $^{80}_{40}$Zr culminating in ^{76}Sr with 125(13) W.u. for the $2^+_1 \rightarrow 0^+_{\text{g.s.}}$ transition [52]. For exotic $^{88}_{44}$Ru large-scale shell-model (LSSM) calculations suggest an enhancement of collectivity in fast-rotating $N = Z$ nuclei [54].

Moreover, nuclei with equal numbers of protons and neutrons are of particular interest in the study of isospin symmetry, as they are the only nuclei which can exhibit isospin-singlet states. Further electromagnetic selection rules are relevant as direct electric-dipole transitions between $T = 0$ states are not allowed due to the isovector character of the $E1$ transition operator [6]. In some cases for which such an $E1$ transition takes place, the isospin symmetry is substantially broken. This is found for the $3^-_1 \rightarrow 2^+_1$ transition in self-conjugate ^{44}Ti where a finite $B(E1)$ value is determined. The utilized effective ZBM2M shell-model interaction conserves isospin symmetry in consequence of which the

calculated $E1$ strengths returns zero. The results on this indication of isospin-symmetry breaking in ^{44}Ti are presented and discussed in Publication II of this thesis [17].

1.6 α-clustering in ^{44}Ti

Within the atomic nucleus, nucleons can build molecule-like cluster structures. Due to its extraordinarily high binding energy and the experimental observation of natural α-particle radioactivity, α-particle clusters were in the focus of all early work in this field [55]. Particular importance is attributed to nuclear systems where an α particle can couple with a doubly closed-shell nucleus. In the prominent case of ^{20}Ne and ^{16}O* such a molecule-like structure was identified by means of the investigation of the two rotational bands with $K^\pi = 0^+$ and $K^\pi = 0^-$ [56] (the K quantum number represents the projection of the total angular momentum on the symmetry axis).

Although ^{44}Ti can be built out of an α particle coupled to doubly-magic ^{40}Ca, it was rather unclear if α correlations can be observed versus the strong spin-orbit force in the pf shell [57]. Later observations of the $K^\pi = 0^-$ band as a partner of the $K^\pi = 0^+$ in the parity doublet bands supported the argument of α-particle structures in pf shell nuclei [58–61]. The authors concluded that the nuclear structure of ^{40}Ca and ^{44}Ti can be considered similar to ^{16}O and ^{20}Ne, which exhibit α structures.

Recent studies on ^{44}Ti within the α-cluster model not only reported detailed level schemes but also provided $B(E2)$ values: Ohkubo *et al.* reproduced all rotational bands in ^{44}Ti within an α-cluster model in which α-like core excitations are produced utilizing a double-folded potential [62]. The group calculated $B(E2)$ values for yrast and non-yrast states up to 8 MeV. Another approach is reported by M. Kimura and H. Horiuchi who use the deformed-basis antisymmetrized molecular dynamics (AMD) by the use of the Gogny D1S force [63]. The authors observed coexistence phenomena of the mean-field structure and the α structure in this nucleus. The extracted $B(E2)$ values from both works showed an enhancement over the hitherto known experimental values for the $2^+_1 \rightarrow 0^+_{\text{g.s.}}$ transition in ^{44}Ti which will be discussed in the first and, in more detail, in the second publication of this thesis [16, 17]. As it turned out, the α-cluster model proves to be competitive with modern shell-model calculations in ^{44}Ti.

1.7 The doubly-magic nucleus ^{56}Ni in comparison with ^{100}Sn

Doubly-magic nuclei represent special cornerstones along the whole table of isotopes. They provide access to intrinsic properties such as excitation energies and reduced transition probabilities which are related to very pure shell-model configurations. Thus, the study of doubly-magic nuclei and their direct neighbors is indispensable for the development of effective shell-model interactions. Special attention is given to the investigation of exotic nuclei far from stability [64] which play a decisive role in the synthesis of heavy elements in nuclear astrophysics. Along the $N \leq Z$ line, the rapid proton-capture (rp) process takes place in explosive hydrogen-burning scenarios such as novae and

X-ray bursts at the surface of accreting neutron stars [65, 66]. The initial material is transformed by sequential proton captures up to the proton drip-line followed by β^+ decays. The rp process is continually competing with the inverse (γ,p) photo-disintegration reactions ending in a closed SnSbTe cycle [67]. Astrophysical models rely on precise knowledge of masses and half-lives of the nuclei in the region of the rp process. Moreover, long-lived isomeric states can impact the process as they may accelerate the reaction flow [66]. Along the rp paths up to the region around ^{100}Sn, the experimental data situation becomes increasingly fragmentary (see Fig. 1 in Ref. [65]). Therefore, shell-model calculations are used to compensate for the lack of experimental data [68, 69].

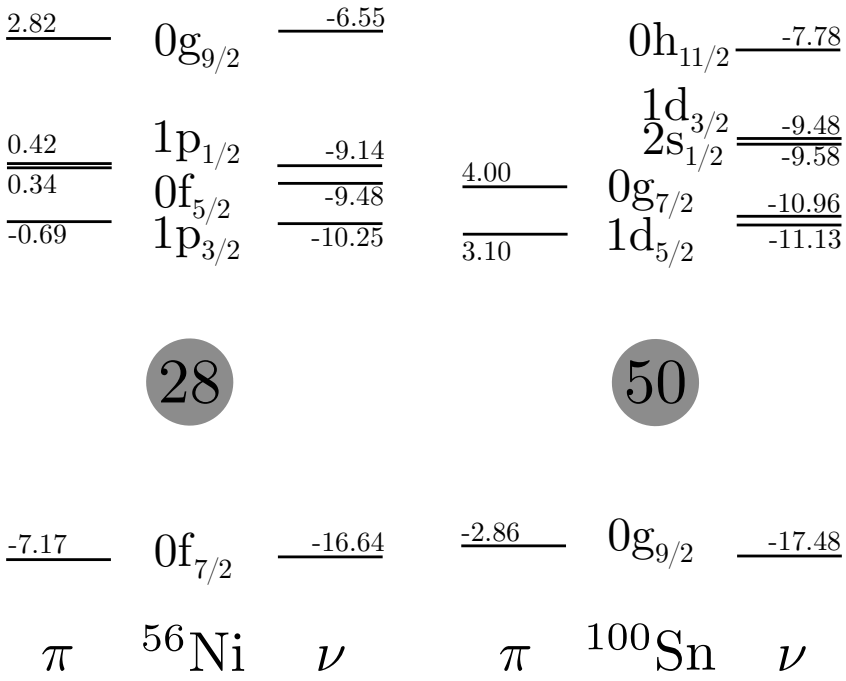

Figure 7: Schematic representation of single-particle energies and single-hole energies for protons (π) and neutrons (ν) in ^{56}Ni and ^{100}Sn. Level energies are normalized to the middle of the shell gaps and account for Coulomb energy differences between protons and neutrons. The shell gaps for $N = Z = 28$ and $N = Z = 50$ are additionally labeled. Plotted with data obtained from Ref. [66] (cf. Fig. 3.1.2 in Ref. [66]).

In spite of considerable experimental efforts, excited nuclear states in doubly-magic ^{100}Sn were not observed until now. Promising results were obtained at the GSI Helmholtzzentrum für Schwerionenforschung [70] and, recently, at the RIKEN Nishina Center [71] radioactive-ion beam facilities (RIBF) where up to a couple of hundreds events of ^{100}Sn were identified after fragmentation reactions of a ^{124}Xe primary beam. On the theoretical side, the existence of a hypothetical $E2$-isomeric 6_1^+ state was discussed recently based on results from LSSM shell-model calculations and from the Hartree-Fock random-phase approximation (HF-RPA) [66, 71].

The region around ^{100}Sn can be described within the gds valence space comprising the $0g_{9/2}$, $1d_{5/2}$,$0g_{7/2}$, $2s_{1/2}$, and $1d_{3/2}$ shell-model orbitals. Within this work a realistic interaction is used based on a renormalized G-matrix derived from the Oslo Group [12], with monopole constraints in order to reproduce shell-gap observables in the region around ^{100}Sn [20]. Results on excitation energies

and $B(E2)$ values of this calculation together with similar results from a HF-RPA calculation [72] are used for a phenomenological comparison of level schemes in both doubly-magic $N = Z$ nuclei ^{100}Sn and ^{56}Ni. Such a comparison is justified, as the single-particle and single-hole energies extrapolated from ^{90}Zr to ^{100}Sn show remarkable similarities to those extracted from ^{56}Ni [66] (a schematic view is shown in Fig. 7). This conspicuousness is related to basic properties as both nuclei are $N = Z$, doubly-magic and have an ℓs open core, i.e. the spin-orbit shell closure splits the $0f_{7/2}$ and $0g_{9/2}$ orbitals from the $0f_{5/2}$ and $0g_{7/2}$ orbits which are entangled by the remaining $\Delta\ell = \Delta j = 2$ ($1p$ and $1d$) orbitals for ^{56}Ni and ^{100}Sn, respectively (see Fig. 7). Based on the similarities in the shell structures of both nuclei, excitation energies and nuclear transition probabilities in ^{56}Ni could give indication for a comparable behavior of analogous states in ^{100}Sn.

1.8 Outline of this thesis

This cumulative doctoral thesis comprises three peer-reviewed publications:

- K. Arnswald *et al.* "Enhanced collectivity along the $N = Z$ line: Lifetime measurements in ^{44}Ti, ^{48}Cr, and ^{52}Fe". *Phys. Lett. B* 772 (2017) 599–606
- K. Arnswald *et al.* "Lifetime measurements in ^{44}Ti". *Phys. Rev. C* 102, 054302 (2020)
- K. Arnswald *et al.* "Enhanced quadrupole collectivity in doubly-magic ^{56}Ni: Lifetime measurements of the 4_1^+ and 6_1^+ states". *Phys. Lett. B* 820 (2021) 136592

The thesis is concerned with experimental results deduced from lifetime measurements of low-lying (non-)yrast states along the $N = Z$ chain between ^{44}Ti and ^{56}Ni. The experimental findings are compared with results from various shell-model interactions (see section 1.2).

The first letter "Enhanced collectivity along the $N = Z$ line: Lifetime measurements in ^{44}Ti, ^{48}Cr, and ^{52}Fe" [16] presents precise lifetime results of the 2_1^+ states in ^{44}Ti, ^{48,50}Cr, and ^{52}Fe employing the recoil-distance Doppler-shift (RDDS) method. The deduced $B(E2; 2_1^+ \rightarrow 0^+_{\text{g.s.}})$ values are compared with similar results from even-even nuclei along the respective chains of isotopes and with results from shell-model calculations using the GXPF1A, KB3G, and FPD6 interactions. In addition, a novel effective shell-model Hamiltonian starting from a realistic nucleon-nucleon potential is used for the calculation of $B(E2)$ values. Preliminary lifetime and shell-model results of this work were already reported in Ref. [7].

The second article "Lifetime measurements in ^{44}Ti" [17] concentrates on the $N = Z$ nucleus ^{44}Ti. Nuclear level lifetimes were measured over a range of 610 fs up to 110 ps using the Doppler-shift attenuation method (DSAM) as well as the RDDS technique. Corresponding $E2$, $E2/M1$, and $E1$ reduced transition strengths are confronted with results from the established GXPF1A, FPD6, and KB3G shell-model interactions. Moreover, the modern ZBM2M shell-model interaction is employed to calculate negative-parity states on the one hand and to shed light on the impact of multi-particle multi-hole cross-shell excitations in ^{44}Ti on the other hand. The experimental findings are furthermore compared with theoretical values from an α-cluster model.

The third publication "Enhanced quadrupole collectivity in doubly-magic ^{56}Ni: Lifetime measurements of the 4_1^+ and 6_1^+ states" [20] focuses on lifetime measurements in the doubly-magic nucleus ^{56}Ni. Exploiting the DSA method, nuclear level lifetimes of the 4_1^+ and 6_1^+ states are determined. The corresponding $B(E2)$ values are compared along the $N = 28$ chain of isotones and confronted with shell-model calculations employing the GXPF1A and PFSDG-U interactions. In addition, valence ab-initio calculations were utilized based on recently derived Hamiltonians from chiral perturbation theory, with and without contributions of three-body forces. Based on similar single-particle and single-hole energies, experimental and theoretical level schemes of ^{56}Ni are finally confronted with theoretical results on the doubly-magic $N = Z$ partner nucleus ^{100}Sn.

This thesis closes with a discussion and conclusions of the acquired results presented in the three publications. A short outlook highlights possible setups for future experiments along the $N = Z$ line.

Publication I:

Enhanced collectivity along the $N = Z$ line: Lifetime measurements in ^{44}Ti, ^{48}Cr, and ^{52}Fe

Physics Letters B 772 (2017) 599–606

Contents lists available at ScienceDirect

Physics Letters B

www.elsevier.com/locate/physletb

Enhanced collectivity along the $N = Z$ line: Lifetime measurements in ^{44}Ti, ^{48}Cr, and ^{52}Fe

K. Arnswald [a,*], T. Braunroth [a], M. Seidlitz [a], L. Coraggio [b], P. Reiter [a], B. Birkenbach [a], A. Blazhev [a], A. Dewald [a], C. Fransen [a], B. Fu [a], A. Gargano [b], H. Hess [a], R. Hirsch [a], N. Itaco [b,c], S.M. Lenzi [d], L. Lewandowski [a], J. Litzinger [a], C. Müller-Gatermann [a], M. Queiser [a], D. Rosiak [a], D. Schneiders [a], B. Siebeck [a], T. Steinbach [a], A. Vogt [a], K. Wolf [a], K.O. Zell [a]

[a] Institut für Kernphysik, Universität zu Köln, Zülpicher Straße 77, D-50937 Köln, Germany
[b] Istituto Nazionale di Fisica Nucleare, Sezione di Napoli, I-80126 Napoli, Italy
[c] Dipartimento di Matematica e Fisica, Università degli Studi della Campania "Luigi Vanvitelli", Viale A. Lincoln 5, I-8110 Caserta, Italy
[d] Dipartimento di Fisica dell'Università and INFN, Sezione di Padova, I-35141 Padova, Italy

ARTICLE INFO

Article history:
Received 8 May 2017
Received in revised form 29 June 2017
Accepted 15 July 2017
Available online 20 July 2017
Editor: V. Metag

Keywords:
$N = Z$ nuclei
Lifetime measurements
RDDS
B(E2) values

ABSTRACT

Lifetimes of the 2_1^+ states in ^{44}Ti, ^{48,50}Cr, and ^{52}Fe were determined with high accuracy exploiting the recoil distance Doppler-shift method. The reduced E2 transition strengths of ^{44}Ti and ^{52}Fe differ considerably from previously known values. A systematic increase in collectivity is found for the $N = Z$ nuclei compared to neighboring isotopes. The B(E2) values along the Ti, Cr, and Fe isotopic chains are compared to shell-model calculations employing established interactions for the $0f1p$ shell, as well as a novel effective shell-model Hamiltonian starting from a realistic nucleon–nucleon potential. The theoretical approaches underestimate the B(E2) values for the lower-mass Ti isotopes. Strong indication is found for particle-hole cross-shell configurations, recently corroborated by similar results for the neighboring isotone ^{42}Ca.

1. Introduction

Reduced transition strengths are sensitive observables to study the properties of atomic nuclei and the evolution of nuclear structure. A basic indicator for the collectivity and for the shape of even–even nuclei is given by the B(E2) values especially for the excited 2_1^+ states. Together with the transition strengths of the 4_1^+ states, the vibrational or rotational character of the individual isotopes can be deduced. The measurement of the reduced transition probability of the $2_1^+ \rightarrow 0_{g.s.}^+$ transition in the $N = Z$ nuclei ^{44}Ti, ^{48}Cr, and ^{52}Fe allows to delineate the evolution of the quadrupole collectivity between the doubly-magic shell closures at $N = Z = 20$ and $N = Z = 28$ where deviations from the spherical shape and its vibrational character are of high interest. Existing experimental results feature puzzling peculiarities with respect to the properties of excited 2_1^+ and 4_1^+ states in these nuclei and motivated the following investigations.

For the neutron-deficient Ti isotopes the $B(E2; 2_1^+ \rightarrow 0_{g.s.}^+)$ value for ^{44}Ti [1–3] appeared to be significantly smaller than the respective B(E2) value in the neighboring semi-magic $N = 20$ isotope ^{42}Ti [4] (cf. Fig. 1). This observation contradicts the general expectation and would question the robustness of the $N = 20$ shell closure for Ti. Moreover, other experimental studies of ^{44}Ti showed a rotational-like excitation-energy spacing on top of the excited 0_2^+ state [5]. Theoretical predictions concur with this observation and claim highly-deformed $12p$–$8h$ and $16p$–$12h$ configurations at 12 MeV and 20 MeV, respectively, as origin of these bands [6]. Recently, shape parameters in the isotone ^{42}Ca were determined from a Coulomb-excitation experiment [7]. As a result, a weakly-deformed ground-state band and a slightly triaxial superdeformed sideband were discovered. Especially, the observed enhanced quadrupole deformation of the 2_1^+ state suggests a possible mixing with the superdeformed 2_2^+ state. An intriguing question is related to the $N = Z$ isotonic neighbor ^{44}Ti where a similar

* Corresponding author.
E-mail address: konrad.arnswald@ikp.uni-koeln.de (K. Arnswald).

http://dx.doi.org/10.1016/j.physletb.2017.07.032

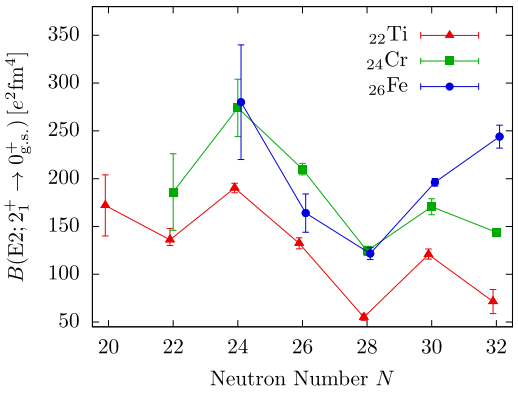

Fig. 1. (Color online.) Previously known $B(\mathrm{E2}; 2_1^+ \to 0^+_{\mathrm{g.s.}})$ values of Ti (red triangles), Cr (green squares), and Fe (blue circles) isotopes. Adopted $B(\mathrm{E2})$ values are taken from Ref. [8]. For ^{56}Cr recent results from Ref. [9] are additionally considered. For better visibility, the data points of the same element are connected and the Ti and Fe chains are slightly shifted horizontally with respect to the Cr data.

structure can be expected. From the interplay between deformed and highly-deformed sidebands and the yrast 2^+ state, like in ^{42}Ca, a clearly enhanced $B(\mathrm{E2}; 2_1^+ \to 0^+_{\mathrm{g.s.}})$ value is anticipated for ^{44}Ti in contradiction to the experimental results.

In addition, the ratio of reduced transition strengths $B_{4/2} = B(\mathrm{E2}; 4_1^+ \to 2_1^+)/B(\mathrm{E2}; 2_1^+ \to 0^+_{\mathrm{g.s.}})$ was exploited in Refs. [2,10] to characterize the nuclei ^{44}Ti, ^{48}Cr and ^{52}Fe. The values indicate a rapid change from a vibrational behavior for ^{44}Ti and ^{52}Fe to an extreme single-particle value at mid-shell for ^{48}Cr. However, the ratios are subject to large experimental uncertainties.

The lifetime of the 2_1^+ state in ^{48}Cr was addressed by several experiments using early recoil distance Doppler-shift measurements after fusion-evaporation reactions [11–13]. A maximum $B(\mathrm{E2})$ value was measured at the $f_{7/2}$ mid-shell position. However, large experimental uncertainties motivated the improved experiments of this publication.

The $B(\mathrm{E2})$ value of the ground-state transition in ^{52}Fe was deduced from a recent Coulomb-excitation experiment at intermediate energies at the National Superconducting Cyclotron Laboratory employing the SeGA detector array [14]. A moderate increase of quadrupole collectivity was found with respect to the neighboring shell closure at the $N = 28$ isotope ^{54}Fe. A complementary approach, based on the RDDS technique, was employed in the new experiment to determine the lifetime of the corresponding 2_1^+ state in ^{52}Fe. A summary of the previously known experimental $B(\mathrm{E2}; 2_1^+ \to 0^+_{\mathrm{g.s.}})$ values is shown in Fig. 1 for the Ti, Cr, and Fe isotopes from $N = 20$ to 32.

From theoretical point of view, the $0f1p$ shell nuclei provide an excellent testing ground for modern shell-model calculations. The following three shell-model interactions FPD6 [15], KB3G [16], and GXPF1A [17] were developed in part by fitting experimental data of the nuclei of interest and are thus suited to describe the envisaged region of the nuclear chart. Detailed new calculations are subject of this letter. Moreover, a new effective shell-model Hamiltonian starting from a realistic nucleon–nucleon potential was employed in order to describe the experimental findings.

As protons and neutrons occupy the same major shell, the neutron–proton interaction becomes important, enhancing collective effects like isoscalar ($T = 0$) neutron–proton pairing. Theoretical investigations on $T = 0$ ground-state correlations were performed for ^{44}Ti [18]. Furthermore, results from Ref. [19] indicate that for $N = Z = 24$ (^{48}Cr) neutron–proton pair correlations become important at higher spin values. Isoscalar neutron–proton pairing is even more relevant for heavier, exotic $N = Z$ nuclei towards doubly-magic ^{100}Sn [18,20]. For example, it is expected that the self-conjugate ^{88}Ru has a significantly enhanced E2 transition strength [21]. A recent study in the neighboring $N = Z = 46$ nucleus ^{92}Pd revealed experimental evidence for $T = 0$ neutron–proton pairing [22].

A different theoretical approach exploits the α-cluster structure in the fp-shell region where a strong spin-orbit force is counteracting the α correlations. However, the observation of an α-cluster band in ^{44}Ti confirmed the applicability of the α-cluster model. Detailed theoretical $B(\mathrm{E2})$ values are available for ^{44}Ti from Ref. [23] which show a considerably enhanced collective behavior. A refined theoretical study in this line exploits deformed-basis antisymmetrized molecular dynamics (AMD) by the use of the Gogny D1S force [24] and yield coexistence phenomena in ^{44}Ti. A mixed character of the mean-field-like structure and the $\alpha + {}^{40}$Ca cluster structure of the yrast band in ^{44}Ti is obtained implying a high $B(\mathrm{E2}; 2_1^+ \to 0^+_{\mathrm{g.s.}})$ value. These results are given in Ref. [24] and exceed the previously measured $B(\mathrm{E2})$ value [1–3].

A new experimental investigation is motivated by the fact that the lifetime of the 2_1^+ state in ^{44}Ti is mainly known from pioneering studies performed in the 1970's with limited precision [1,2]. The same is true for the 2_1^+ state in ^{48}Cr which was addressed by earlier experiments [11–13]. The determined lifetime values were given with considerable error bars. Nowadays, the recoil distance Doppler-shift (RDDS) method has proven to provide precise, reliable, and model-independent lifetime values in the picosecond range for excited nuclear states. The method is applicable for stable-beam experiments as well as for the measurement of transition strengths in exotic nuclei [9,25–28].

A measurement of the reduced transition strengths with increased precision for the $N = Z$ nuclei ^{44}Ti, ^{48}Cr, and ^{52}Fe was performed to address the open questions and puzzling observations. Nuclear level lifetimes in the isotopes of interest were studied employing the RDDS techniques with stable ion beams, which allows high accuracy by exploitation of $\gamma\gamma$-correlation gated spectra and by elimination of systematic errors like unobserved side-feeding effects.

2. Experiment

Three experiments were performed at the FN tandem accelerator at the Institute for Nuclear Physics, University of Cologne, combining a setup of twelve high-purity germanium (HPGe) detectors and the Cologne coincidence-plunger device [29]. Excited states in the nuclei of interest were populated by the following fusion-evaporation reactions: $^{\mathrm{nat.}}$Mg(^{23}Na, $x$np)^{44}Ti, ^{40}Ca(^{10}B, np)^{48}Cr, and ^{27}Al(^{28}Si, 2np)^{52}Fe.

The plunger targets were made of $^{\mathrm{nat.}}$Mg (^{40}Ca, ^{27}Al) with a thickness of 1 mg/cm^2 (0.50 mg/cm^2, 0.58 mg/cm^2) for the ^{44}Ti (^{48}Cr, ^{52}Fe) recoils. While the magnesium target was self-supporting, the calcium and aluminum target material was evaporated onto a 2.0-mg/cm^2 gold backing facing the beam. The calcium target was additionally protected against oxidation by a 0.1-mg/cm^2 gold layer. Recoiling nuclei left the target with 2.7% (1.1%, 3.1%) of the speed of light which corresponds to mean velocities of 8.1 µm/ps (3.3 µm/ps, 9.3 µm/ps). Reaction products were finally stopped in a 9.6-mg/cm^2 thick gold foil. During the experiment data were recorded at 6 (12, 7) different target-to-stopper distances, i.e. different flight times of the recoiling nuclei. These distances reach from 21.5 to 47.5 µm (20.4 to 321 µm, 28.6 to 151.6 µm) and were measured with an accuracy of better than 2%. Beam-depending changes, such as thermal expansion of the target, were compensated by a feedback system employing a piezoelectric linear motor. The experimental details are summarized in Table 1.

Emitted γ rays were detected by twelve HPGe detectors with relative efficiencies between 55% and 80% which were placed in

Table 1
Experimental details: Reactions, target properties, and offset-corrected relative target-to-stopper distances of the plunger device for each of the three experiments.

Reaction	E_{beam} [MeV]	Target thickness [mg/cm^2]	Recoil velocity [μm/ps]	Target-to-stopper distances	Target-to-stopper range [μm]
$^{nat.}$Mg(^{23}Na, $x$np)^{44}Ti	62	1	8.1(4)	6	21.5–47.5
^{40}Ca(^{10}B, np)^{48}Cr	26	0.50	3.3(2)	12	20.4–321
^{27}Al(^{28}Si, 2np)^{52}Fe	86	0.58	9.3(4)	7	28.6–151.6

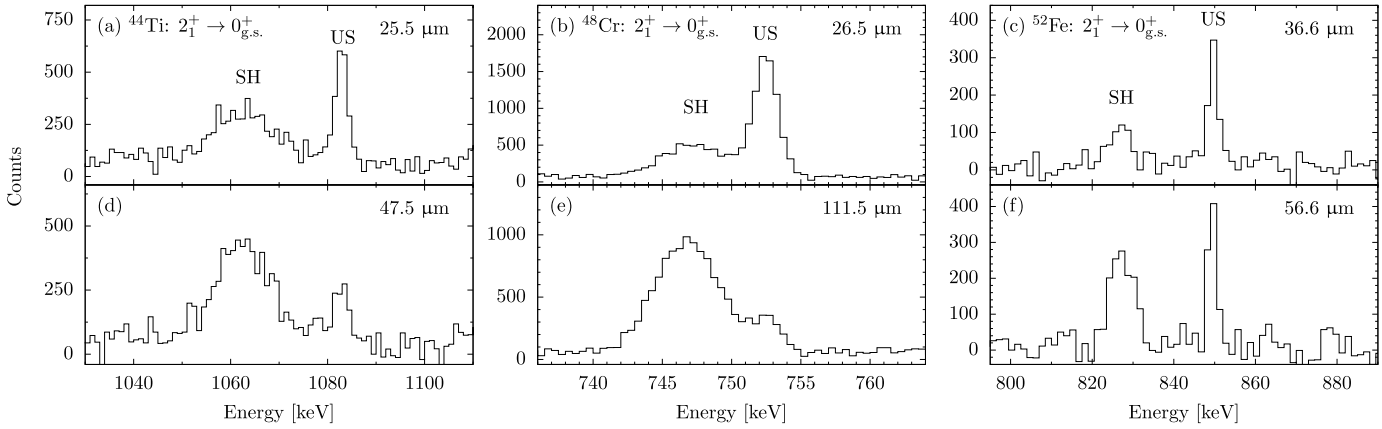

Fig. 2. Exemplary γ-ray energy spectra from the $2_1^+ \rightarrow 0_{g.s.}^+$ decay at (a, d) 1083 keV in ^{44}Ti, at (b, e) 752 keV in ^{48}Cr, and at (c, f) 849 keV in ^{52}Fe. Spectra are produced from cuts on the shifted component of the $4_1^+ \rightarrow 2_1^+$ transition and are shown for a short (a, b, c) and a larger (d, e, f) target-to-stopper distance at backward angles. Doppler-shifted (SH) components and unshifted (US) components are additionally labeled.

rings centered at polar angles of $\theta_0 = 0°$ (1 detector), $\theta_1 = 45°$ (6 detectors), and $\theta_2 = 143°$ (5 detectors) with respect to the beam axis. Each HPGe detector was shielded with sheets of lead and copper between target and endcap with a total thickness of 2 mm in order to reduce pile up and additional dead time caused by low-energy X rays. Furthermore, a hardware $\gamma\gamma$-coincidence trigger was used to suppress single γ-ray events, which do not contribute to the $\gamma\gamma$-coincidence analysis. Coincident γ-ray events were finally sorted into $\gamma\gamma$ matrices with respect to the different target-to-stopper distances and the correlation groups defined by the individual detector rings. The total statistics in the projected $\gamma\gamma$ matrices amount to 6.8×10^9 (3.5×10^9, 7.3×10^9) events for the experiments to populate ^{44}Ti, (^{48}Cr, and ^{52}Fe), respectively.

3. Analysis and results

The lifetime analysis is based on the recoil distance Doppler-shift (RDDS) technique in conjunction with the differential decay-curve method (DDCM) [29]. Due to sufficient production yields of recoiling nuclei of interest, the DDCM was utilized in the $\gamma\gamma$-coincidence mode. Employing gates on the Doppler-shifted (SH) component of feeding transitions, or on the unshifted (US) part of the $2_1^+ \rightarrow 0_{g.s.}^+$ transitions, the lifetime of the 2_1^+ states was determined by analyzing the intensity ratios of shifted and unshifted components of the depopulating and feeding transitions, respectively (cf. Fig. 2). A lifetime τ_i is deduced for each distance i in the sensitive range. The τ curve is expected to be constant and the weighted mean value of the different τ_i corresponds to the analyzed lifetime. Lifetimes determined from different $\gamma\gamma$ matrices are statistically independent. The statistical uncertainty of the lifetime value is dominated by the distribution of the single τ_i values. Systematic errors of the lifetime arise from (i) the uncertainty of the recoil velocity which is inversely included in the lifetime value. The mean velocity was determined from the Doppler shift of the direct feeding transition observed at forward and backward angles. The uncertainty of the mean polar angle $\Delta\theta = 3°$ results in $\Delta\beta = 1.2 \times 10^{-3} (0.5 \times 10^{-3}, 1.3 \times 10^{-3})$ for ^{44}Ti (^{48}Cr, ^{52}Fe). (ii) The relative target-to-stopper distances can be measured with a high precision of $\Delta x \leq 0.4$ μm in the sensitive range. Thus, its contribution to the total uncertainty of τ was neglected. (iii) Contaminating transitions in the $\gamma\gamma$ coincidence gate may impact the experimental lifetimes. This was excluded in the analysis by the careful selection of narrow energy gates. Finally, the total systematic error of the lifetime was calculated via the Gaussian error propagation.

In the case of ^{44}Ti a gate from below was set on the unshifted part of the $2_1^+ \rightarrow 0_{g.s.}^+$ transition at 1083 keV to avoid any background contribution in the region of interest. The lifetime of the 2_1^+ state is finally determined from the shifted and the total intensities (I_{SH} and I_{SH+US}) of the $4_1^+ \rightarrow 2_1^+$ feeding transition at 1371 keV and yields $\tau(2_1^+) = 2.68\,(21)_{stat.}\,(12)_{sys.}$ ps.

The ^{10}B + ^{40}Ca reaction caused a small Doppler shift for the γ rays of interest in ^{48}Cr due to a moderate momentum transfer. Therefore, the shifted and unshifted components of the γ-ray line are not separated completely from each other (see spectra in Figs. 2(b), (e)). To avoid any contamination of unshifted fractions in the selected gate, an indirect gate on the $8_1^+ \rightarrow 6_1^+$ transition at 1742 keV was used in the analysis. For this transition only a shifted component was observed indicating a fast behavior of the feeding structure (cf. Ref. [30]). Moreover, the low momentum transfer of the reaction and the large energy loss in the target result in a broad velocity distribution of the recoiling nuclei after the target, i.e. a wide range of flight times between target and stopper foil. Thus, the observed velocity distribution of the nuclei that emit a γ ray in flight, depends on the target-to-stopper distance. A correction was applied which normalizes the distances to the observed maximum recoil velocities. The lifetime of the first 2^+ state in ^{48}Cr was determined from the feeding-corrected intensity distribution of the $2_1^+ \rightarrow 0_{g.s.}^+$ transition at 752 keV, which yields $\tau(2_1^+) = 12.16\,(14)_{stat.}\,(69)_{sys.}$ ps.

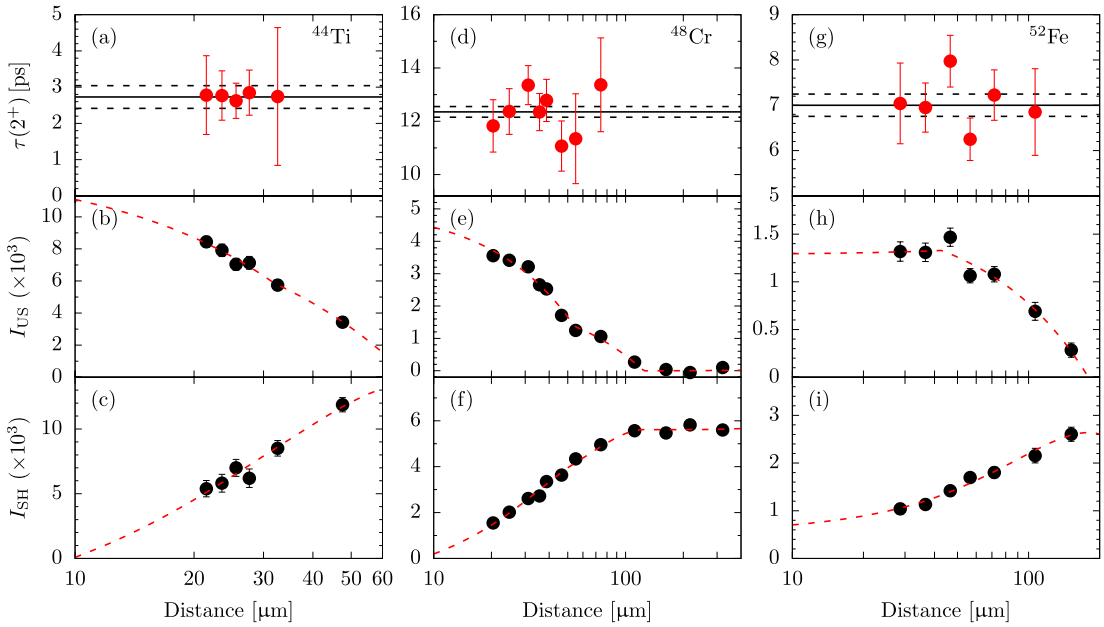

Fig. 3. (Color online.) τ curves of the 2^+_1 states (a, d, g) are presented for the nuclei ^{44}Ti, ^{48}Cr, and ^{52}Fe, respectively. Black solid lines indicate the weighted mean value of the lifetime; dashed lines mark the statistical uncertainty. Furthermore, the unshifted (b) and shifted (c) intensities of the direct populating transition in ^{44}Ti are shown, as well as the unshifted intensities (e, h) and the shifted intensities (f, i) of the depopulating $2^+_1 \rightarrow 0^+_{g.s.}$ transition in ^{48}Cr and ^{52}Fe, respectively. The polynomial fit function to the given intensities is presented in dashed red. Lifetimes and γ-ray intensities are presented in dependence of the target-to-stopper distances. Note the logarithmic distance scale.

Table 2
Experimental lifetimes for the 2^+_1 states in ^{44}Ti, ^{48,50}Cr, and ^{52}Fe from the present experiment are compared to previous experimental values taken from Ref. [8,14]. The corresponding experimental and theoretical $B(E2; 2^+_1 \rightarrow 0^+_{g.s.})$ values are included. The results are compared to four different shell-model calculations (for details see text).

Nucleus	Experiment				Theory			
	Lifetime [ps]		$B(E2)$ [e^2 fm^4]		$B(E2)$ [e^2 fm^4]			
	Present	Previous	Present	Previous	GXPF1A	KB3G	FPD6	Realistic
^{44}Ti	2.7(2)	$4.03^{+0.18}_{-0.32}$ [a]	205^{+20}_{-17}	136^{+12}_{-6} [a]	105	119	140	120
^{48}Cr	12.2(7)	12.4(14) [a]	279^{+17}_{-15}	274(30) [a]	251	253	314	272
^{50}Cr	13.0(4)	$13.15^{+0.41}_{-0.29}$ [a]	214^{+7}_{-6}	210(6) [a]	218	218	276	243
^{52}Fe	7.0(4)	11.3(14) [b]	265^{+15}_{-13}	163(20) [b]	221	217	292	273

[a] From Ref. [8].
[b] Adapted from $B(E2; 0^+_{g.s.} \rightarrow 2^+_1) = 817\,(102)\,e^2$ fm^4 in Ref. [14].

In ^{52}Fe a narrow gate was applied to the shifted component of the $4^+_1 \rightarrow 2^+_1$ transition at 1535 keV. In the gated spectra a contaminant within the range of the shifted component of the $2^+_1 \rightarrow 0^+_{g.s.}$ transition at 849 keV obstructed a lifetime analysis in the forward detector rings. Therefore, the lifetime of the first 2^+ state was determined using the upstream detector ring, yielding $\tau(2^+_1) = 7.00\,(24)_{stat.}\,(28)_{sys.}$ ps. In order to cross-check the modified analysis with only one detector-ring combination in ^{52}Fe, an independent analysis of the lifetime of the 2^+_1 state in the neighboring ^{50}Cr was performed as a consistency check. This transition was observed with higher statistics and its analysis yields $\tau(2^+_1) = 13.0\,(3)_{stat.}\,(3)_{sys.}$ ps, which is in good agreement with the adopted lifetime of $\tau(2^+_1) = 13.15^{+0.41}_{-0.29}$ ps from Ref. [8].

The final τ curves of the 2^+_1 states and the corresponding γ-ray intensities are presented for the nuclei ^{44}Ti, ^{48}Cr, and ^{52}Fe in Fig. 3. Lifetime measurements of higher-lying yrast states were not feasible because these states are too short-lived for the applied target-to-stopper distances. Experimental results of measured lifetimes and corresponding $B(E2)$ values are summarized in Table 2. The final experimental error of the lifetime includes the root sum squared of the statistical and the systematic uncertainties.

4. Discussion

The measured lifetimes were converted into $B(E2; 2^+_1 \rightarrow 0^+_{g.s.})$ values and are compared to previous experimental values (see Table 2). Results on $B(E2)$ values from new shell-model calculations were obtained and are also confronted with the new findings. Emphasize is given to the evolution along $N = Z$ and the respective even–even isotopic chains. The latter comparison is shown in Fig. 4 for the 2^+_1 excitation energies (a, b, c) and the $B(E2)$ values (d, e, f).

The newly determined 2^+_1 lifetime in ^{44}Ti corresponds to a reduced transition probability $B(E2; 2^+_1 \rightarrow 0^+_{g.s.}) = 205^{+20}_{-17}\,e^2$ fm^4; while the adopted lifetime is $\tau = 4.03^{+0.18}_{-0.32}$ ps with $B(E2; 2^+_1 \rightarrow 0^+_{g.s.}) = 136^{+12}_{-6}\,e^2$ fm^4 [8]. Thus, there is a 4σ deviation between both values. The adopted value includes results deduced from lifetime experiments employing the Doppler-shift attenuation method (DSAM) following α-capture and α-transfer reactions on a ^{40}Ca target [2,3]. For this type of experiments, systematic uncertainties

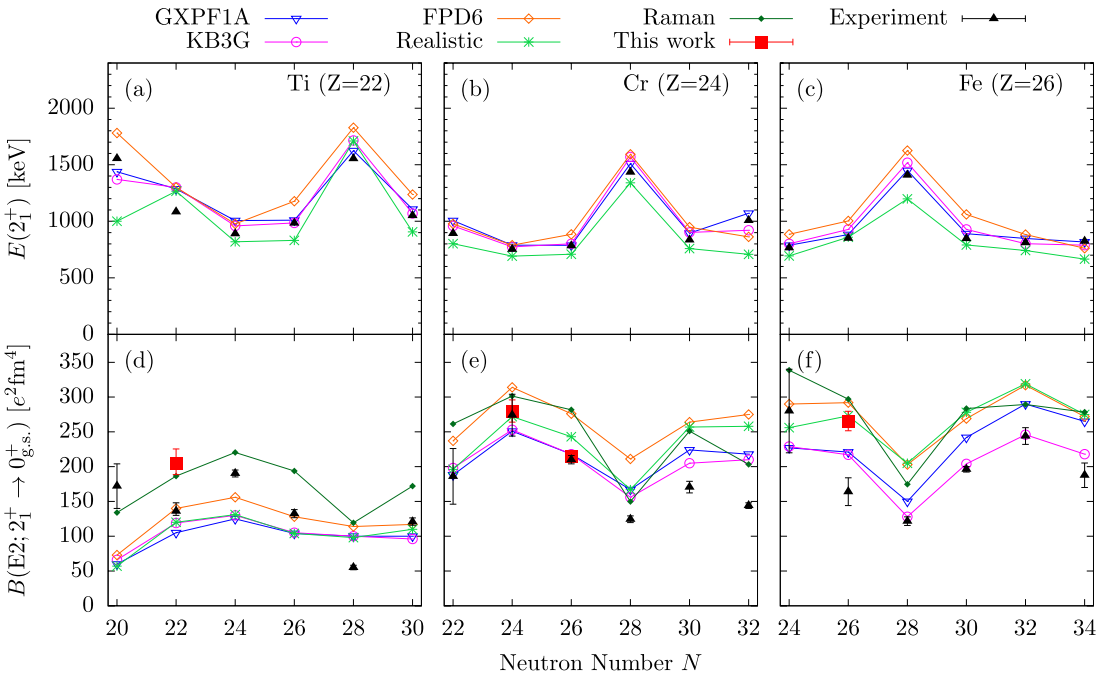

Fig. 4. (Color online.) Experimental and theoretical 2_1^+ excitation energies (a, b, c) and $B(E2)$ values of the $2_1^+ \rightarrow 0_{g.s.}^+$ transition (d, e, f). Both values are plotted against the neutron number for (a, d) titanium, (b, e) chromium, and (c, f) iron isotopes, respectively. $B(E2)$ values from this work are given in red squares. Previously adopted $B(E2)$ values (black triangles) are taken from Refs. [8,9]. The global best fit given by Raman et al. [38] is presented by dark green diamonds. Moreover, shell-model calculations employing the GXPF1A (blue open triangles), KB3G (purple open circles), and FPD6 (orange open diamonds) interactions, as well as a shell-model calculation using a realistic effective Hamiltonian (green stars) are shown.

arise from the lack of precise knowledge of the stopping power, unknown feeding contributions, and the decreasing sensitivity of the DSAM for lifetimes longer than 1 ps. As stated above, the previous $B(E2)$ value is lower than the value for the $N = 20$ isotope ^{42}Ti and does not match the expectation along the titanium isotopic chain. The new larger $B(E2)$ value for ^{44}Ti resolves the discrepancy (cf. Fig. 4(d)) and a more collective behavior than in the neighboring semi-magic even–even nucleus ^{42}Ti is suggested.

For ^{48}Cr the reduced transition probability of $B(E2; 2_1^+ \rightarrow 0_{g.s.}^+) = 279^{+17}_{-15}\, e^2\,\mathrm{fm}^4$ deduced in this work agrees well with the previously adopted value $B(E2; 2_1^+ \rightarrow 0_{g.s.}^+) = 274(30)\, e^2\,\mathrm{fm}^4$ from Ref. [8]. The adopted value includes the results from Refs. [11–13]. The relative uncertainty can now be further reduced and amounts to 5.8%. The value follows nicely the overall tendency along the chromium isotopes (cf. Fig. 4(e)) with its maximum value at mid-shell.

In ^{52}Fe there is a discrepancy between the new $B(E2; 2_1^+ \rightarrow 0_{g.s.}^+) = 265^{+15}_{-13}\, e^2\,\mathrm{fm}^4$ value and the previously measured $B(E2; 2_1^+ \rightarrow 0_{g.s.}^+) = 163\,(20)\, e^2\,\mathrm{fm}^4$ value by Yurkewicz et al. [14] (cf. Fig. 4(f)), suggesting a significantly stronger collectivity at $N = Z = 26$. While a small $B(E2)$ value at the $N = 28$ shell closure is expected, a clearly increased $B(E2)$ value in ^{52}Fe, like it is reported here, cannot be excluded. The difference of both experimental values for ^{52}Fe is subject of theoretical discussion presented below.

In summary, the new $B(E2; 2_1^+ \rightarrow 0_{g.s.}^+)$ values in ^{44}Ti and ^{52}Fe are significantly larger than previously measured, corroborating enhanced collectivity close to the doubly-magic nuclei ^{40}Ca and ^{56}Ni at $N = Z$. For Ti and Cr, the $N = Z$ nuclei show largest $B(E2)$ values in comparison to the neighboring even–even isotopes, while for the Fe isotopes, the values at $N = Z$ for ^{52}Fe and the lighter mid-shell neighbor ^{50}Fe are comparable within the experimental uncertainties.

For the theoretical description of the excitation energy of the 2_1^+ states and the new $B(E2; 2_1^+ \rightarrow 0_{g.s.}^+)$ values, shell-model calculations were performed along the isotopic chains of Ti, Cr, and Fe for a wide range where experimental data on $B(E2; 2_1^+ \rightarrow 0_{g.s.}^+)$ values were accessible. The NuShellX@MSU code [31] was employed using three already established interactions for comparison with the present experimental data: FPD6 [15], KB3G [16], and GXPF1A [17]. The model space comprises the $f_{7/2}$, $p_{3/2}$, $p_{1/2}$, and $f_{5/2}$ orbitals, coupled to a ^{40}Ca core. Effective charges $e_\pi = 1.5\, e$ and $e_\nu = 0.5\, e$ were used for protons and neutrons, respectively. The calculated $B(E2)$ values for the nuclei of interest agree with published calculations employing the FPD6 and GXPF1 interactions [32,33].

In addition, realistic shell-model calculations, using the shell-model code Antoine [34], have been performed. The two-body matrix elements of the residual interaction were derived from many-body perturbation theory, including all diagrams up to third-order in the perturbative expansion of the effective shell-model Hamiltonian [35]. Effective operators to calculate the electromagnetic transition rates have been consistently derived within this perturbative approach. The starting realistic nucleon–nucleon potential is a low-momentum potential derived from the CD-Bonn potential [36] within the $V_{\mathrm{low-k}}$ approach, and using a cutoff momentum $\Lambda = 2.6\,\mathrm{fm}^{-1}$ [37]. The single-proton and single-neutron energies have been chosen to reproduce the excitation energies of single-particle states in ^{57}Cu and ^{49}Ca, respectively, and to reproduce the odd-even mass difference around ^{56}Ni and ^{48}Ca. Consequently, two-body matrix elements of the residual interaction and effective electromagnetic operators are derived from theory, while single-particle energies are taken from experiment. The $B(E2; 2_1^+ \rightarrow 0_{g.s.}^+)$ values from all four calculations are reported in Table 2.

Along the chain of titanium isotopes, there is only poor agreement between the experimental and theoretical $B(E2; 2_1^+ \rightarrow 0_{g.s.}^+)$ values for all interactions (see Fig. 4(d)). A strong discrepancy is observed for $N = 20$ to 24 due to small theoretical results. This derivation decreases with the increasing number of neutrons to-

ward $N = 26$. At the shell closure at $N = 20$ a factor of three difference is obtained; and the new experimental value for ^{44}Ti is approximately a factor of two higher than the calculated value. The $N = 26, 30$ values are reproduced quite well. However, at the $N = 28$ sub-shell closure the experimental result of a small $B(E2)$ value is not reproduced by the calculations.

A recent study in the neighboring even–even isotone ^{42}Ca showed a similar result [7]. Enhanced $B(E2; 2_1^+ \rightarrow 0_{g.s.}^+)$ values were measured in contrast to lower shell-model results. It was suggested by Ref. [39] that the experimental enhancement arises from $2\hbar\omega$ sd-shell excitations, which are not included in the fp model space. In addition, a sizable quadrupole moment of the 2_1^+ state in ^{42}Ca is proposed to originate from a mixing of the 2_1^+ state with a superdeformed 2_2^+ state [7]. In ^{44}Ti a mixing of the 2_1^+ state with non-yrast 2^+ states will have a minor effect due to larger level-energy differences. Thus, the underestimated transition probability is most likely caused by core excitations from the sd shell. Furthermore, an overestimated theoretical excitation energy of the 2_1^+ state is obtained. Neglecting core excitations, the different shell-model calculations predict the energy of the 2_1^+ state to be $E(2^+) = 1266$ to 1300 keV which exceeds the experimentally observed $E(2^+) = 1083$ keV (cf. Fig. 4 (a)).

The importance of core excitations north-east of ^{40}Ca is also essential in the schematic α-cluster model discussed by Ohkubo et al. [23]. Excitation energies of all rotational bands in ^{44}Ti are reproduced using an $\alpha + ^{40}\mathrm{Ca}(I^\pi)$ system. Moreover, $B(E2)$ values were determined for the low-lying bands and yield $B(E2; 2_1^+ \rightarrow 0_{g.s.}^+) = 18$ W.u. [23] which reproduces the present experimental value of $B(E2) = 22(2)$ W.u. best.

The different shell-model calculations follow the measured $B(E2)$ systematics for $N < 28$ in the chromium isotopic chain as shown in Fig. 4(e). Deviations are visible only for the FPD6 interaction, which tends to larger $B(E2)$s than experimentally determined. The GXPF1A and KB3G interactions as well as the realistic one are in good agreement with the experimental data at $N < 28$. For $N \geq 28$ the transition strength is overestimated by theory. Especially, the experimental data can hardly be reproduced at the (sub-)shell closures $N = 28$ and $N = 32$.

The comparison between experiment and theory shows only partial agreement for the iron isotopes (see Fig. 4(f)). While the $B(E2)$ values for the two lightest isotopes at $N = 24, 26$, which are calculated within the realistic scheme and the FPD6 interaction, are in a good agreement with the new experimental data, the values from GXPF1A and KB3G calculations are too small. However, the latter two interactions reproduce nicely the values for $N \geq 28$. It is noteworthy, that no calculation describes the huge experimental difference of $\sim 143\, e^2\,\mathrm{fm}^4$ between $N = Z = 26$ and the shell closure at $N = 28$; it is underestimated by all interactions.

Experimental and theoretical $B(E2; 2_1^+ \rightarrow 0_{g.s.}^+)$ values for the even–even $N = Z$ nuclei are shown in Fig. 5. For the doubly-magic ^{56}Ni at $N = Z = 28$, each of the employed four shell-model interactions overestimate the experimental $B(E2)$ value from Ref. [40]. The global best fit of Raman et al. [38] is in agreement with the new values.

The present $B(E2; 2_1^+ \rightarrow 0_{g.s.}^+)$ values allow for a refined assessment of the aforementioned $B_{4/2}$ values in these isotopes which are shown in Table 3. For the $B_{4/2}$ ratios the following data were taken: (i) The adopted $B(E2; 2_1^+ \rightarrow 0_{g.s.}^+)$ values from Ref. [8] and $B(E2; 4_1^+ \rightarrow 2_1^+)$ values from Refs. [41–43] are used to determine the $B_{4/2}$ ratios (labeled Previous). (ii) The new $B(E2; 2_1^+ \rightarrow 0_{g.s.}^+)$ values from Table 2 are combined with values from Refs. [41–43] (labeled Present). The corresponding $R_{4/2} = E(4_1^+)/E(2_1^+)$ ratio is also summarized in Table 3.

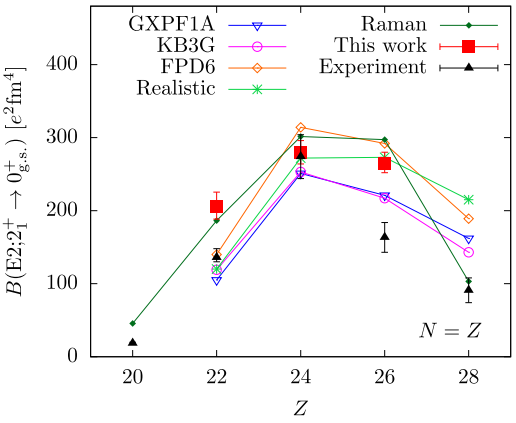

Fig. 5. (Color online.) $B(E2; 2_1^+ \rightarrow 0_{g.s.}^+)$ values for even–even $N = Z$ nuclei between ^{40}Ca and ^{56}Ni. Same color code as in Fig. 4 is used. See text for details.

Table 3
$B_{4/2}$ and $R_{4/2}$ ratios for ^{44}Ti, ^{48}Cr, and ^{52}Fe. Geometrical limits are $B_{4/2} = R_{4/2} = 2.0$ for an ideal vibrator, $B_{4/2} = 1.43$ and $R_{4/2} = 3.33$ for an ideal rotor and $B_{4/2} = 1$ as well as $R_{4/2} < 2$ for a non-collective behavior. See text for details.

Isotope	$B_{4/2}$		$R_{4/2}$
	Present	Previous	
^{44}Ti	$1.36^{+0.29}_{-0.22}$	$2.04^{+0.42}_{-0.32}$	2.27
^{48}Cr	$1.00^{+0.11}_{-0.08}$	$1.02^{+0.16}_{-0.14}$	2.47
^{52}Fe	$1.14^{+0.32}_{-0.21}$	$1.83^{+0.57}_{-0.38}$	2.81

The present $B_{4/2}$ ratios for ^{44}Ti and ^{52}Fe differ distinctively from the previous results. For both isotopes the former results indicate a vibrator-like behavior, whereas the new $B_{4/2}$ ratios are reduced. The $B_{4/2} = 1.36^{+0.29}_{-0.22}$ in ^{44}Ti suggests a rotational behavior. In ^{52}Fe the $B_{4/2} = 1.14^{+0.32}_{-0.21}$ ratio lies between the rotor and the single-particle limit. The ratio given for ^{48}Cr remains nearly unchanged with a new value $B_{4/2} = 1.00^{+0.11}_{-0.08}$ which is at the limit for a collective behavior. The observed fluctuations which were discussed for the previous $B_{4/2}$ ratios in Ref. [10] are not confirmed.

Moreover, the comparison of $R_{4/2}$ and $B_{4/2}$ ratios does not allow a consistent description. While the $R_{4/2}$ ratios suggest a transition from vibrational to rotational character, the new $B_{4/2}$ ratios show collective behavior with similarities to a rotational motion. Nonetheless, it has to be noted that the $B_{4/2}$ ratios depend also on the $B(E2; 4_1^+ \rightarrow 2_1^+)$ values which were not subject of this work. Especially for ^{44}Ti, but also for ^{52}Fe, these values are only known with considerable uncertainties.

5. Summary

To summarize, lifetimes in the self-conjugated nuclei ^{44}Ti, ^{48}Cr, and ^{52}Fe were measured with the RDDS method and precise reduced transition probabilities for the 2_1^+ ground-state transition were determined. The present results yield clearly increased $B(E2; 2_1^+ \rightarrow 0_{g.s.}^+)$ values than previously known for ^{44}Ti and ^{52}Fe in the vicinity of two doubly-magic nuclei. The new results indicate enhanced collectivity for all investigated $N = Z$ nuclei. The deduced $B_{4/2}$ ratio suggests a rotational behavior for ^{44}Ti.

The comparison with state-of-the-art shell-model calculations shows an ambiguous outcome; none of the four effective interactions reproduces all known $B(E2; 2_1^+ \rightarrow 0_{g.s.}^+)$ values from ^{40}Ca to ^{56}Ni in a consistent way. There is a strong evidence that the

observed discrepancy between experiment and theory for ^{44}Ti is related to multi-particle-hole cross-shell configurations similar to recent observations in the neighboring isotone ^{42}Ca. Also the possible rotational character of ^{44}Ti could be explained by particle-hole *sd*-shell core excitations which are typically related to a deformed nucleus. At mid $f_{7/2}$ shell, the different calculations reproduce the experimental B(E2) values for ^{48}Cr. Here, the reduced $B_{4/2}$ ratio close to unity remains an open question. The agreement is reduced for ^{52}Fe; the calculations applying the FPD6 interaction and the effective shell-model Hamiltonian reproduce well the measured B(E2) values. At the $N = Z = 28$ shell closure ^{56}Ni the B(E2) values are overestimated by all considered interactions.

Therefore, on the theory side, challenging future shell-model calculations, which include core excitations from the *sd* shell, are needed to resolve the open questions and to obtain a consistent description of the mass region including also the isotopic evolution where even larger discrepancies exist currently, while on the experimental side, improved lifetime measurements of higher-lying states, especially the 4_1^+ and other members of the ground-state band are of high importance.

Acknowledgement

A.V. acknowledges support from the Bonn-Cologne Graduate School of Physics and Astronomy (BCGS).

References

[1] R.B. Huber, W. Kutschera, C. Signorini, P. Blasi, Gamma transitions in ^{44}Ti and ^{48}Cr from heavy ion induced reactions, J. Phys., Colloq. 32 (1971) C6-207–C6-208.
[2] W.R. Dixon, R.S. Storey, J.J. Simpson, Lifetimes of ^{44}Ti levels, Nucl. Phys. A 202 (3) (1973) 579–592.
[3] S. Schielke, K.-H. Speidel, O. Kenn, J. Leske, N. Gemein, M. Offer, Y.Y. Sharon, L. Zamick, J. Gerber, P. Maier-Komor, First measurement and shell model interpretation of the g factor of the 2_1^+ state in self-conjugate radioactive ^{44}Ti, Phys. Lett. B 567 (3–4) (2003) 153–158.
[4] R. Hartmann, H. Grawe, K. Kändler, The γ-decay of ^{42}Sc and ^{42}Ti, Nucl. Phys. A 203 (2) (1973) 401–413.
[5] C.D. O'Leary, M.A. Bentley, B.A. Brown, D.E. Appelbe, R.A. Bark, D.M. Cullen, S. Ertürk, A. Maj, A.C. Merchant, Nonyrast high-spin states in $N = Z$ ^{44}Ti, Phys. Rev. C 61 (2000) 064314.
[6] D.C. Zheng, L. Zamick, D. Berdichevsky, Superdeformed many-particle–many-hole states in $N = Z$ nuclei: beyond the 8p–8h state in ^{40}Ca, Phys. Rev. C 42 (1990) 1004–1008.
[7] K. Hadyńska-Klęk, P.J. Napiorkowski, M. Zielińska, J. Srebrny, A. Maj, F. Azaiez, J.J. Valiente Dobón, M. Kicińska Habior, F. Nowacki, H. Naïdja, B. Bounthong, T.R. Rodríguez, G. de Angelis, T. Abraham, G. Anil Kumar, D. Bazzacco, M. Bellato, D. Bortolato, P. Bednarczyk, G. Benzoni, L. Berti, B. Birkenbach, B. Bruyneel, S. Brambilla, F. Camera, J. Chavas, B. Cederwall, L. Charles, M. Ciemała, P. Cocconi, P. Coleman-Smith, A. Colombo, A. Corsi, F.C.L. Crespi, D.M. Cullen, A. Czermak, P. Désesquelles, D.T. Doherty, B. Dulny, J. Eberth, E. Farnea, B. Fornal, S. Franchoo, A. Gadea, A. Giaz, A. Gottardo, X. Grave, J. Grębosz, A. Görgen, M. Gulmini, T. Habermann, H. Hess, R. Isocrate, J. Iwanicki, G. Jaworski, D.S. Judson, A. Jungclaus, N. Karkour, M. Kmiecik, D. Karpiński, M. Kisieliński, N. Kondratyev, A. Korichi, M. Komorowska, M. Kowalczyk, W. Korten, M. Krzysiek, G. Lehaut, S. Leoni, J. Ljungvall, A. Lopez-Martens, S. Lunardi, G. Maron, K. Mazurek, R. Menegazzo, D. Mengoni, E. Merchán, W. Męczyński, C. Michelagnoli, J. Mierzejewski, B. Million, S. Myalski, D.R. Napoli, R. Nicolini, M. Niikura, A. Obertelli, S.F. Özmen, M. Palacz, L. Próchniak, A. Pullia, B. Quintana, G. Rampazzo, F. Recchia, N. Redon, P. Reiter, D. Rosso, K. Rusek, E. Sahin, M.-D. Salsac, P.-A. Söderström, I. Stefan, O. Stézowski, J. Styczeń, C. Theisen, N. Toniolo, C.A. Ur, V. Vandone, R. Wadsworth, B. Wasilewska, A. Wiens, J.L. Wood, K. Wrzosek-Lipska, M. Zięblíński, Superdeformed and triaxial states in ^{42}Ca, Phys. Rev. Lett. 117 (2016) 062501.
[8] B. Pritychenko, M. Birch, B. Singh, M. Horoi, Tables of E2 transition probabilities from the first 2^+ states in even–even nuclei, At. Data Nucl. Data Tables 107 (2016) 1–139.
[9] M. Seidlitz, P. Reiter, A. Dewald, O. Möller, B. Bruyneel, S. Christen, F. Finke, C. Fransen, M. Górska, H. Grawe, A. Holler, G. Ilie, T. Kotthaus, P. Kudejová, S.M. Lenzi, S. Mandal, B. Melon, D. Mücher, J.-M. Regis, B. Saha, P. von Brentano, A. Wiens, K.O. Zell, Precision lifetime measurements of the first 2^+ and 4^+ states in ^{56}Cr at the $N = 32$ subshell closure, Phys. Rev. C 84 (2011) 034318.
[10] D. Hertz-Kintish, L. Zamick, S.J.Q. Robinson, $B(E2, 4 \to 2)/B(E2, 2 \to 0)$ ratio in even–even nuclei: apparent anomalous behavior of the chromium isotopes, Phys. Rev. C 90 (2014) 034307.
[11] W. Kutschera, R.B. Huber, C. Signorini, P. Blasi, Gamma-ray spectroscopy of ^{48}Cr, Nucl. Phys. A 210 (3) (1973) 531–543.
[12] B. Haas, P. Taras, J.C. Merdinger, R. Vaillancourt, Yrast states in ^{48}Cr and reaction mechanism of the ^{34}S + ^{16}O reaction at $E_{\text{lab}} = 30$–36 MeV, Nucl. Phys. A 238 (2) (1975) 253–268.
[13] L.P. Ekström, G.D. Jones, F. Kearns, T.P. Morrison, O.M. Mustaffa, D.N. Simister, H.G. Price, P.J. Twin, R. Wadsworth, N.J. Ward, Gamma-ray spectroscopy on ^{48}Cr, J. Phys. G 5 (6) (1979) 803.
[14] K.L. Yurkewicz, D. Bazin, B.A. Brown, C.M. Campbell, J.A. Church, D.-C. Dinca, A. Gade, T. Glasmacher, M. Honma, T. Mizusaki, W.F. Mueller, H. Olliver, T. Otsuka, L.A. Riley, J.R. Terry, Intermediate-energy Coulomb excitation of ^{52}Fe, Phys. Rev. C 70 (2004) 034301.
[15] W.A. Richter, M.G. Van Der Merwe, R.E. Julies, B.A. Brown, New effective interactions for the 0f1p shell, Nucl. Phys. A 523 (2) (1991) 325–353.
[16] A. Poves, J. Sánchez-Solano, E. Caurier, F. Nowacki, Shell model study of the isobaric chains $A = 50$, $A = 51$ and $A = 52$, Nucl. Phys. A 694 (1–2) (2001) 157–198.
[17] M. Honma, T. Otsuka, B.A. Brown, T. Mizusaki, Shell-model description of neutron-rich pf-shell nuclei with a new effective interaction GXPF1, Eur. Phys. J. A 25 (1) (2005) 499–502.
[18] S. Frauendorf, A.O. Macchiavelli, Overview of neutron–proton pairing, Prog. Part. Nucl. Phys. 78 (2014) 24–90.
[19] C. Qi, R. Wyss, N = Z nuclei: a laboratory for neutron–proton collective mode, Phys. Scr. 91 (1) (2016) 013009.
[20] M. Honma, T. Otsuka, B.A. Brown, T. Mizusaki, New effective interaction for pf-shell nuclei and its implications for the stability of the $N = Z = 28$ closed core, Phys. Rev. C 69 (2004) 034335.
[21] K. Kaneko, Y. Sun, G. de Angelis, Enhancement of high-spin collectivity in $N = Z$ nuclei by the isoscalar neutron–proton pairing, Nucl. Phys. A 957 (2017) 144–153.
[22] B. Cederwall, F.G. Moradi, T. Bäck, A. Johnson, J. Blomqvist, E. Clément, G. de France, R. Wadsworth, K. Andgren, K. Lagergren, A. Dijon, G. Jaworski, R. Liotta, C. Qi, B.M. Nyakó, J. Nyberg, M. Palacz, H. Al-Azri, A. Algora, G. de Angelis, A. Ataç, S. Bhattacharyya, T. Brock, J.R. Brown, P. Davies, A. Di Nitto, Z. Dombrádi, A. Gadea, J. Gál, B. Hadinia, F. Johnston-Theasby, P. Joshi, K. Juhász, R. Julin, A. Jungclaus, G. Kalinka, S.O. Kara, A. Khaplanov, J. Kownacki, G. La Rana, S.M. Lenzi, J. Molnár, R. Moro, D.R. Napoli, B.S.N. Singh, A. Persson, F. Recchia, M. Sandzelius, J.-N. Scheurer, G. Sletten, D. Sohler, P.-A. Söderström, M.J. Taylor, J. Timár, J.J. Valiente-Dobón, E. Vardaci, S. Williams, Evidence for a spin-aligned neutron–proton paired phase from the level structure of ^{92}Pd, Nature 469 (7328) (2011) 68–71.
[23] S. Ohkubo, Y. Hirabayashi, T. Sakuda, α-cluster structure of ^{44}Ti in core-excited α + ^{40}Ca model, Phys. Rev. C 57 (1998) 2760–2762.
[24] M. Kimura, H. Horiuchi, Coexistence of cluster structure and superdeformation in ^{44}Ti, Nucl. Phys. A 767 (2006) 58–80.
[25] J. Ljungvall, A. Görgen, M. Girod, J.-P. Delaroche, A. Dewald, C. Dossat, E. Farnea, W. Korten, B. Melon, R. Menegazzo, A. Obertelli, R. Orlandi, P. Petkov, T. Pissulla, S. Siem, R.P. Singh, J. Srebrny, C. Theisen, C.A. Ur, J.J. Valiente-Dobón, K.O. Zell, M. Zielińska, Shape coexistence in light Se isotopes: evidence for oblate shapes, Phys. Rev. Lett. 100 (2008) 102502.
[26] W. Rother, A. Dewald, H. Iwasaki, S.M. Lenzi, K. Starosta, D. Bazin, T. Baugher, B.A. Brown, H.L. Crawford, C. Fransen, A. Gade, T.N. Ginter, T. Glasmacher, G.F. Grinyer, M. Hackstein, G. Ilie, J. Jolie, S. McDaniel, D. Miller, P. Petkov, T. Pissulla, A. Ratkiewicz, C.A. Ur, P. Voss, K.A. Walsh, D. Weisshaar, K.-O. Zell, Enhanced quadrupole collectivity at $N = 40$: the case of neutron-rich Fe isotopes, Phys. Rev. Lett. 106 (2011) 022502.
[27] T. Braunroth, A. Dewald, H. Iwasaki, S.M. Lenzi, M. Albers, V.M. Bader, T. Baugher, T. Baumann, D. Bazin, J.S. Berryman, C. Fransen, A. Gade, T. Ginter, A. Gottardo, M. Hackstein, J. Jolie, A. Lemasson, J. Litzinger, S. Lunardi, T. Marchi, V. Modamio, C. Morse, D.R. Napoli, A. Nichols, F. Recchia, S.R. Stroberg, R. Wadsworth, D. Weisshaar, K. Whitmore, K. Wimmer, Reduced transition strengths of low-lying yrast states in chromium isotopes in the vicinity of $N = 40$, Phys. Rev. C 92 (2015) 034306.
[28] K. Kolos, D. Miller, R. Grzywacz, H. Iwasaki, M. Al-Shudifat, D. Bazin, C.R. Bingham, T. Braunroth, G. Cerizza, A. Gade, A. Lemasson, S.N. Liddick, M. Madurga, C. Morse, M. Portillo, M.M. Rajabali, F. Recchia, L.L. Riedinger, P. Voss, W.B. Walters, D. Weisshaar, K. Whitmore, K. Wimmer, J.A. Tostevin, Direct lifetime measurements of the excited states in ^{72}Ni, Phys. Rev. Lett. 116 (2016) 122502.
[29] A. Dewald, O. Möller, P. Petkov, Developing the recoil distance Doppler-shift technique towards a versatile tool for lifetime measurements of excited nuclear states, Prog. Part. Nucl. Phys. 67 (3) (2012) 786–839.
[30] F. Brandolini, S.M. Lenzi, D.R. Napoli, R.V. Ribas, H. Somacal, C.A. Ur, D. Bazzacco, J.A. Cameron, G. de Angelis, M.D. Poli, C. Fahlander, A. Gadea, S. Lunardi, G. Martínez-Pinedo, N.H. Medina, C.R. Alvarez, J. Sánchez-Solano, C.E. Svensson, Precise DSAM lifetime measurements in ^{48}Cr and ^{50}Cr as a test of large scale shell model calculations, Nucl. Phys. A 642 (3–4) (1998) 387–406.

[31] B.A. Brown, W.D.M. Rae, The Shell-model code NuShellX@MSU, Nucl. Data Sheets 120 (2014) 115–118.
[32] S.J.Q. Robinson, T. Hoang, L. Zamick, A. Escuderos, Y.Y. Sharon, Shell model calculations of $B(E2)$ values, static quadrupole moments, and g factors for a number of $N = Z$ nuclei, Phys. Rev. C 89 (2014) 014316.
[33] L. Zamick, Y.Y. Sharon, S.J.Q. Robinson, M. Harper, Consequences of omitting spin-orbit partner configurations for $B(E2)$ values and quadrupole moments in nuclei, Phys. Rev. C 91 (2015) 064321.
[34] E. Caurier, G. Martínez-Pinedo, F. Nowacki, A. Poves, A.P. Zuker, The shell model as a unified view of nuclear structure, Rev. Mod. Phys. 77 (2005) 427–488.
[35] L. Coraggio, A. Covello, A. Gargano, N. Itaco, T.T.S. Kuo, Effective shell-model Hamiltonians from realistic nucleon–nucleon potentials within a perturbative approach, Ann. Phys. 327 (9) (2012) 2125–2151.
[36] R. Machleidt, High-precision, charge-dependent Bonn nucleon–nucleon potential, Phys. Rev. C 63 (2001) 024001.
[37] S. Bogner, T.T.S. Kuo, L. Coraggio, A. Covello, N. Itaco, Low momentum nucleon–nucleon potential and shell model effective interactions, Phys. Rev. C 65 (2002) 051301.
[38] S. Raman, C.W. Nestor Jr., P. Tikkanen, Transition probability from the ground to the first-excited 2^+ state of even–even nuclides, At. Data Nucl. Data Tables 78 (1) (2001) 1–128.
[39] B.A. Brown, The nuclear shell model towards the drip lines, Prog. Part. Nucl. Phys. 47 (2) (2001) 517–599.
[40] K.L. Yurkewicz, D. Bazin, B.A. Brown, C.M. Campbell, J.A. Church, D.C. Dinca, A. Gade, T. Glasmacher, M. Honma, T. Mizusaki, W.F. Mueller, H. Olliver, T. Otsuka, L.A. Riley, J.R. Terry, Nuclear structure in the vicinity of $N = Z = 28$ ^{56}Ni, Phys. Rev. C 70 (2004) 054319.
[41] J. Chen, B. Singh, J.A. Cameron, Nuclear data sheets for $A = 44$, Nucl. Data Sheets 112 (9) (2011) 2357–2495.
[42] T.W. Burrows, Nuclear data sheets for $A = 48$, Nucl. Data Sheets 107 (7) (2006) 1747–1922.
[43] Y. Dong, H. Junde, Nuclear data sheets for $A = 52$, Nucl. Data Sheets 128 (2015) 185–314.

Publication II:
Lifetime measurements in ^{44}Ti

Lifetime measurements in ^{44}Ti

K. Arnswald,[1,*] P. Reiter,[1] A. Blazhev,[1] T. Braunroth,[1] A. Dewald,[1] M. Droste,[1] C. Fransen,[1] A. Goldkuhle,[1] R. Hetzenegger,[1] R. Hirsch,[1] E. Hoemann,[1] L. Kaya,[1] L. Lewandowski,[1] C. Müller-Gatermann,[1,†] P. Petkov,[2,1] D. Rosiak,[1] M. Seidlitz,[1] B. Siebeck,[1] A. Vogt,[1] D. Werner,[1] K. Wolf,[1] and K.-O. Zell[1]

[1]*Institut für Kernphysik, Universität zu Köln, 50937 Köln, Germany*

[2]*"Horia Hulubei" National Institute for Physics and Nuclear Engineering, R-76900 Bucharest-Măgurele, Romania*

(Received 24 July 2020; accepted 14 October 2020; published 2 November 2020)

Lifetimes of excited nuclear states were determined in ^{44}Ti using the recoil distance Doppler-shift technique and the Doppler-shift attenuation method. Results from the $K^\pi = 3^-$ band confirm isospin-symmetry breaking for the $3^-_1 \rightarrow 2^+_1$ $E1$ transition. The lifetime of the 4^-_1 state differs considerably from the previously known value. Good agreement is found for the 4^+_1 and 6^+_1 level lifetimes with respect to previous values. The experimental values are compared with large-scale shell-model calculations employing established interactions in the $0f1p$ shell, as well as a modern effective Hamiltonian including multiparticle multihole cross-shell configurations. Extended configuration spaces of this shell-model calculation allow for a detailed comparison with newly determined negative-parity states.

DOI: 10.1103/PhysRevC.102.054302

I. INTRODUCTION

The self-conjugated nucleus ^{44}Ti is a benchmark for present-day large-scale shell-model (LSSM) calculations in the full $0f1p$ shell northeast of the doubly magic nucleus ^{40}Ca. Several interactions such as the well-established FPD6 [1], KB3G [2], and GXPF1A [3] yield good agreement with various experimental observables, such as energy spectra or—with the inclusion of the Coulomb contributions—isospin-dependent effects like the mirror-energy differences (cf. Refs. [4–6]). However, for even-even nuclei these interactions are restricted to positive-parity states in the fp shell.

The latest calculations with the ZBM2M interaction [7] use the extended *hasp* model space [8] comprising the proton and neutron $1s_{1/2}$, $1d_{3/2}$, $0f_{7/2}$, $1p_{3/2}$ orbitals and surmount limitations of previous truncated schemes of the *sd* and fp main shells. They provide access to negative-parity states which—in the case of ^{44}Ti—cannot be calculated from the odd-parity fp orbitals. This interaction is based on the ZBM2 interaction [9] with adjustments of the $d_{3/2}$-$d_{3/2}$ monopole matrix elements. It demonstrated good agreement with experimental observations, i.e., excitation energies and charge radii, in ^{38}K and confirmed the relevance of cross-shell correlations in the vicinity of ^{40}Ca [7]. Moreover, results from the non-modified ZBM2 interaction reproduce well the experimentally observed energy spectra and reduced $E2$ strengths in stable Ca isotopes [9]. These results also include the even-even neighboring isotone ^{42}Ca and the $T_z = +2$ isobar ^{44}Ca of ^{44}Ti. However, the ZBM2M interaction was predominantly employed for calculations in the $Z \leqslant 20$ region [10–12]. Lifetime investigations in ^{44}Ti provide a fertile study ground for these calculations above the $Z = 20$ shell closure.

Recently, the first 2^+ level lifetimes in even-even $N = Z$ nuclei have been studied with an improved accuracy employing the Cologne coincidence-plunger setup [13]. The authors of this article report an increased $B(E2; 2^+_1 \rightarrow 0^+_{\text{g.s.}}) = 205^{+20}_{-17}\ e^2\,\text{fm}^4$ value in ^{44}Ti compared with previous measurements. Moreover, this result was not in agreement with values from shell-model interactions of the fp model space. This discrepancy was explained by multi-particle-hole (ph) cross-shell configurations in the vicinity of the $Z = 20$ shell closure.

The nuclear level lifetimes from higher-lying positive-parity states in ^{44}Ti are known from pioneering studies performed in the 1970s with limited precision [14–19]. Lifetimes of negative-parity states were studied by Kolata *et al.*, who determined a lifetime of $\tau = 3.9(13)$ ps for the 4^-_1 state [20]. From later lifetime and angular distribution measurements, performed by Dixon *et al.* [18], a lower lifetime limit of $\tau > 50$ ps was proposed for this state based on spin and parity arguments contradicting the lifetime value from Ref. [20]. The only evaluated lifetime exists for the negative-parity 3^-_1 bandhead [21] and it refers to a preliminary lifetime analysis from a conference proceeding in 2011 [22]. In this study a $B(E3; 3^-_1 \rightarrow 0^+_{\text{g.s.}}) \approx 3$ W.u. value is presented which corresponds to a lifetime of ≈31 ps including an adopted branching ratio of $I(3^-_1 \rightarrow 0^+_{\text{g.s.}})/I(3^-_1 \rightarrow 2^+_1) = 2.0(3)\%$ [21].

High-spin states in ^{44}Ti were investigated by O'Leary *et al.*, who observed rotational-like energy-level spacings between states placed upon the first-excited 0^+ state [23]. The energy levels were well reproduced by *df* shell-model calculations. These calculations use the positive-parity $d_{3/2}$ and negative-parity $f_{7/2}$ orbitals and allow for the derivation of the negative-parity band built upon the 3^-_1 state.

*konrad.arnswald@ikp.uni-koeln.de

†Present address: Physics Division, Argonne National Laboratory, 9700 South Cass Avenue, Lemont, Illinois 60439, USA.

On the theoretical side, ^{44}Ti is of importance for the investigation of α-cluster structures. These correlations are considerably distorted due to the strong effect of the spin-orbit force in the fp shell. Recent studies confirmed the applicability of the ^{40}Ca $+\alpha$ model (cf. Ref. [24]). Moreover, coexistence phenomena of the mean-field structure and α structures were investigated by the use of deformed-basis antisymmetrized molecular dynamics (AMD) exploiting the Gogny D1S force [25]. The authors verified the $\beta_2 = 0.25$ normally deformed $K^\pi = 3^-$ band with a dominant $1p1h$ intrinsic configuration. Detailed $B(E2)$ values from these approaches are available for positive-parity states [24,25].

The scarce and contradictory lifetime information of negative-parity states in ^{44}Ti together with recent theoretical advances of LSSM calculations motivates a refined study of lifetimes and reduced transition strengths in this nucleus. In this article, we report and discuss new results on lifetimes and reduced transition strengths in ^{44}Ti. This paper is organized as follows: the experimental setup is described in Sec. II, the data analysis and results are presented in Sec. III. A detailed comparison with results from shell-model calculations and systematics is reported in Sec. IV. The article closes with a summary and conclusions in Sec. V.

II. EXPERIMENTS

The lifetime experiments on ^{44}Ti were performed at the FN tandem accelerator at the Institute for Nuclear Physics, University of Cologne, Germany, using the setup of the Cologne coincidence plunger [26]. Excited states were populated by ^{40}Ca(^{6}Li, pn)^{44}Ti fusion-evaporation reactions at 20 MeV beam energy. The plunger target was made of 0.2 mg/cm^2 enriched ^{40}Ca evaporated on a 2 mg/cm^2 gold backing facing the beam. In addition, the target was sandwiched by a 0.1-mg/cm^2-thin gold layer which was evaporated onto the other side to reduce oxidation effects. Recoiling nuclei which left the target with a mean velocity of 0.81(5)% of the speed of light—which corresponds to $v = 2.43(15)$ μm/ps—were finally stopped in a 3.6-mg/cm^2-thick gold stopper. During the experiment, data were collected at seven target-to-stopper distances between 46 and 626 μm. Emitted γ rays were detected by twelve high-purity germanium (HPGe) detectors with relative efficiencies between 55% and 80% placed in three rings at polar angles of 0° (one detector), 45° (six detectors), and 142.3° (five detectors) with respect to the beam axis. Pileup and additional dead time were significantly reduced by 2-mm-thick sheets of lead and copper which were placed between target and end cap to shield the detectors from low-energy x-rays. In total, 10^{10} coincident γ-ray events were processed and recorded utilizing a synchronized 80-MHz XIA® Digital Gamma Finder (DGF) data-acquisition system and stored to disk. The data were sorted into γ-γ matrices employing the SOCO-V2 sort code [27] and analyzed utilizing the TV [28] software package.

Subsequently to the RDDS measurements, a DSAM run was performed employing a 0.2 mg/cm^2 enriched ^{40}Ca target which was centrally evaporated onto a 2 mg/cm^2 gold backing using a 2-mm aperture. To reduce oxidation effects of the target material, the ^{40}Ca layer was subsequently covered completely by a 0.5-mg/cm^2-thin gold fronting. The DSAM experiment was performed under similar experimental conditions with respect to the previous RDDS run. In total, 3.6×10^9 γ-γ events were recorded and stored to disk.

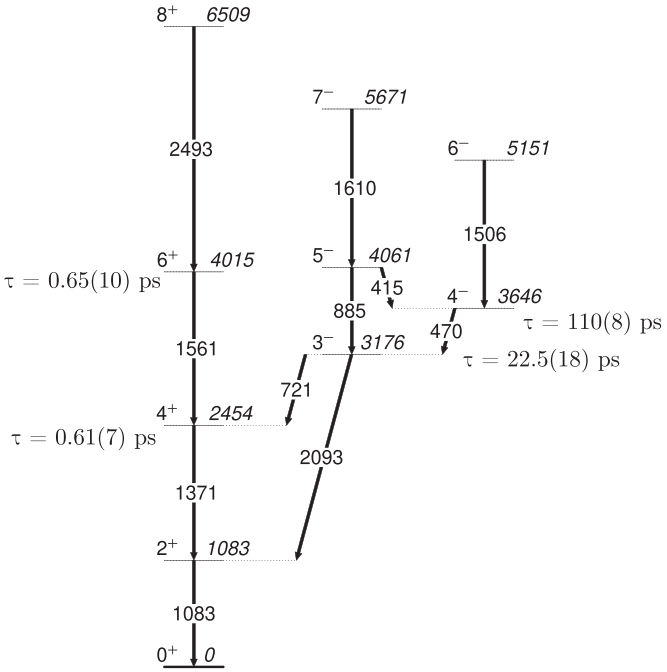

FIG. 1. Partial level scheme of ^{44}Ti. Dominant decay branches observed in both experiments as well as obtained level lifetimes are shown. All energies are given in keV.

III. DATA ANALYSIS AND RESULTS

The observed level scheme of populated excited states and measured lifetimes in ^{44}Ti is displayed in Fig. 1. The lifetime results, obtained in both experiments, are summarized in Table I.

A. Recoil distance Doppler shift

The lifetime analysis of the 3^-_1 and 4^-_1 states in ^{44}Ti is based on the recoil distance Doppler-shift (RDDS) technique and the differential decay-curve method (DDCM) [26,29]. The analysis was performed in the γ-γ coincidence mode using gates on completely shifted parts of directly feeding

TABLE I. Experimental lifetimes in ^{44}Ti from the present experiment are compared with previous experimental values. For each state the applied method and gating energies are summarized.

		Lifetime (ps)			E_γ (keV)	
E_x (keV)	J^π	Present	Literature	Method	Gate	Analyzed
1083	2^+		2.7(2) [13]			
2454	4^+	0.61(7)	0.60(11) [15]	DSAM	1561	1371
4015	6^+	0.65(10)	0.56(8) [18]	DSAM	2493	1561
3176	3^-	22.5(18)	≈31 [21,22]	RDDS	885	2093
3646	4^-	110(8)	3.9(13)[a] [20]	RDDS	1506	470

[a]Contradicts $\tau > 50$ ps as proposed in Ref. [18].

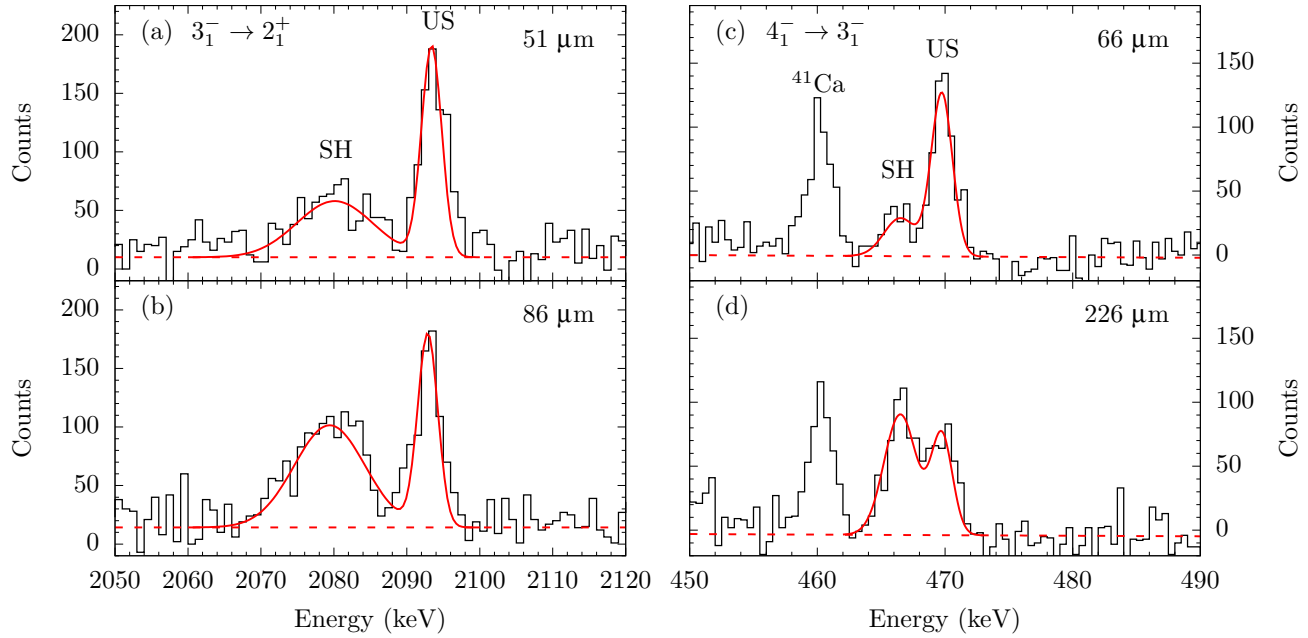

FIG. 2. Exemplary γ-ray energy spectra for the (a), (b) $3_1^- \rightarrow 2_1^+$ transition at 2093 keV and the (c), (d) $4_1^- \rightarrow 3_1^-$ transition at 470 keV for two different target-to-stopper distances. Spectra are produced by a gate on the shifted part of the direct feeders at 885 and 1506 keV, respectively. Unshifted (US) and shifted (SH) components as well as a contamination of ^{41}Ca to the $4_1^- \rightarrow 3_1^-$ transition are labeled. The Gaussian fits to the experimental spectra are given in a red solid lines, and the background is marked as dashed red (see text for details).

transitions from above. Lifetimes of the states of interest were subsequently determined from the peak volumes of shifted (SH) and unshifted (US) components of the depopulating transition. Exemplary gated γ-ray spectra are presented in Fig. 2 for the $3_1^- \rightarrow 2_1^+$ [Figs. 2(a) and 2(b)] and $4_1^- \rightarrow 3_1^-$ [Figs. 2(c) and 2(d)] transitions. Both spectra are shown for shorter target-to-stopper distances [Figs. 2(a) and 2(c)] and are compared with larger ones [Figs. 2(b) and 2(d)]. The peak volumes are determined via Gaussian fits. For consistency purposes, position and peak width of the unshifted component are assumed constant. Further details on RDDS analyses are contained in Ref. [26].

For each target-to-stopper distance x_i in the sensitive range, one lifetime τ_i is determined. The mean lifetime τ is determined from the weighted mean of all τ_i. γ-ray spectra from different detector-ring combinations are statistically independent and the final lifetime is determined from the weighted mean of the τ of each detector-ring combination. The statistical error is dominated by the variance of the single τ_i. The systematic uncertainties result from three main contributions. First, the error of the mean velocity. The mean velocity is deduced from the Doppler-shift of the 2093 keV transition at forward and backward angles. The uncertainty of the mean polar angle $\Delta\theta = 3^\circ$ results in a $\Delta\beta = 0.05\%$ systematic uncertainty of the velocity distribution. Second, the relative target-to-stopper distances were measured with a high precision of $\Delta x \leqslant 0.5\%$ relative to the absolute distances. Finally, contaminating transitions in general can have an impact on the experimental lifetime results but could be excluded by carefully selected narrow energy gates. The uncertainty of the final lifetime is deduced from the Gaussian error propagation.

The analysis of the 3_1^- and 4_1^- lifetimes is performed with the RDDS code NAPATAU [30]. In the case of the 3_1^- state, a gate was set on the shifted component of the direct-feeding $5_1^- \rightarrow 3_1^-$ transition at 885 keV. The lifetime is deduced from the unshifted and shifted intensities (I_{US} and I_{SH}) of the depopulating $3_1^- \rightarrow 2_1^+$ transition at 2093 keV displayed in Figs. 3(b) and 3(c). For the four distances in the sensitive range, lifetimes were obtained [see Fig. 3(a)] from second-order polynomial-fit functions to the experimental intensities of the Doppler-shifted components I_{SH}. The τ curve for the unshifted intensities is the derivative of this function with the proportionality constant $v \cdot \tau$. Both the fit function to I_{SH} as well as the τ curve for I_{US} are simultaneously χ^2 minimized to the experimental values. From both curves a lifetime τ_i is determined at each distance. The weighted mean lifetime from all distances in the sensitive range is determined from forward and backward angles for the 3_1^- state, yielding $\tau = 21.8(10)_{\mathrm{stat.}}(16)_{\mathrm{sys.}}$ ps and $\tau = 23.4(11)_{\mathrm{stat.}}(16)_{\mathrm{sys.}}$ ps, respectively. The weighted mean of both lifetimes amounts to $\tau(3_1^-) = 22.5(7)_{\mathrm{stat.}}(16)_{\mathrm{sys.}}$ ps.

Likewise, the lifetime of the 4_1^- state is determined via a gate on the shifted component of the direct-feeding $6_1^- \rightarrow 4_1^-$ transition at 1506 keV. Subsequently, unshifted and shifted intensities of the $4_1^- \rightarrow 3_1^-$ transition at 470 keV are analyzed [see Figs. 3(e) and 3(f)] for five distances in the sensitive range. The mean lifetime is obtained from the single τ_i in Fig. 3(d) and yields $\tau = 108(3)_{\mathrm{stat.}}(8)_{\mathrm{sys.}}$ ps and $\tau = 113(4)_{\mathrm{stat.}}(8)_{\mathrm{sys.}}$ ps from forward and backward angles, respectively. The weighted mean is $\tau(4_1^-) = 110(3)_{\mathrm{stat.}}(8)_{\mathrm{sys.}}$ ps. Exemplary τ curves of the 3_1^- and 4_1^- states are presented in Fig. 3.

B. Doppler-shift attenuation method

The Doppler-shift attenuation method (DSAM) was applied for the analysis of the short-lived 4_1^+ and 6_1^+ states. The

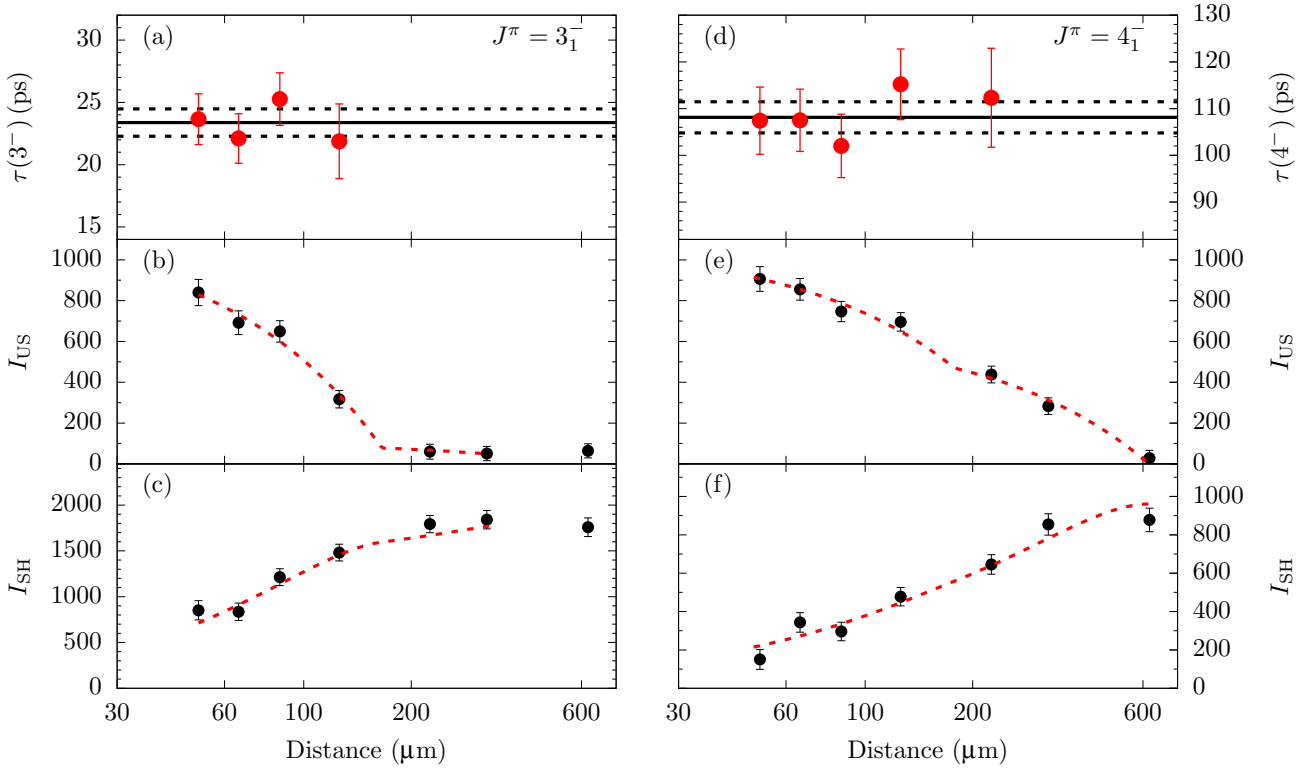

FIG. 3. Exemplary τ curves of the (a) 3_1^- state and (d) 4_1^- state at backward and forward angles, respectively. The weighted mean value is marked with a black solid line, the black dashed line indicates the statistical uncertainty. The respective (b), (e) unshifted and (c), (f) shifted intensities are presented with the corresponding polynomial-fit functions (dashed red curves). Lifetimes and γ-ray intensities are plotted against the offset-corrected relative target-to-stopper distances. Note the logarithmic distance scale.

slowing-down process of the nuclei of interest in the target and stopper material is described via Monte Carlo simulations performed by a modified version of the DESASTOP computer code [31,32]. The Monte Carlo simulations include the reaction kinematics, target and stopper properties, as well as the detector setup including finite opening angles. The electronic stopping powers for ^{44}Ti are obtained from Ref. [33]. For the contribution of the nuclear stopping, the LSS description [34] is considered as well as the parametrization of the universal scattering function for a Thomas-Fermi potential [35]. Microchanneling effects in the stopping medium are taken into account and are corrected for by a reduction factor of $f_n = 0.7$ (cf. Refs. [36–38] for further details).

In general, lifetime information can be obtained from the correlation of the slowing-down process of the recoiling nuclei of interest and the decay pattern of the studied nuclear states if both processes happen on the same timescales [39]. For the data analysis the differential decay-curve method was applied by using γ-γ gates on the directly feeding transition [40,41]. An energy gate onto any purely shifted part of the feeding transition generates a γ-ray spectrum of the depopulating transition which afterwards will be analyzed. The lineshape of this spectrum is a convolution of the Doppler-shifted energy spectrum (i.e., the energy spectrum projected on the recoil velocities corresponding to the energy gate) and the detector-response function. The lifetime analysis is based on a lineshape simulation which is compared with the experimental spectra. The simulation includes (i) the γ-ray energies of the unshifted feeding and depopulating transitions, (ii) the detector-response function, (iii) the time dependence of the velocity projections of the Doppler-shifted energies onto the observation angle of the detector setup, and (iv) the time-dependence of the population scheme of the level of interest. Further details on DSAM analyses are given in Refs. [40,41].

The lifetimes of the 4_1^+ and 6_1^+ states are analyzed by employing gates on the shifted component of the $6_1^+ \rightarrow 4_1^+$ and $8_1^+ \rightarrow 6_1^+$ feeding transitions, respectively. The resulting γ-ray spectra with the corresponding simulated lineshapes for the $4_1^+ \rightarrow 2_1^+$ and $6_1^+ \rightarrow 4_1^+$ transitions are presented in Figs. 4(a) and 4(b), respectively. Obviously, as both spectra show similar amounts of Doppler-shifted components with respect to the unshifted peak, the analyzed lifetimes cannot differ considerably. While the γ-γ statistics of the $4_1^+ \rightarrow 2_1^+$ transition amounts to 1500 counts in a single ring-ring combination, it diminishes to 400 counts for the elusive $6_1^+ \rightarrow 4_1^+$ transition. Nevertheless, the background level is reduced to $<$10 counts. Similar to the RDDS analysis, the generated γ-ray spectra are analyzed separately for forward and backward angles. The obtained lifetimes of the 6_1^+ state is determined from forward and backward angles, yielding $\tau = 0.64(12)$ ps and $\tau = 0.69(18)$ ps, respectively. The weighted mean of both values amounts to $\tau(6_1^+) = 0.65(10)$ ps. In the lifetime analysis of the 4_1^+ state this lifetime was included to the feeding scheme. The obtained lifetime of the 4_1^+ state is $\tau = 0.69(11)$ ps and $\tau = 0.56(9)$ ps for forward and backward angles,

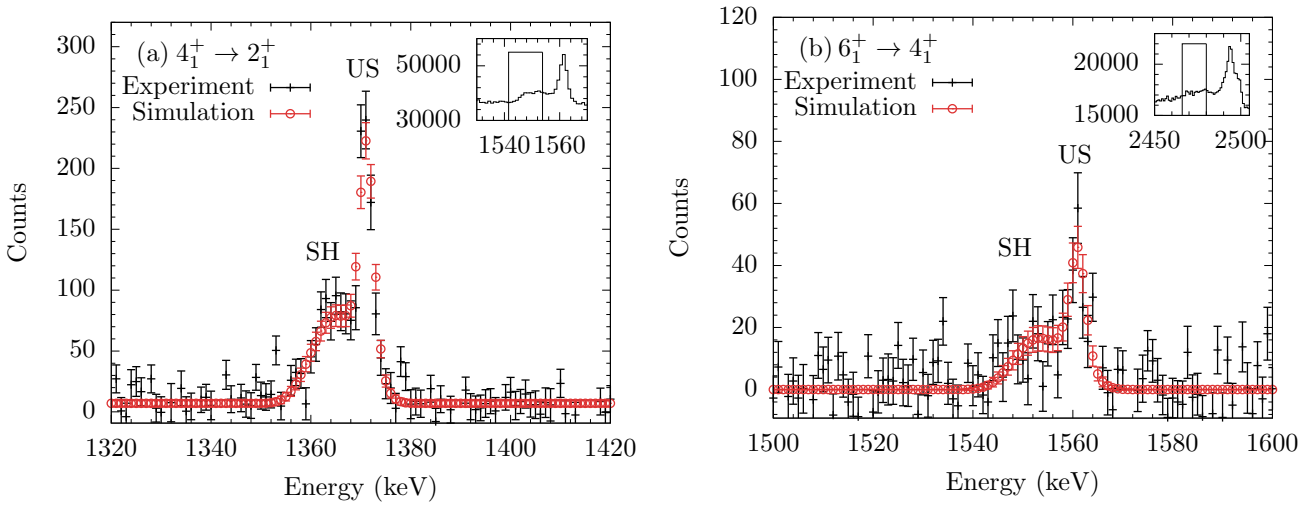

FIG. 4. γ-ray spectrum of the (a) $4_1^+ \rightarrow 2_1^+$ transition with a γ-energy gate on the purely shifted part of the $6_1^+ \rightarrow 4_1^+$ transition at 1541–1553 keV at backward angles. Similar data for the (b) $6_1^+ \rightarrow 4_1^+$ transition gated on the $8_1^+ \rightarrow 6_1^+$ transition at 2466–2480 keV. The γ-energy gates onto the direct feeding transitions are shown in the insets. The experimental data are shown as black crosses. The simulated lineshapes are given in open red circles.

respectively. The weighted mean yields $\tau(4_1^+) = 0.61(7)$ ps. The experimental uncertainties are dominated by the statistical errors which yield 90 and 40 fs for the 6_1^+ and 4_1^+ states, respectively. Systematic errors occur from the uncertainty of the slowing-down process, which is distributed over the uncertainties of the electronic and nuclear stopping powers and to the target width. These errors were conservatively estimated to not exceed 10% (cf. Ref. [41]) and are included in the final uncertainties.

IV. DISCUSSION

The measured lifetimes were converted to $B(\sigma\lambda)$ values and are compared with previous experimental data (see Table II). Furthermore, results for $B(\sigma\lambda)$ values from shell-model calculations were obtained and confronted with the new experimental findings. Comparisons are drawn along the ground-state band of ^{44}Ti up to the 12_1^+ state. The results are presented in Fig. 5.

The newly determined lifetimes of the 4_1^+ and 6_1^+ states correspond to $B(E2; 4_1^+ \rightarrow 2_1^+) = 276^{+36}_{-28}\ e^2\,\mathrm{fm}^4$ and $B(E2; 6_1^+ \rightarrow 4_1^+) = 135^{+25}_{-18}\ e^2\,\mathrm{fm}^4$, respectively. Both values are in a good agreement with previous measurements from the 1970s. The experimental uncertainty for the 4_1^+ lifetime was improved by 7%. The 3_1^- state decays via a 2093-keV $E1$ transition to the 2_1^+ state. The lifetime corresponds to $B(E1; 3_1^- \rightarrow 2_1^+) = 3.0^{+0.3}_{-0.2} \times 10^{-6}\ e^2\,\mathrm{fm}^2$ and is in a fair agreement with the preliminary results from Ref. [22]. The

TABLE II. Experimental reduced transition strengths of ^{44}Ti from the present experiment are compared with previous experimental values. The results on reduced transition strengths and excitation energies from Ref. [21] are compared with four different shell-model calculations with $e_\pi = 1.5e$, $e_\nu = 0.5e$. See text for details.

	E_i (keV)					$B(\sigma\lambda)$ (W.u.)					
	Experiment	Theory				Experiment		Theory			
$J_i^\pi \xrightarrow{\sigma\lambda} J_f^\pi$	Literature	GXPF1A	KB3G	FPD6	ZBM2M	Present	Previous	GXPF1A	KB3G	FPD6	ZBM2M
$2_1^+ \xrightarrow{E2} 0_{\mathrm{g.s.}}^+$	1083	1287	1300	1300	1096		$22.0^{+1.8}_{-1.5}$ [13]	11.4	12.9	15.2	24.5
$4_1^+ \xrightarrow{E2} 2_1^+$	2454	2381	2430	2498	2696	30^{+4}_{-3}	30^{+7}_{-5} [15]	14.8	17.0	20.6	35.4
$6_1^+ \xrightarrow{E2} 4_1^+$	4015	3113	3317	3776	4511	15^{+3}_{-2}	17^{+3}_{-2} [18]	11.6	14.2	17.4	22.5
$8_1^+ \xrightarrow{E2} 6_1^+$	6509	5210	5589	6248	6081		>1.3[a][17]	7.8	10.1	12.1	23.2
$10_1^+ \xrightarrow{E2} 8_1^+$	7671	6368	6868	7614	7292		16^{+4}_{-2}[a] [17]	10.0	11.3	11.8	3.7
$12_1^+ \xrightarrow{E2} 10_1^+$	8040	6776	7484	8312	7723		$4.4^{+1.1}_{-0.7}$ [19]	5.9	6.6	6.8	4.1
$3_1^- \xrightarrow{E1} 2_1^+$	3176				3544	$3.7(3) \times 10^{-6}$	$\approx 2.7 \times 10^{-6}$ [22]				0
$4_1^- \xrightarrow{E2} 3_1^-$[b]	3646				2844	32^{+3}_{-2}	1000^{+500}_{-200} [20]				0.3
$4_1^- \xrightarrow{M1} 3_1^-$[b]						$1.4^{+0.7}_{-0.4} \times 10^{-4}$	$4^{+3}_{-2} \times 10^{-3}$ [20]				1.7×10^{-6}

[a] $B(E2)$ value assumes 100% branching.
[b] With $|\delta| = 4.2(8)$ [42].

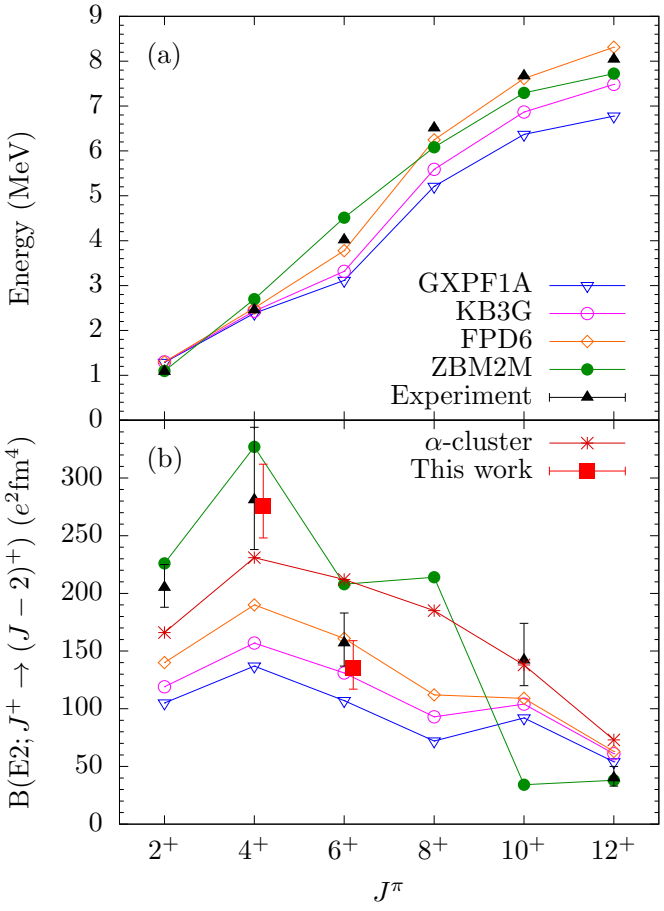

FIG. 5. (a) Experimental and theoretical excitation energies and (b) $B(E2)$ values of the ground-state band in ^{44}Ti. $B(E2)$ values from this work are given by red squares. Previously adopted experimental transition strengths (black filled triangles) are taken from the corresponding lifetimes given in Refs. [13,15,17–19]. Shell-model calculations employing the GXPF1A (blue open triangles), KB3G (purple open circles), FPD6 (orange open diamonds), and ZBM2M (green filled circles) interactions are shown. $B(E2)$ values are compared with results from an α-cluster model (dark red stars) taken from Ref. [24].

4_1^- state is depopulated via a mixed $E2$-$M1$ transition. The lifetime converts into $B(E2; 4_1^- \rightarrow 3_1^-) = 290(20)\ e^2\,\mathrm{fm}^4$ and $B(M1; 4_1^- \rightarrow 3_1^-) = 2.6^{+1.3}_{-0.7} \times 10^{-4}\ \mu_N^2$. The applied mixing ratio is given in Ref. [42] and yields $\delta = 4.2(8)$. The obtained result differs considerably from the value given in Ref. [20]. However, a larger lifetime was already indicated by Dixon *et al.* [18] and fits the present observations.

For the theoretical description of the excitation energies and the $B(E2)$ values of the ground-state band, shell-model calculations were performed employing the *K*-SHELL code [43,44] as well as the code NUSHELLX@MSU [45]. The fp model space comprises the $0f_{7/2}$, $1p_{3/2}$, $1p_{1/2}$, and $0f_{5/2}$ orbitals coupled to a ^{40}Ca core. Three interactions were employed for comparison with the present experimental data: FPD6 [1], KB3G [2], and GXPF1A [3]. Moreover, the ZBM2M shell-model interaction [7] was employed for the calculation of negative-parity states and to investigate the impact of cross-shell correlations in ^{44}Ti. This interaction uses the extended *hasp* model space comprising the proton and neutron $1s_{1/2}$, $1d_{3/2}$, $0f_{7/2}$, $1p_{3/2}$ orbitals coupled to a ^{28}Si core. For nuclei in the region of the *sd* and fp shells, reduced proton charges of $e_\pi = 1.15e$ to $1.31e$ provided reasonable results along $N = Z$ [46,47]. However, standard effective charges $e_\pi = 1.5e$ and $e_\nu = 0.5e$ are used for all shell-model calculations in order to approach the impact of core excitations in ^{44}Ti. For the derivation of $B(M1)$ strengths, effective spin g-factors with $g^s_{\mathrm{effective}} = 0.7 g^s_{\mathrm{free}}$ (i.e., $g^s_\pi = 3.91$ and $g^s_\nu = -2.678$) were used, which is justified because the spin-orbit partners are not present in the model space. Furthermore, these values exactly reproduce the experimental g-factors of the 2_1^+ reference state [48]. The shell-model results are summarized in Table II and displayed in Fig. 5.

As observed in Fig. 5(a), the four shell-model interactions reproduce the trend of the excitation energies of the ground-state band in ^{44}Ti quite well. Nevertheless, there are some deviations which have significant impact on the evolution of the $B(E2)$ values discussed hereinafter. The excitation energy of the 2_1^+ state is in very good agreement with the result from the ZBM2M interaction but is overestimated by the other three interactions by approximately 200 keV. The 4_1^+ state excitation energy is well reproduced by the three fp shell interactions and is overestimated by the ZBM2M interaction by $\approx$250 keV. The energy of the 6_1^+ state is still overestimated by the ZBM2M interaction while being underpredicted by the other three interactions. Thenceforward, the ZBM2M, GXPF1A, and KB3G interactions underestimate the evolution of the 8_1^+, 10_1^+, and 12_1^+ excitation energy, whereas the FPD6 interaction is in fair agreement with the experimental observations. In addition, the ZBM2M interaction opens the possibility to calculate excitation energies from negative-parity states. The energy of the 3_1^- state yields 3544 keV compared with the experimental value of 3176 keV. However, the excitation energy of the 4_1^- state is not reproduced (2844 keV compared with 3646 keV), moving the 4_1^- state below the 3_1^- bandhead.

The derived $B(E2)$ values exhibit a very different evolution along the yrast band for the GXPF1A, KB3G, and FPD6 interactions on the one hand and the ZBM2M interaction on the other hand [see Fig. 5(b)]. The three fp-shell interactions show a very similar evolution along the ground-state band. As already discussed in Ref. [13], the theoretical description of the first-excited 2^+ state underestimates the experimental result. This behavior continues for the 4_1^+ state. The theoretical results match the experimental results first for the $6_1^+ \rightarrow 4_1^+$ transition where the $B(E2)$ nearly halves. Thenceforward, all three interactions are in good agreement with the experimental observations. The ^{40}Ca core excitations have predominantly low-spin configurations which, therefore, influence most the wave functions of the low-spin states. Even by the use of standard effective charges, the fp shell interactions do not match the experimental values. For the $2_1^+ \rightarrow 0^+_{\mathrm{g.s.}}$ and $4_1^+ \rightarrow 2_1^+$ transitions only the new ZBM2M interaction with the extended *hasp* model space provides a good description. This is due to the account of particle-hole excitations for the low-spin states. Their amount is deduced from the wave functions and it yields more than 88% of core-excited configurations for the states up to 6_1^+. The higher-lying states are predominantly of

$f_{7/2}$ character manifested by a general decrease in collectivity. This is differently modeled by the ZBM2M calculation. Clear deviations between the different theoretical approaches are observed for the 8_1^+ and 10_1^+ states. The ZBM2M interaction overestimates the values of the other interactions for the 8_1^+ state, whereas experimental and theoretical values for the 10_1^+ state are considerably underestimated. The 12_1^+ isomer is in good agreement with the shell-model result. The ZBM2M interaction is competitive for the description of low-spin yrast states in ^{44}Ti although its predictive power decreases with higher spins.

The experimental $B(E2)$ values from the ground-state band are furthermore compared with theoretical values from the α-cluster model reported by Ohkubo *et al.* [24]. The group uses an α-like excitation of a ^{40}Ca core employing density-dependent M3Y (DDM3Y) double folding potentials without any effective charges. $B(E2)$ values extracted from this model are displayed in Fig. 5(b). They show a trend similar to the ZBM2M values although they evolve smoother along the ground-state band. This model reproduces the enhanced collectivity for the 2_1^+ and 4_1^+ states well and is in perfect agreement with the $B(E2)$ value of the 10_1^+ state. Similar to the ZBM2M calculation, the $B(E2)$ value from the 6_1^+ state is overestimated by the α-cluster model. Overall, the evolution of the ground-state band transition strengths are reproduced quite well by this model. This also supports the argument of the importance of an excited ^{40}Ca core for an adequate description of transition strengths from low-energy states in ^{44}Ti.

Transition strengths from negative-parity states were calculated with the ZBM2M interaction. However, the calculated $B(E1; 3_1^- \rightarrow 2_1^+)$ value is equal to zero. At first glance, the shell model supports the exceptionally low $B(E1) = 3.7(3) \times 10^{-6}$ W.u. value. The finite experimental value can be explained by isospin-symmetry breaking as both states—the 3_1^- and 2_1^+—are calculated to have isospin $T = 0$. Due to the isovector character of the $E1$ transition operator, the shell model yields $B(E1) = 0$. This slow $E1$ transition in ^{44}Ti exhibits a drop in collectivity with respect to the isotopic and isotonic neighbors ^{46}Ti and ^{42}Ca of two to three orders of magnitude. Even for the $T_z = +2$ isospin partner ^{44}Ca the $B(E1; 3_1^- \rightarrow 2_1^+)$ value amounts to $2.5(12) \times 10^{-4}$ W.u. [21]. The calculated $M1$ and $E2$ reduced transition strengths of the $4_1^- \rightarrow 3_1^-$ transition underpredict the experimental values by two orders of magnitude (see Table II). The shell-model calculations support a dominating $E2$ character of the $4_1^- \rightarrow 3_1^-$ transition. The interaction yields a multipole-mixing ratio of 6.3 and is comparable with the experimentally determined $|\delta| = 4.2(8)$ [42].

To give a more detailed interpretation of the lifetime of the 4_1^- state, the decomposition of the total wave function configuration into its proton and neutron components was calculated for selected states with the ZBM2M interaction. The decomposition matrix is symmetric due to the self-conjugated nature of ^{44}Ti. The 4_1^- state can be predominantly decomposed into $4^- \otimes 0^+$ (22%), $4^- \otimes 2^+$ (28%), and $5^- \otimes 2^+$ (15%) coupled proton or neutron configurations. While the 0^+ and 2^+ configurations are of $2p2h$ (24%) and $4p4h$ (16%) character, the configurations coupled to 4^- and 5^- are predominantly of $3p3h$ character: $d_{3/2}^{-1}s_{1/2}^{-2}f_{7/2}^{5}$ (30%), $d_{3/2}^{-2}s_{1/2}^{-1}f_{7/2}^{5}$ (9%), and $d_{3/2}^{-1}s_{1/2}^{-2}p_{3/2}^{1}f_{7/2}^{4}$ (5%). Major components of the 3_1^- state originate from $3^- \otimes 0^+$ (31%), $2^- \otimes 2^+$ (22%), and $5^- \otimes 2^+$ (13%) nucleon couplings. Similar to the 4^- state, the positive-parity configurations are $2p2h$ (23%) and $4p4h$ (4%) excitations plus an additional amount of $0p0h$ (12%) configurations. In contrast with the 4_1^- state, the negative-parity configurations of the 3_1^- are dominated by $1p1h$ (28%) (19% $s_{1/2}^{-1}f_{7/2}^{3}$ and 9% $d_{3/2}^{-1}f_{7/2}^{3}$) nucleon configurations. The $3p3h$ configurations $d_{3/2}^{-2}s_{1/2}^{-1}f_{7/2}^{5}$ (12%) and $d_{3/2}^{-1}s_{1/2}^{-2}f_{7/2}^{5}$ (2%) are calculated to an amount of 14%.

As the $E2$ and $M1$ one-body transition operators in the shell-model calculation can only connect configurations differing by maximum $1p1h$ excitation, the transition $4_1^- \rightarrow 3_1^-$ is limited to $3p3h$ configurations and is predominantly of $d_{3/2} \leftrightarrow s_{1/2}$ character. This explains the small transition strength calculated by the ZBM2M interaction, especially as the spin-orbit partners are not available in the given model space, the $B(M1)$ strength is hindered. Therefore, calculations in the full $sdpf$ model space are needed for a refined theoretical description of the $4_1^- \rightarrow 3_1^-$ transition.

V. CONCLUSIONS

In summary, lifetimes of negative and positive-parity states in the $N = Z$ nucleus ^{44}Ti were measured with the RDDS technique and the DSA method. The present results for the 4_1^+ and 6_1^+ states yield good agreement with previous measurements. Deviations were found for the 3_1^- and 4_1^- states. In the case of the 3_1^- state, only preliminary values are available in the literature. The higher lifetime of the 4_1^- state has been predicted by Dixon *et al.* [18]. The comparison with shell-model calculations yield ambiguous conclusions. The ZBM2M interaction reproduces the 2_1^+ and 4_1^+ transition probabilities well but falls short for higher spins. The GXPF1A, KB3G, and FPD6 interaction are in good agreement with the $B(E2; 6_1^+ \rightarrow 4_1^+)$ value and reproduce the trend up to the 12^+ isomer. $B(E2)$ values from the ground-state band were well reproduced by results from the $\alpha + ^{40}\mathrm{Ca}(I^\pi)$ model reported in Ref. [24]. Reduced transition strengths from the negative-parity band in ^{44}Ti were compared with shell-model results for the first time. The finite experimental value of $B(E1; 3_1^- \rightarrow 2_1^+) = 3.7(3) \times 10^{-6}$ W.u. indicates isospin-symmetry breaking and remains challenging to be reproduced within the shell model. The derived transition strengths of the $4_1^- \rightarrow 3_1^-$ transition show the same trend to a higher lifetime but even underestimate the present $B(\sigma\lambda)$ values. For the 8_1^+ state only an upper lifetime limit of $\tau < 0.7$ ps is available in literature. Precise lifetime measurements of this state can close the gap within the yrast band towards the 12^+ isomer and will help to solve the puzzle of the different shell-model descriptions. On the theory side, full $sdpf$ shell-model calculations are needed to properly discuss the $B(M1)$ strength of the $4_1^- \rightarrow 3_1^-$ transition.

ACKNOWLEDGMENTS

We acknowledge fruitful discussions with N. Shimizu. We thank the IKP FN Tandem accelerator team for the professional support during the experiment.

[1] W. A. Richter, M. G. Van Der Merwe, R. E. Julies, and B. A. Brown, New effective interactions for the $0f1p$ shell, Nucl. Phys. A **523**, 325 (1991).

[2] A. Poves, J. Sánchez-Solano, E. Caurier, and F. Nowacki, Shell model study of the isobaric chains $A = 50$, $A = 51$ and $A = 52$, Nucl. Phys. A **694**, 157 (2001).

[3] M. Honma, T. Otsuka, B. A. Brown, and T. Mizusaki, Shell-model description of neutron-rich pf-shell nuclei with a new effective interaction GXPF1, Eur. Phys. J. A **25**, 499 (2005).

[4] S. M. Lenzi and M. A. Bentley, Test of Isospin Symmetry-isospin symmetry Along the $N = Z$ Line, in *The Euroschool Lectures on Physics with Exotic Beams, Vol. III*, edited by J. S. Al-Khalili and E. Roeckl (Springer, Berlin, Heidelberg, 2009), Vol. 764, pp. 57–98.

[5] F. Brandolini, S. M. Lenzi, D. R. Napoli, R. V. Ribas, H. Somacal, C. A. Ur, D. Bazzacco, J. A. Cameron, G. de Angelis, M. De Poli, C. Fahlander, A. Gadea, S. Lunardi, G. Martínez-Pinedo, N. H. Medina, C. Rossi Alvarez, J. Sánchez-Solano, and C. E. Svensson, Precise DSAM lifetime measurements in ^{48}Cr and ^{50}Cr as a test of large scale shell model calculations, Nucl. Phys. A **642**, 387 (1998).

[6] M. A. Bentley, S. J. Williams, D. T. Joss, C. D. O'Leary, A. M. Bruce, J. A. Cameron, M. P. Carpenter, P. Fallon, L. Frankland, W. Gelletly, C. J. Lister, G. Martínez-Pinedo, A. Poves, P. H. Regan, P. Reiter, B. Rubio, J. Sanchez Solano, D. Seweryniak, C. E. Svensson, S. M. Vincent, and D. D. Warner, Mirror symmetry at high spin in ^{51}Fe and ^{51}Mn, Phys. Rev. C **62**, 051303(R) (2000).

[7] M. L. Bissell, J. Papuga, H. Naïdja, K. Kreim, K. Blaum, M. De Rydt, R. F. Garcia Ruiz, H. Heylen, M. Kowalska, R. Neugart, G. Neyens, W. Nörtershäuser, F. Nowacki, M. M. Rajabali, R. Sanchez, K. Sieja, and D. T. Yordanov, Proton-Neutron Pairing Correlations in the Self-Conjugate Nucleus ^{38}K Probed via a Direct Measurement of the Isomer Shift, Phys. Rev. Lett. **113**, 052502 (2014).

[8] H. Hasper, Large scale shell-model calculations in the upper part of the *sd* shell: General description and energy levels for $A = 36$–39, Phys. Rev. C **19**, 1482 (1979).

[9] E. Caurier, K. Langanke, G. Martínez-Pinedo, F. Nowacki, and P. Vogel, Shell model description of isotope shifts in calcium, Phys. Lett. B **522**, 240 (2001).

[10] R. F. Garcia Ruiz, M. L. Bissell, K. Blaum, A. Ekström, N. Frömmgen, G. Hagen, M. Hammen, K. Hebeler, J. D. Holt, G. R. Jansen, M. Kowalska, K. Kreim, W. Nazarewicz, R. Neugart, G. Neyens, W. Nörtershäuser, T. Papenbrock, J. Papuga, A. Schwenk, J. Simonis, K. A. Wendt, and D. T. Yordanov, Unexpectedly large charge radii of neutron-rich calcium isotopes, Nat. Phys. **12**, 594 (2016).

[11] D. M. Rossi, K. Minamisono, H. B. Asberry, G. Bollen, B. A. Brown, K. Cooper, B. Isherwood, P. F. Mantica, A. Miller, D. J. Morrissey, R. Ringle, J. A. Rodriguez, C. A. Ryder, A. Smith, R. Strum, and C. Sumithrarachchi, Charge radii of neutron-deficient ^{36}K and ^{37}K, Phys. Rev. C **92**, 014305 (2015).

[12] J. Kostensalo, J. Suhonen, and K. Zuber, Shell-model computed cross sections for charged-current scattering of astrophysical neutrinos off ^{40}Ar, Phys. Rev. C **97**, 034309 (2018).

[13] K. Arnswald, T. Braunroth, M. Seidlitz, L. Coraggio, P. Reiter, B. Birkenbach, A. Blazhev, A. Dewald, C. Fransen, B. Fu, A. Gargano, H. Hess, R. Hirsch, N. Itaco, S. M. Lenzi, L. Lewandowski, J. Litzinger, C. Müller-Gatermann, M. Queiser, D. Rosiak, D. Schneiders, B. Siebeck, T. Steinbach, A. Vogt, K. Wolf, and K. O. Zell, Enhanced collectivity along the $N = Z$ line: Lifetime measurements in ^{44}Ti, ^{48}Cr, and ^{52}Fe, Phys. Lett. B **772**, 599 (2017).

[14] R. B. Huber, W. Kutschera, C. Signorini, and P. Blasi, Gamma transitions in ^{44}Ti and ^{48}Cr from heavy ion induced reactions, J. Phys. Colloques **32**, C6–207 (1971).

[15] W. R. Dixon, R. S. Storey, and J. J. Simpson, Lifetimes of ^{44}Ti levels, Nucl. Phys. A **202**, 579 (1973).

[16] J. J. Simpson, W. R. Dixon, and R. S. Storey, Evidence for Rotational Bands in ^{44}Ti, Phys. Rev. Lett. **31**, 946 (1973).

[17] J. J. Simpson, W. Dünnweber, J. P. Wurm, P. W. Green, J. A. Kuehner, W. R. Dixon, and R. S. Storey, Yrast levels in ^{44}Ti, Phys. Rev. C **12**, 468 (1975).

[18] W. R. Dixon, R. S. Storey, and J. J. Simpson, Levels of ^{44}Ti from the ^{40}Ca$(\alpha, \gamma)^{44}$Ti reaction, Phys. Rev. C **15**, 1896 (1977).

[19] J. Britz, A. Chevallier, J. Chevallier, and B. Haas, Lifetime of the 8040 keV state in ^{44}Ti, Nucl. Phys. A **262**, 189 (1976).

[20] J. J. Kolata, J. W. Olness, and E. K. Warburton, High-spin states in ^{44}Ti and ^{44}Sc, Phys. Rev. C **10**, 1663 (1974).

[21] Evaluated Nuclear Structure Data File (ENSDF), (2020), http://www.nndc.bnl.gov/ensdf.

[22] C. Michelagnoli, C. A. Ur, E. Farnea, S. M. Lenzi, S. Lunardi, F. Recchia, N. Marginean, D. Bucurescu, G. Cata-Danil, D. Delenau, D. Filipescu, D. Ghita, T. Glodariu, R. Marginean, C. Mihai, A. Negret, S. Pascu, T. Sava, L. Stroe, and G. Suliman, Lifetime measurement in $N = Z$ nucleus ^{44}Ti, Acta Phys. Pol., B **42**, 825 (2011).

[23] C. D. O'Leary, M. A. Bentley, B. A. Brown, D. E. Appelbe, R. A. Bark, D. M. Cullen, S. Ertürk, A. Maj, and A. C. Merchant, Nonyrast high-spin states in $N = Z$ ^{44}Ti, Phys. Rev. C **61**, 064314 (2000).

[24] S. Ohkubo, Y. Hirabayashi, and T. Sakuda, α-cluster structure of ^{44}Ti in core-excited $\alpha + ^{40}$Ca model, Phys. Rev. C **57**, 2760 (1998).

[25] M. Kimura and H. Horiuchi, Coexistence of cluster structure and superdeformation in ^{44} Ti, Nucl. Phys. A **767**, 58 (2006).

[26] A. Dewald, O. Möller, and P. Petkov, Developing the recoil distance Doppler-shift technique towards a versatile tool for lifetime measurements of excited nuclear states, Prog. Part. Nucl. Phys. **67**, 786 (2012).

[27] N. Saed-Samii, Ph.D. thesis, Universität zu Köln, 2013 (unpublished).

[28] J. Theuerkauf, S. Esser, S. Krink, M. Luig, N. Nicolay, O. Stuch, and H. Wolters, Program TV, Institute for Nuclear Physics, Cologne, Germany.

[29] A. Dewald, S. Harissopulos, and P. von Brentano, The differential plunger and the differential decay curve method for the analysis of recoil distance Doppler-shift data, Z. Phys. A **334**, 163 (1989).

[30] B. Saha, Bestimmung der Lebensdauern kollektiver Kernanregungen in 124-Xe und Entwicklung von entsprechender Analysesoftware, Ph.D. thesis, Universität zu Köln, 2004, https://kups.ub.uni-koeln.de/1246/.

[31] G. Winter, The application of lineshape analysis in plunger measurements, Nucl. Instrum. Methods Phys. Res. **214**, 537 (1983).

[32] G. Winter, ZfK Rossendorf Report ZfK-497 (1983).

[33] L. C. Northcliffe and R. F. Schilling, Range and stopping-power tables for heavy ions, At. Data Nucl. Data Tables **7**, 233 (1970).

[34] J. Lindhard, M. Scharff, and H. E. Schiøtt, Kgl. Dan. Vid. Selsk. Mat. Fys. Medd. **33**, 14 (1963).
[35] W. M. Currie, A Monte Carlo programme for Doppler shift analysis, Nucl. Instrum. Methods **73**, 173 (1969).
[36] J. Keinonen, Use of capture reactions to measure short lifetimes by the DSA method, AIP Conf. Proc. **125**, 557 (1985).
[37] J. F. Ziegler and J. P. Biersack, The Stopping and Range of Ions in Matter, in *Treatise on Heavy-Ion Science: Volume 6: Astrophysics, Chemistry, and Condensed Matter*, edited by D. A. Bromley (Springer US, Boston,1985), pp. 93–129.
[38] J. Keinonen, Reliability of short lifetimes measured by the Doppler shift attenuation method, AIP Conf. Proc. **238**, 383 (1991).
[39] T. K. Alexander and J. S. Forster, Lifetime Measurements of Excited Nuclear Levels by Doppler-Shift Methods, in *Advances in Nuclear Physics: Volume 10*, edited by M. Baranger and E. Vogt (Springer US, Boston,1978), pp. 197–331.
[40] P. Petkov, D. Tonev, J. Gableske, A. Dewald, and P. von Brentano, Lifetime analysis using the Doppler-shift attenuation method with a gate on feeding transition, Nucl. Instrum. Methods Phys. Res., Sect. A **437**, 274 (1999).
[41] P. Petkov, C. Müller-Gatermann, D. Werner, A. Dewald, A. Blazhev, C. Fransen, J. Jolie, S. Ohkubo, and K. O. Zell, New lifetime measurements for the lowest quadrupole states in ^{20,22}Ne and possible explanations of the high collectivity of the depopulating $E2$ transitions, Phys. Rev. C **100**, 024312 (2019).
[42] W. R. Dixon, R. S. Storey, and J. J. Simpson, Spins of the 3176 and 3646 keV levels of ^{44}Ti, Nucl. Phys. A **363**, 173 (1981).
[43] Noritaka Shimizu, Nuclear shell-model code for massive parallel computation, KSHELL, arXiv:1310.5431.
[44] N. Shimizu, T. Mizusaki, Y. Utsuno, and Y. Tsunoda, Thick-restart block Lanczos method for large-scale shell-model calculations, Comput. Phys. Commun. **244**, 372 (2019).
[45] B. A. Brown and W. D. M. Rae, The shell-model code NuShellX@MSU, Nucl. Data Sheets **120**, 115 (2014).
[46] R. du Rietz, J. Ekman, D. Rudolph, C. Fahlander, A. Dewald, O. Möller, B. Saha, M. Axiotis, M. A. Bentley, C. Chandler, G. de Angelis, F. Della Vedova, A. Gadea, G. Hammond, S. M. Lenzi, N. Mărginean, D. R. Napoli, M. Nespolo, C. Rusu, and D. Tonev, Effective Charges in the fp Shell, Phys. Rev. Lett. **93**, 222501 (2004).
[47] M. Dufour and A. P. Zuker, Realistic collective nuclear Hamiltonian, Phys. Rev. C **54**, 1641 (1996).
[48] S. Schielke, K.-H. Speidel, O. Kenn, J. Leske, N. Gemein, M. Offer, Y. Y. Sharon, L. Zamick, J. Gerber, and P. Maier-Komor, First measurement and shell model interpretation of the g factor of the 2_1^+ state in self-conjugate radioactive ^{44}Ti, Phys. Lett. B **567**, 153 (2003).

Publication III:

Enhanced quadrupole collectivity in doubly-magic ^{56}Ni: Lifetime measurements of the 4_1^+ and 6_1^+ states

Physics Letters B 820 (2021) 136592

Contents lists available at ScienceDirect

Physics Letters B

www.elsevier.com/locate/physletb

Enhanced quadrupole collectivity in doubly-magic ^{56}Ni: Lifetime measurements of the 4_1^+ and 6_1^+ states

K. Arnswald [a,*], A. Blazhev [a], F. Nowacki [b], P. Petkov [c,a], P. Reiter [a], T. Braunroth [a], A. Dewald [a], M. Droste [a], C. Fransen [a], R. Hirsch [a], V. Karayonchev [a], L. Kaya [a], L. Lewandowski [a], C. Müller-Gatermann [a,1], M. Seidlitz [a], B. Siebeck [a], A. Vogt [a], D. Werner [a], K.O. Zell [a]

[a] Institut für Kernphysik, Universität zu Köln, Zülpicher Straße 77, D-50937 Köln, Germany
[b] Université de Strasbourg, CNRS, IPHC UMR 7178, F-67000 Strasbourg, France
[c] "Horia Hulubei" National Institute for Physics and Nuclear Engineering, R-76900 Bucharest-Măgurele, Romania

ARTICLE INFO

Article history:
Received 21 May 2021
Received in revised form 16 July 2021
Accepted 17 August 2021
Available online 19 August 2021
Editor: B. Blank

Keywords:
Doubly-magic nuclei
$N = Z$ nuclei
Lifetime measurements
DSAM
B(E2) values

ABSTRACT

Lifetime measurements of excited states in doubly-magic ^{56}Ni have been performed exploiting the Doppler-shift attenuation method in order to determine reduced transition probabilities. For the 4_1^+ and 6_1^+ states, the deduced B(E2) values are compared with results from shell-model calculations employing the GXPF1A and the modern PFSDG-U interactions. In addition, valence ab-initio calculations were performed using a novel realistic Hamiltonian derived from chiral perturbation theory including three-body potential contributions and are confronted with the experimental findings. The new results show maximum E2 strength in comparison with known values along the $N = 28$ chain of isotones. The results corroborate the high collectivity for the double shell closure at $N = Z = 28$ which was anticipated from the large $B(\mathrm{E2}; 2_1^+ \rightarrow 0^+_{\mathrm{g.s.}})$ value despite the considerable increase of its excitation energy as compared to neighboring semi-magic nuclei. Based on similarities in the shell structures of the self-conjugate doubly-magic nuclei ^{56}Ni and ^{100}Sn, the new values could be an indication for an expected comparable collective behavior of the 6_1^+ state in ^{100}Sn.

1. Introduction

Doubly-magic atomic nuclei act as cornerstones for the description of nuclear structure. They provide access to basic properties such as excitation energies and nuclear transition rates as signatures for very pure shell-model configurations outside an inert core [1–4]. The $N = Z$ nucleus ^{56}Ni with the magic numbers $N = Z = 28$ plays a special role for the development of the nuclear shell model. The introduction of a strong spin-orbit interaction by Goeppert-Mayer and Jensen et al. facilitated the magic number 28, while the magic numbers 2, 8, and 20 are also present without spin-orbit coupling [5,6]. Within the pf shell, comprising the $1f_{7/2}$, $2p_{3/2}$, $2p_{1/2}$, and $1f_{5/2}$ proton and neutron orbitals, the spin-orbit splitting of the $f_{7/2}$ orbital from the other three orbits creates an energy gap at $N, Z = 28$. However, ^{56}Ni as a doubly-magic nucleus within the pf major shells is also the first doubly magic $N = Z$ nucleus that is not stable and this feature has hampered studies of the properties of nuclear levels relevant to the $N = Z = 28$ shell gaps.

Although ^{56}Ni is only two neutrons away from its stable neighboring isotope ^{58}Ni, previous studies on excited states in this nucleus required highest experimental efforts. High-spin states in ^{56}Ni were investigated by Rudolph et al. [7] who used a 143 MeV ^{36}Ar beam impinging on a ^{28}Si target provided by the 88-Inch Cyclotron at the Lawrence Berkeley National Laboratory. The 2α exit channel after fusion-evaporation reaction was selected by employing the 4π CsI ball Microball [8]. Subsequent γ rays from excited states were measured with the Gammasphere array comprising 82 Ge crystals [9]. The 2_1^+ lifetime was directly obtained from a pioneering experiment using the Doppler-shift attenuation method in 1973 by Schulz et al. [10]. The transition probability to the first excited state was determined by Coulomb-excitation measurements at intermediate energies by Kraus et al. [11] and Yurkewicz et al. [12] using a ^{56}Ni radioactive beam.

* Corresponding author.
E-mail address: konrad.arnswald@ikp.uni-koeln.de (K. Arnswald).
[1] Present address: Physics Division, Argonne National Laboratory, 9700 South Cass Avenue, Lemont, Illinois 60439, USA.

https://doi.org/10.1016/j.physletb.2021.136592

Both nuclear properties, the excitation energy of the 2_1^+ state and the transition strength to the ground state, are key signatures for shell closures. Unlike other doubly magic nuclei such as ^{40}Ca with $N = Z = 20$, in ^{56}Ni both values show contradictory behavior for the $N = Z = 28$ shell gap. While the excitation energy shows a considerable increase at $N, Z = 28$, the shell gap does not result in a particularly small B(E2) value for the lowest 2^+ state [12]. This can be understood in relation with the nature of the shell-closure: in Harmonic Oscillator (HO) shell closures such as ^{40}Ca, quadrupole excitations of the ground state do not connect to the first low-lying 2^+ states (usually of many particle-hole nature) whereas in spin-orbit shell-closures, such as in ^{56}Ni or ^{100}Sn, the first excited 2^+ state is a direct quadrupole excitation of the doubly-magic core, resulting in an enhanced B(E2) value. Such evolution of gaps have been studied in detail through spin-tensor analysis [13] and evolve mainly due to the central component of the monopole nuclear interaction. This has been interpreted as a relative *softness* of the shell closure at ^{56}Ni [14,15]. The Kumar quadrupole invariants also point to large quadrupole fluctuations resulting in a relatively non-defined spherical shape [16].

For the *pf* shell, shell-model interactions are available which well describe the features of corresponding nuclei [17–19]. These interactions are usually based on renormalized realistic nucleon-nucleon potentials with phenomenological corrections. These corrections are believed to take into account (in an ad-hoc manner) the missing three-body contributions [20]. In addition, nowadays, explicit 2N and 2N+3N interactions built on chiral perturbation theory potentials are also available and can be challenged for an ab-initio description of nuclear structure properties [21].

Nuclear structure studies in ^{56}Ni provide guidance for the description of the self-conjugate doubly-magic nucleus ^{100}Sn [22–24]. Several analogies between both nuclei exist and they have their origin in similar single-particle energies (SPE) and single-hole energies (SHE) [25]. Therefore, a concurrent description of ^{56}Ni and ^{100}Sn is sought by theory and investigations were performed e.g. by Nowacki who compared theoretical 2_1^+ excitation energies and B(E2) values of both nuclei [26]. Furthermore, a detailed comparison between both nuclei was given by Faestermann et al. who elaborate on the systematics of $E(2_1^+)$, $B(\mathrm{E2}; 2_1^+ \rightarrow 0^+_{\mathrm{g.s.}})$, and on the similarities of the theoretical description [27].

The collectivity of excited states in $N = Z$ nuclei is subject of most recent investigations [28–31]. For the even-even nuclei $^{44}_{22}$Ti, $^{48}_{24}$Cr, and $^{52}_{26}$Fe within the $1f_{7/2}$ orbital, enhanced E2 strengths were obtained with respect to the relevant isotope chain systematics [29]. These studies predominantly focus on the first excited 2^+ state. Along the $N = Z$ line ^{56}Ni is located between the even-even nuclei $^{52}_{26}$Fe and $^{60}_{30}$Zn. While for ^{52}Fe B(E2) values from higher-lying states are available (cf. Ref. [32]), for ^{60}Zn no lifetime values from excited states are known. In ^{56}Ni, the $B(\mathrm{E2}; 2_1^+ \rightarrow 0^+_{\mathrm{g.s.}})$ value is only known with a sizeable uncertainty [33]. In spite of considerable experimental effort, no valid lifetime values were available for higher lying yrast states like the 4_1^+ and 6_1^+ states in this nucleus. These values are needed to answer the question whether the collective behavior is restricted to the 2_1^+ state and how it evolves along the yrast line. Therefore, a measurement was performed to determine the reduced transition strengths of these states in the $N = Z$ doubly-magic system. Nuclear level lifetimes were studied employing the Doppler-shift attenuation method in a stable ion-beam experiment, which allows for high accuracy by exploitation of $\gamma\gamma$-correlation gated spectra reducing the background.

This paper is organized as follows: the experimental details and the results of the data analysis are described in the first two sections. A detailed comparison with results from modern shell-model calculations is presented in the following section before the paper closes with a summary and conclusions.

2. Experiment

The lifetime experiment on ^{56}Ni was performed at the FN tandem accelerator at the Institute for Nuclear Physics, University of Cologne, Germany, using the setup of the Cologne coincidence plunger [34]. Excited states were populated by ^{27}Al(^{32}S, 2np)^{56}Ni fusion-evaporation reactions at 78 MeV beam energy. The target was made of 0.5-mg/cm^2 aluminum evaporated on a 2.8-mg/cm^2 natural magnesium backing. Emitted γ rays were detected by twelve high-purity germanium (HPGe) detectors with relative efficiencies between 55% and 80% placed in three rings at polar angles of 0° (one detector), 45° (six detectors), and 142.3° (five detectors) with respect to the beam axis. Pile up and additional dead time caused by low-energy X rays were significantly reduced by detector shields consisting of 2-mm thick sheets of lead and copper which were placed between target and HPGe detector end cap. Coincident γ-ray events were processed and recorded utilizing synchronized 80-MHz XIA® Digital Gamma Finder (DGF) data-acquisition system and stored to disk. The data were sorted into $\gamma - \gamma$ matrices employing the soco-v2 sort code [35] and analyzed utilizing the TV [36] software package. In total 11×10^9 $\gamma - \gamma$ events were recorded.

3. Analysis and results

The Doppler-shift attenuation method (DSAM) was applied for the lifetime analysis of the 4_1^+ and 6_1^+ states. For the description of the slowing-down process of the nuclei of interest in the target and stopper material, Monte Carlo simulations were performed by a modified version [37] of the DESASTOP computer code [38,39]. These Monte Carlo simulations describe the slowing-down process of the recoiling nuclei by taking into account the reaction kinematics, as well as target and stopper properties and the detector setup including finite opening angles. The electronic stopping powers for ^{56}Ni are obtained from Ref. [40]. For the contribution of the nuclear stopping the J. Lindhard, M. Scharff, H.E. Schiøtt (LSS) description [41] is considered as well as the parametrization of the universal scattering function for a Thomas-Fermi potential [42]. Microchanneling effects in the stopping medium are taken into account and are corrected for by a reduction factor of $f_n = 0.7$ (cf. Refs. [43–45] for further details).

In general, lifetime information can be obtained from the correlation of the decay pattern of the studied nuclear states and the slowing-down process of the recoiling nuclei of interest if both processes are happening at the same time scales [46]. Due to the small cross section of the elusive reaction channel, which leads to low statistics in γ-gated spectra, the lifetime analysis is performed in singles mode with γ gates applied to the complete Doppler-broadened lineshape of the $2_1^+ \rightarrow 0^+_{\mathrm{g.s.}}$ transition at 2701 keV to select the higher lying states of interest, to clean up the spectrum, and to reduce the background. γ-ray spectra from the lifetime analyses of the 4_1^+ and 6_1^+ states are shown in Fig. 1. The γ-ray lineshapes in these quasi-singles spectra are a convolution of the Doppler-shifted energy spectrum (corresponding to the velocity projections on a given observation axis) and the detector response function. The lifetime analysis is based on a numerical lineshape simulation, the calculated lineshape is compared iteratively with the experimental spectra. The line shape simulation takes into account: (i) the γ-ray energies of the unshifted feeding and depopulating transitions, (ii) the level lifetimes of feeding states, (iii) the detector-response function, (iv) the time dependence of the velocity projections of the Doppler-shifted energies onto the observation angle of the detector setup, and (v) the time dependence of the population scheme of the level of interest. Further details on the DSAM analysis are given in Refs. [31,47].

Table 1
Experimental excitation energies and reduced transition strengths of ^{56}Ni from the present experiment are compared with previous experimental values taken from Refs. [10–12]. The results are compared with four different shell-model calculations. Effective charges $e_\pi = 1.12\,e$, $e_\nu = 0.67\,e$ were used. See text for details.

J_i^π	E [keV]					B(E2; $J_i^\pi \to (J-2)_i^\pi$) [e^2 fm^4]					
	Exp.[a]	Theory				Experiment		Theory			
		GXPF1A	2N	2N+3N	PFSDG-U	Present	Previous	GXPF1A	2N	2N+3N	PFSDG-U
2_1^+	2701	2597	977	2567	2964	-	74^{+24}_{-48}[a]	130	270	132	150
4_1^+	3924	3687	1887	3567	4701	128^{+24}_{-18}	< 296[b]	124	504	132	107
6_1^+	5316	5289	3139	5286	5658	59^{+10}_{-7}	-	87	533	119	69

[a] From Ref. [33].
[b] From Ref. [10].

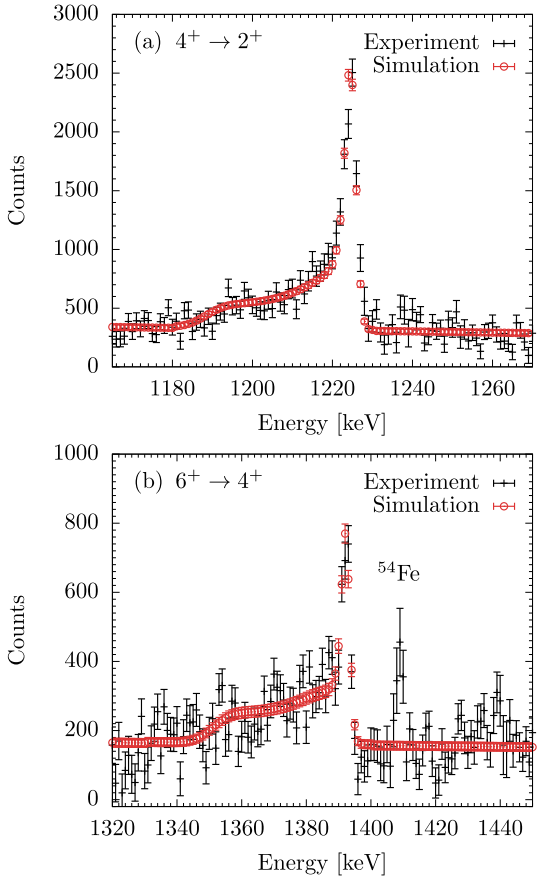

Fig. 1. Exemplary γ-ray spectrum of the (a) $4_1^+ \to 2_1^+$ transition of ^{56}Ni observed at polar angles of 142.3° with respect to the direction of beam. Similar data for the (b) $6_1^+ \to 4_1^+$ transition. Both spectra are obtained by applying a γ-energy gate on the complete $2_1^+ \to 0_{g.s.}^+$ transition to reduce the background. Experimental data are shown as black horizontal bars. The simulated line shapes are given in open red circles. A contaminating ^{54}Fe transition is marked (see text for details).

The 6_1^+ lifetime is obtained from a χ^2 minimization of the differences between the simulated lineshape and the experimental spectrum of the $6_1^+ \to 4_1^+$ transition in an energy range from 1331 keV to 1400 keV. The final result is shown in Fig. 1(b). The direct feeding $8_1^+ \to 6_1^+$ transition is observed with very weak intensity in the experimental spectrum. The feeding contribution from the 8_1^+ state is taken into account as contribution to the experimental lifetime uncertainty. Since no lifetime value is known for the 8^+ state, its upper limit is conservatively estimated to $\Delta\tau_{\text{feeder}} = 150$ fs as for the large transition energy of 2638 keV a short lifetime can be expected (in comparison: the 2^+ state lifetime amounts to 76 fs [33] with a similar transition energy of 2701 keV). Apart from the $8_1^+ \to 6_1^+$ transition, no further feeding transitions for the 4_1^+ and 6_1^+ states are observed in the experimental spectra. In the γ-ray spectrum shown in Fig. 1(b) the $2_1^+ \to 0_{g.s.}^+$ transition from ^{54}Fe is observed at 1408 keV as a small contamination. This transition can be traced back to random coincidences of this strong evaporation channel. However, the lifetime analysis of the 6_1^+ state in ^{56}Ni is not affected by this transition which has no contaminating lineshape. For the analysis of the 6_1^+ level lifetime, γ-ray spectra from two different detector-ring combinations (i.e. 45° and 142.3° spectra with γ-energy gates on 142.3°) are analyzed which are statistically independent. The final lifetime $\tau(6_1^+) = 2.66(38)$ ps is determined from the weighted mean of both values.

Likewise, the level lifetime of the 4_1^+ state was determined (cf. Fig. 1(a)). The considered feeding includes the lifetime and initial population of the 6_1^+ level. The final lifetime is determined from two detector-ring combinations (i.e. 142.3° spectra with γ-energy gates on 45° and 142.3°) and yields $\tau(4_1^+) = 2.31(37)$ ps. The statistical uncertainties are 300 fs and 100 fs for the 6_1^+ and 4_1^+ states, respectively. Systematic errors arise partly from the uncertainties of the slowing-down process which originates from the uncertainties of the electronic and nuclear stopping powers and from the target thickness. These errors were conservatively estimated to not exceed 10% (cf. Ref. [31]). Additional systematic errors of $\Delta\tau_{\text{feeder}} = 150$ fs and $\Delta\tau_{\text{feeder}} = 120$ fs stem from the effective feeding lifetimes for the 6_1^+ and 4_1^+ states, respectively. In the case of the 4_1^+ state, the initial population of the feeding 6_1^+ state is also taken into account. For each detector-ring combination, the uncertainty is determined from a variation of the different error sources within their given error margins. From these varied simulations, lifetimes τ_i were obtained which mark the range of the uncertainty distribution. From the sum over all $\Delta\tau_i = |\tau - \tau_i|$, the total uncertainty for a single detector-ring combination is obtained. The final uncertainty of each lifetime is determined from the error of the weighted mean of two detector-ring combinations.

4. Discussion

The newly measured lifetimes for the 4_1^+ and 6_1^+ states are converted into B(E2) values. The reduced transition strengths yield $B(\text{E2}; 6_1^+ \to 4_1^+) = 59^{+10}_{-7}$ e^2 fm^4 and $B(\text{E2}; 4_1^+ \to 2_1^+) = 128^{+24}_{-18}$ e^2 fm^4 (see Table 1 and Fig. 2). The latter result is in agreement with the experimental estimate of < 296 e^2 fm^4 corresponding to the lower lifetime limit of > 1 ps in Ref. [10]. Fig. 2 shows the excitation energies of the (e) 2_1^+, (c) 4_1^+, and (a) 6_1^+ states and the B(E2) values of the (f) $2_1^+ \to 0_{g.s.}^+$, (d) $4_1^+ \to 2_1^+$, and (b) $6_1^+ \to 4_1^+$ transitions for the $N = 28$ isotones between the doubly-magic nucleus ^{48}Ca and ^{58}Zn, two protons above ^{56}Ni. A comparison of the new B(E2) values shows an enhancement and highest values along the $N = 28$ even-even isotonic chain within the experimental uncertainties.

Theoretical results from shell-model calculations are obtained and confronted with the new experimental findings (see Table 1). For the theoretical description of the excitation energies and the

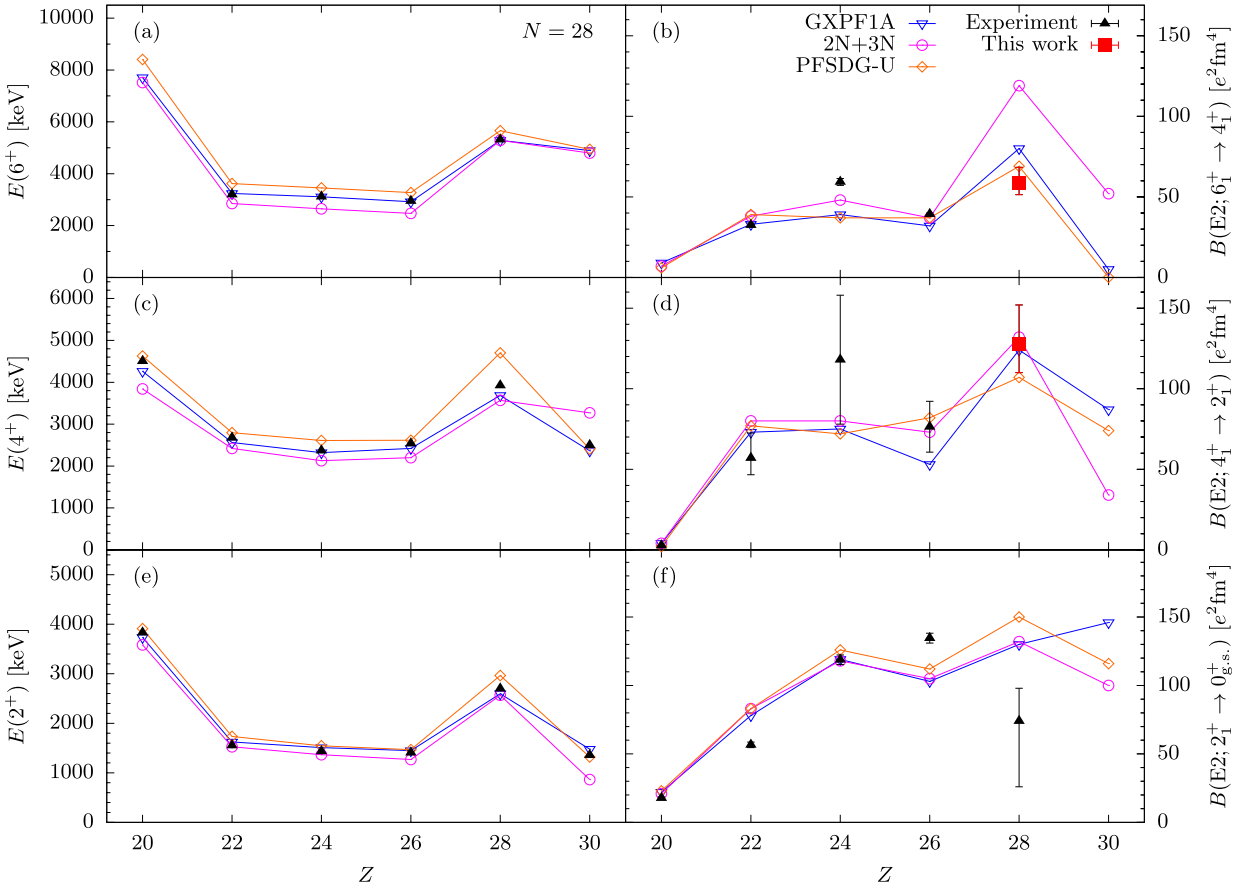

Fig. 2. Experimental and theoretical excitation energies (a, c, e) and B(E2) values (b, d, f) of the 2_1^+ (e, f), 4_1^+ (c, d), and 6_1^+ (a, b) states in $N = 28$ isotones. B(E2) values from this work are given in red squares. The previously adopted experimental values (black triangles) are taken from Refs. [33,48]. Moreover, shell-model calculations employing the GXPF1A (blue open triangles), 2N+3N (purple open circles), and PFSDG-U (orange open diamonds) interactions are shown using the effective charges $e_\pi = 1.12\,e$ and $e_\nu = 0.67\,e$. See text for details.

B(E2) values of the ground-state band, shell-model calculations were performed employing the KSHELL [49] and ANTOINE [50,51] codes. The model space comprises the $1f_{7/2}$, $2p_{3/2}$, $2p_{1/2}$, and $1f_{5/2}$ proton and neutron orbitals, coupled to a ^{40}Ca core. For comparison with the present experimental data: we use the standard pf effective interaction GXPF1A [17] as well as the novel PFSDG-U interaction using only its pf orbitals for both protons and neutrons [18,19]. This latter interaction is a monopole constrained realistic interaction in the spirit of the older KB3G [52]. In addition, for sake of completeness, valence ab-initio calculations were performed using the recently derived Hamiltonians from chiral perturbation theory, with (2N+3N) and without (2N) three-body potential contributions [21]. In all cases, the effective charges $e_\pi = 1.12\,e$ and $e_\nu = 0.67\,e$ were used for protons and neutrons, respectively. These charges reproduce the $27/2^- \to 23/2^-$ transition strengths in the ^{51}Fe and ^{51}Mn mirror partners [53] and provided a good description of B(E2) values in Ni isotopes [54].

An inspection of Table 1 shows that the 2N interaction has problems in describing the energy spectrum of the lowest yrast states in ^{56}Ni as well as clearly overestimates the experimental B(E2) values. These issues are improved by adding 3N forces [21]. The main difference between the 2N and 2N+3N calculations is found in the shell gap at $N = Z = 28$. With the 2N interaction, the calculated neutron and proton shell gaps Δ_n and Δ_p defined as $S_n(^{57}\mathrm{Ni})$-$S_n(^{56}\mathrm{Ni})$ and $S_p(^{57}\mathrm{Cu})$-$S_p(^{56}\mathrm{Ni})$, respectively, result in ∼4.6 MeV compared to ∼6.45 MeV experimentally. As a consequence, these smaller gaps lower the deformed multi-particle multi-hole ($npnh$) configurations by several MeV with respect to the expected closed-shell configuration. Inspection of the obtained ground state wave-function shows considerable amount of $2p2h$ and $4p4h$ mixing in the leading configurations while the closed-shell configuration amounts to only 20%. Associated strong B(E2) values are observed along the yrast band. Inclusion of 3N contributions restores the physics picture: the proton and neutron shell gaps $\Delta_{n,p}$ are increased to ∼5.5 MeV (which is still smaller than experimentally observed), and the closed-shell configuration rises up to order 61% as expected for a doubly-magic nucleus. The $A = 57$ spectrum shows a reduced binding of the $1f_{5/2}$ state with respect to the $2p_{3/2}$ state, which counterbalances the smaller gap. This results in B(E2) values which are in good agreement with the experimental data with the exception of the $6^+ \to 4^+$ transition that is slightly overestimated. The latter observation may be traced back to the enhanced $2p_{3/2}$ occupancy with respect to the $1f_{5/2}$ one, provoking (slightly) larger $f_{7/2} - p_{3/2} = \Delta_j = 2$ quadrupole coherence.

Comparison between calculated and measured B(E2) values show rather similar behavior (see Fig. 2). For the $2_1^+ \to 0_{\mathrm{g.s.}}^+$ and $4_1^+ \to 2_1^+$ transitions, all interactions show overall good agreement over the whole isotonic chain. The experimental trend of the $B(\mathrm{E2}; 6_1^+ \to 4_1^+)$ values is also very well reproduced by the GXPF1A and PFSDG-U interactions while the 2N+3N calculations start to deviate at ^{56}Ni. It is noteworthy, the nature of the 2_1^+, 4_1^+, and 6_1^+ states changes along the $N = 28$ isotonic chain from proton valence $f_{7/2}$ recoupling to $1p1h$ excitations from both protons and neutrons in ^{56}Ni. The detailed occupancies and $npnh$ components are provided in Table 2 for the ^{56}Ni case. For all excited states up to 6_1^+, the $1p1h$, $2p2h$, and $3p3h$ configurations dominate (except for the 2N interaction). This reflects the correlations beyond

Table 2
Occupation of neutron orbitals and percentage of particle-hole excitations across the $N = 28$ gap for the 2^+, 4^+, and 6^+ states in ^{56}Ni.

Interaction	J^π	$\nu f_{7/2}$	$\nu p_{3/2}$	$\nu f_{5/2}$	$\nu p_{1/2}$	1p1h	2p2h	3p3h	4p4h	5p5h
2N	2^+	5.82	1.27	0.59	0.32	7.5	6.4	15	16	18
	4^+	5.74	1.30	0.62	0.35	5.2	6.7	13	17	19
	6^+	5.69	1.27	0.67	0.36	3.7	7.2	13	17	19
2N + 3N	2^+	6.89	0.75	0.26	0.11	42	12	25	9.6	7.3
	4^+	7.00	0.60	0.26	0.14	46	14	23	8.6	5.7
	6^+	6.80	0.52	0.53	0.16	34	25	20	12	5.9
PFSDG-U	2^+	6.63	0.88	0.39	0.10	35	10	28	10	10
	4^+	6.69	0.68	0.48	0.14	37	12	27	10	8.8
	6^+	6.82	0.37	0.72	0.09	44	11	26	8.0	7.1
GXPF1A	2^+	6.79	0.82	0.30	0.10	43	13	27	9.8	6.8
	4^+	6.89	0.62	0.41	0.09	46	16	20	8.7	5.2
	6^+	6.94	0.39	0.58	0.09	47	19	19	7.8	4.3

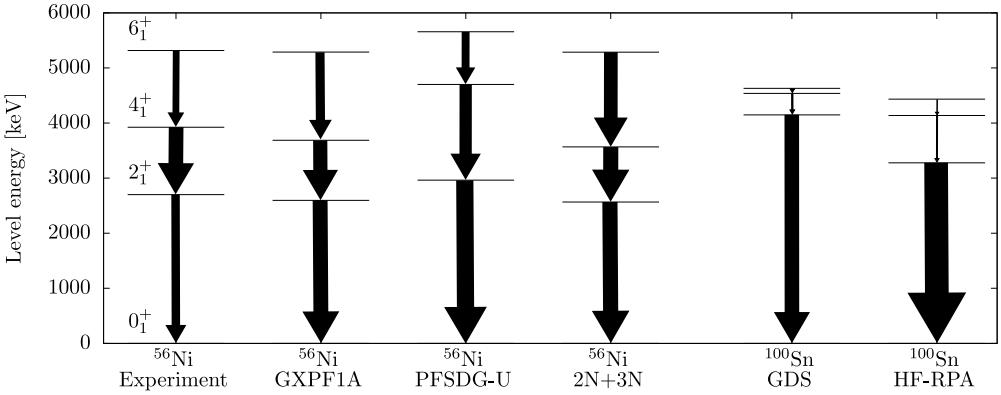

Fig. 3. Experimental and theoretical excitation energies and $B(E2)$ values of ^{56}Ni (see Table 1) are compared with results from the LSSM GDS interaction as well as the HF-RPA [55] calculation for ^{100}Sn (see Table 3). The $B(E2)$ strengths are shown in W.u. and indicated by the arrow widths relative to the experimental $B(E2; 2_1^+ \rightarrow 0^+_{g.s.}) = 5.8$ W.u. value in ^{56}Ni.

the pure single-particle excitations across the shell gap that may be expected for a doubly closed-shell nucleus. Such deviation from the independent-particle model has already been discussed by several authors [56,57] as a consequence of the competing short-range and long-range correlations.

While the softness of the shell closure in ^{56}Ni was deduced from the $B(E2)$ value of the $2_1^+ \rightarrow 0^+_{g.s.}$ (see Fig. 2(f)), an extraordinary high collectivity of the 4_1^+ and 6_1^+ states along the even-even isotonic chain between ^{48}Ca and ^{58}Zn is found in the doubly-magic system ^{56}Ni due to the proton and neutron particle-hole excitations of these states at the shell closure. Beyond the shell closure, theoretical results of the GXPF1A and PFSDG-U interactions naturally predict a very low value of the $6_1^+ \rightarrow 4_1^+$ transition since the 6_1^+ is beyond the natural spin cut-off of two protons above the ^{56}Ni core.

The evolution of reduced transition strengths along the yrast band in ^{56}Ni can be used to give insight into doubly-magic ^{100}Sn. A comparison of excitation energies and transition strengths is justified, as both nuclei are $N = Z$, doubly-magic, and have an open-ℓs core (both having a $j\uparrow$ orbital below the shell gap and the $j\downarrow$ as well as the $\Delta\ell = \Delta j = 2$ orbitals above with similar SPE and SHE). The similarity between the spin-orbit shell closures at $Z = N = 28$ and $Z = N = 50$ has been noticed and addressed already long ago [25–27].

With the newly measured transition strengths of the 4_1^+- and 6_1^+-state decays, it is now possible to extend this discussion and comparison to the higher spin states up to 6_1^+. We perform LSSM calculations in the full *gds* valence space (comprising the $1g_{9/2}$, $1g_{7/2}$, $2d_{5/2}$, $2d_{3/2}$, and $3s_{1/2}$ proton and neutron orbitals) up to $6p6h$ level. The realistic interaction is a renormalized G-matrix from the Oslo group [58], with monopole constraints to reproduce gap observables in the vicinity of ^{100}Sn. The effective charges $e_\pi = 1.11e$ and $e_\nu = 0.84e$ are the ones recently extracted from ^{98}Cd and ^{102}Sn E2 decay rates [59].

Table 3
Theoretical excitation energies and $B(E2)$ values of ^{100}Sn from the LSSM GDS shell-model calculation and the HF-RPA approach [55].

$J_i^\pi \xrightarrow{E2} J_f^\pi$	E_i [keV]		$B(E2)$ [W.u.]	
	GDS	HF-RPA	GDS	HF-RPA
$2_1^+ \rightarrow 0^+_{g.s.}$	4149	3278	9.99	16.25
$4_1^+ \rightarrow 2_1^+$	4539	4138	1.59	1.38
$6_1^+ \rightarrow 4_1^+$	4597	4435	1.46	1.06

The new values for ^{56}Ni are furthermore compared with level energies and $B(E2)$ values from the LSSM *gds* interaction (GDS) and results from calculations exploiting the Hartree-Fock random-phase approximation (HF-RPA) [55] in ^{100}Sn (see Fig. 3) while the values of the theoretical calculations in ^{100}Sn are shown in Table 3.

For the $2_1^+ \rightarrow 0^+_{g.s.}$ transitions the different $B(E2)$ values are in agreement albeit the 2_1^+ energy level for the GDS calculation of ^{100}Sn is considerably increased. However, distinct deviations in reduced transition strength and transition energy are obtained for the 4_1^+ and 6_1^+ decays. Here, the GDS shell-model calculation gives $B(E2; 4_1^+ \rightarrow 2_1^+) = 1.59$ W.u. and $B(E2; 6_1^+ \rightarrow 4_1^+) = 1.46$ W.u. and a narrowed level-energy spacing. Similar results are given by the HF-RPA calculation with $B(E2)$ values of 1.06 W.u. and 1.38 W.u. for the 6_1^+ and 4_1^+ decays, respectively. Within the HF-

RPA calculation, the $4_1^+ \rightarrow 2_1^+$ energy gap is comparable with those from ^{56}Ni, while the $6_1^+ \rightarrow 4_1^+$ transition energy resembles the GDS calculation. Both experimental observations and shell-model predictions in ^{56}Ni show a more collective behavior for the $4_1^+ \rightarrow 2_1^+$ and $6_1^+ \rightarrow 4_1^+$ transitions expressed in B(E2) values of 5 to 10 W.u.. With the increased amount of core-excited configurations of the 4_1^+ and 6_1^+ states now being confirmed by the experimental findings, following the analogy, we can expect a similar situation to arise in the ℓs-open core ^{100}Sn.

Motivated by ^{100}Sn calculations in the past, the possible existence of E2 isomerism for the 6_1^+ state has been discussed [25,27]. However, up to now, no experimental evidence has been found for such an isomeric state [1,60]. A possible explanation to this can be given by our new results. Due to the comparable shell structure with analogous SPE/SHE in the $N = 3$ and $N = 4$ harmonic oscillator shells in ^{56}Ni and ^{100}Sn, respectively, enhanced collectivity can also be expected in ^{100}Sn. The isomeric character of the $6_1^+ \rightarrow 4_1^+$ transition in ^{100}Sn depends on the transition energy and the B(E2) value. Assuming an increased $B(\mathrm{E2}; 6_1^+ \rightarrow 4_1^+)$ strengths of ≈ 5 W.u., as found in ^{56}Ni, and a transition energy of 58 keV and 297 keV from the GDS and HF-RPA predictions, respectively, the lifetime of the 6_1^+ state will be 700 ns and 3 ns. Isomeric lifetimes smaller than 300 ns were below the detection capabilities of the previously performed experiments at fragmentation facilities [1,60].

On the other hand, the actual differences noticed between the E2 transitions along the yrast states of ^{56}Ni and ^{100}Sn may be understood in the following way: even though the degrees of freedom available at the Fermi surface in some isotopes may exhibit similarities, the physics regime may develop differently. In the Ni and Sn chains, it was recently emphasized [61] that the physics in ^{78}Ni and ^{132}Sn had common geometrical features: these two nuclei have double spin-orbit shell closures as well direct quadrupole partners lying at the Fermi surface (see lower part of Fig. 41 in Ref. [61]).

Nevertheless, the physics developing in these two nuclei is rather different: ^{78}Ni shows coexistence of deformed and spherical shapes at a rather low-excitation energy (below 3 MeV), while in ^{132}Sn, due to the stronger spin-orbit contribution to the neutron shell gap, such coexistence disappears which is expressed in the absence of low-lying deformed states (below 4 MeV) in this nucleus. Therefore, such situation is expected to happen in ^{100}Sn with respect to ^{56}Ni: the increased spin-orbit contribution favors the closed-shell configuration provoking a paradoxical behavior: strong instability with respect to the weak interaction (super-allowed Gamow-Teller transition) and strong stability with respect to the strong interaction and electromagnetic excitations.

5. Summary

Lifetimes were obtained for the 4_1^+ and 6_1^+ states in the nucleus ^{56}Ni utilizing the DSA method. The corresponding B(E2) values are the highest along the $N = 28$ chain of isotones between ^{48}Ca and ^{58}Zn within the experimental uncertainties. The extended systematics of B(E2) values are in good agreement with the calculations from the GXPF1A and PFSDG-U shell-model interactions. The results from ab-initio calculations illustrate the necessity of three-body potentials in order to reproduce the experimental findings. The new results are confronted with theoretical predictions in the doubly-magic $N = Z$ ℓs open-shell partner nucleus ^{100}Sn. The strong E2 collectivity in ^{56}Ni could suggest a lifetime in the ns range of a predicted 6_1^+ isomer in ^{100}Sn. Along the $N = Z$ line, the newly obtained values close a gap of excited states lifetimes above the first excited 2_1^+ state and draw attention to the even-even neighbor ^{60}Zn – only one α particle away from ^{56}Ni – for which no lifetime information on excited states is available.

Declaration of competing interest

The authors declare that they have no known competing financial interests or personal relationships that could have appeared to influence the work reported in this paper.

Acknowledgements

We are deeply indebted to our friend and colleague Hubert Grawe who followed us and gave us advice related to numerous shell-model questions in the past and also for this paper. Unexpectedly and sadly, he passed away in November 2020.

References

[1] C.B. Hinke, M. Böhmer, P. Boutachkov, T. Faestermann, H. Geissel, J. Gerl, R. Gernhäuser, M. Górska, A. Gottardo, H. Grawe, J.L. Grębosz, R. Krücken, N. Kurz, Z. Liu, L. Maier, F. Nowacki, S. Pietri, Z. Podolyák, K. Sieja, K. Steiger, K. Straub, H. Weick, H.-J. Wollersheim, P.J. Woods, N. Al-Dahan, N. Alkhomashi, A. Ataç, A. Blazhev, N.F. Braun, I.T. Čeliković, T. Davinson, I. Dillmann, C. Domingo-Pardo, P.C. Doornenbal, G. de France, G.F. Farrelly, F. Farinon, N. Goel, T.C. Habermann, R. Hoischen, R. Janik, M. Karny, A. Kaşkaş, I.M. Kojouharov, T. Kröll, Y. Litvinov, S. Myalski, F. Nebel, S. Nishimura, C. Nociforo, J. Nyberg, A.R. Parikh, A. Procházka, P.H. Regan, C. Rigollet, H. Schaffner, C. Scheidenberger, S. Schwertel, P.-A. Söderström, S.J. Steer, A. Stolz, P. Strmeň, Superallowed Gamow–Teller decay of the doubly magic nucleus ^{100}Sn, Nature 486 (7403) (2012) 341–345, https://doi.org/10.1038/nature11116.

[2] D. Kahl, P. Woods, T. Poxon-Pearson, F. Nunes, B. Brown, H. Schatz, T. Baumann, D. Bazin, J. Belarge, P. Bender, B. Elman, A. Estrade, A. Gade, A. Kankainen, C. Lederer-Woods, S. Lipschutz, B. Longfellow, S.-J. Lonsdale, E. Lunderberg, F. Montes, W. Ong, G. Perdikakis, J. Pereira, C. Sullivan, R. Taverner, D. Weisshaar, R. Zegers, Single-particle shell strengths near the doubly magic nucleus ^{56}Ni and the ^{56}Ni(p,γ)^{57}Cu reaction rate in explosive astrophysical burning, Phys. Lett. B 797 (2019) 134803, https://doi.org/10.1016/j.physletb.2019.134803.

[3] D. Rosiak, M. Seidlitz, P. Reiter, H. Naïdja, Y. Tsunoda, T. Togashi, F. Nowacki, T. Otsuka, G. Colò, K. Arnswald, T. Berry, A. Blazhev, M.J.G. Borge, J. Cederkäll, D.M. Cox, H. De Witte, L.P. Gaffney, C. Henrich, R. Hirsch, M. Huyse, A. Illana, K. Johnston, L. Kaya, T. Kröll, M.L.L. Benito, J. Ojala, J. Pakarinen, M. Queiser, G. Rainovski, J.A. Rodriguez, B. Siebeck, E. Siesling, J. Snäll, P. Van Duppen, A. Vogt, M. von Schmid, N. Warr, F. Wenander, K.O. Zell, Enhanced quadrupole and octupole strength in doubly magic ^{132}Sn, Phys. Rev. Lett. 121 (2018) 252501, https://doi.org/10.1103/PhysRevLett.121.252501.

[4] T.E. Cocolios, A.N. Andreyev, B. Bastin, N. Bree, J. Büscher, J. Elseviers, J. Gentens, M. Huyse, Y. Kudryavtsev, D. Pauwels, T. Sonoda, P. Van den Bergh, P. Van Duppen, Magnetic dipole moment of ^{57,59}Cu measured by in-gas-cell laser spectroscopy, Phys. Rev. Lett. 103 (2009) 102501, https://doi.org/10.1103/PhysRevLett.103.102501.

[5] M. Goeppert Mayer, On closed shells in nuclei. II, Phys. Rev. 75 (1949) 1969–1970, https://doi.org/10.1103/PhysRev.75.1969.

[6] O. Haxel, J.H.D. Jensen, H.E. Suess, On the "magic numbers" in nuclear structure, Phys. Rev. 75 (1949) 1766, https://doi.org/10.1103/PhysRev.75.1766.2.

[7] D. Rudolph, C. Baktash, M.J. Brinkman, E. Caurier, D.J. Dean, M. Devlin, J. Dobaczewski, P.-H. Heenen, H.-Q. Jin, D.R. LaFosse, W. Nazarewicz, F. Nowacki, A. Poves, L.L. Riedinger, D.G. Sarantites, W. Satuła, C.-H. Yu, Rotational bands in the doubly magic nucleus ^{56}Ni, Phys. Rev. Lett. 82 (1999) 3763–3766, https://doi.org/10.1103/PhysRevLett.82.3763.

[8] D.G. Sarantites, P.-F. Hua, M. Devlin, L.G. Sobotka, J. Elson, J.T. Hood, D.R. LaFosse, J.E. Sarantites, M.R. Maier, "The microball" design, instrumentation and response characteristics of a 4π-multidetector exit channel-selection device for spectroscopic and reaction mechanism studies with Gammasphere, Nucl. Instrum. Methods Phys. Res. A 381 (2) (1996) 418–432, https://doi.org/10.1016/S0168-9002(96)00785-1.

[9] I.-Y. Lee, The GAMMASPHERE, Nucl. Phys. A 520 (1990) c641–c655, https://doi.org/10.1016/0375-9474(90)91181-P.

[10] N. Schulz, J. Chevallier, B. Haas, J. Richert, M. Toulemonde, Electromagnetic transition rates in ^{56}Ni, Phys. Rev. C 8 (1973) 1779–1781, https://doi.org/10.1103/PhysRevC.8.1779.

[11] G. Kraus, P. Egelhof, C. Fischer, H. Geissel, A. Himmler, F. Nickel, G. Münzenberg, W. Schwab, A. Weiss, J. Friese, A. Gillitzer, H.J. Körner, M. Peter, W.F. Henning, J.P. Schiffer, J.V. Kratz, L. Chulkov, M. Golovkov, A. Ogloblin, B.A. Brown, Proton inelastic scattering on ^{56}Ni in inverse kinematics, Phys. Rev. Lett. 73 (1994) 1773–1776, https://doi.org/10.1103/PhysRevLett.73.1773.

[12] K.L. Yurkewicz, D. Bazin, B.A. Brown, C.M. Campbell, J.A. Church, D.C. Dinca, A. Gade, T. Glasmacher, M. Honma, T. Mizusaki, W.F. Mueller, H. Olliver, T. Otsuka, L.A. Riley, J.R. Terry, Nuclear structure in the vicinity of $N = Z = 28$ ^{56}Ni, Phys. Rev. C 70 (2004) 054319, https://doi.org/10.1103/PhysRevC.70.054319.

[13] N.A. Smirnova, K. Heyde, B. Bally, F. Nowacki, K. Sieja, Nuclear shell evolution and in-medium NN interaction, Phys. Rev. C 86 (2012) 034314, https://doi.org/10.1103/PhysRevC.86.034314.

[14] T. Otsuka, M. Honma, T. Mizusaki, Structure of the $N = Z = 28$ closed shell studied by Monte Carlo shell model calculation, Phys. Rev. Lett. 81 (1998) 1588–1591, https://doi.org/10.1103/PhysRevLett.81.1588.

[15] M. Honma, T. Otsuka, B.A. Brown, T. Mizusaki, New effective interaction for pf-shell nuclei and its implications for the stability of the $N = Z = 28$ closed core, Phys. Rev. C 69 (2004) 034335, https://doi.org/10.1103/PhysRevC.69.034335.

[16] A. Poves, F. Nowacki, Y. Alhassid, Limits on assigning a shape to a nucleus, Phys. Rev. C 101 (5) (2020) 054307, https://doi.org/10.1103/PhysRevC.101.054307.

[17] M. Honma, T. Otsuka, B.A. Brown, T. Mizusaki, Shell-model description of neutron-rich pf-shell nuclei with a new effective interaction GXPF1, Eur. Phys. J. A 25 (1) (2005) 499–502, https://doi.org/10.1140/epjad/i2005-06-032-2.

[18] F. Nowacki, A. Poves, E. Caurier, B. Bounthong, Shape coexistence in ^{78}Ni as the portal to the fifth island of inversion, Phys. Rev. Lett. 117 (2016) 272501, https://doi.org/10.1103/PhysRevLett.117.272501.

[19] R. Taniuchi, C. Santamaria, P. Doornenbal, A. Obertelli, K. Yoneda, G. Authelet, H. Baba, D. Calvet, F. Château, A. Corsi, A. Delbart, J.-M. Gheller, A. Gillibert, J.D. Holt, T. Isobe, V. Lapoux, M. Matsushita, J. Menéndez, S. Momiyama, T. Motobayashi, M. Niikura, F. Nowacki, K. Ogata, H. Otsu, T. Otsuka, C. Péron, S. Péru, A. Peyaud, E.C. Pollacco, A. Poves, J.-Y. Roussé, H. Sakurai, A. Schwenk, Y. Shiga, J. Simonis, S.R. Stroberg, S. Takeuchi, Y. Tsunoda, T. Uesaka, H. Wang, F. Browne, L.X. Chung, Z. Dombradi, S. Franchoo, F. Giacoppo, A. Gottardo, K. Hadyńska-Klęk, Z. Korkulu, S. Koyama, Y. Kubota, J. Lee, M. Lettmann, C. Louchart, R. Lozeva, K. Matsui, T. Miyazaki, S. Nishimura, L. Olivier, S. Ota, Z. Patel, E. Şahin, C. Shand, P.-A. Söderström, I. Stefan, D. Steppenbeck, T. Sumikama, D. Suzuki, Z. Vajta, V. Werner, J. Wu, Z.Y. Xu, ^{78}Ni revealed as a doubly magic stronghold against nuclear deformation, Nature 569 (7754) (2019) 53–58, https://doi.org/10.1038/s41586-019-1155-x.

[20] A.P. Zuker, Three body monopole corrections to the realistic interactions, Phys. Rev. Lett. 90 (2003) 042502, https://doi.org/10.1103/PhysRevLett.90.042502.

[21] Y.Z. Ma, L. Coraggio, L. De Angelis, T. Fukui, A. Gargano, N. Itaco, F.R. Xu, Contribution of chiral three-body forces to the monopole component of the effective shell-model Hamiltonian, Phys. Rev. C 100 (3) (2019) 034324, https://doi.org/10.1103/PhysRevC.100.034324.

[22] M. Lipoglavšek, D. Seweryniak, C. Davids, C. Fahlander, M. Górska, R. Janssens, J. Nyberg, J. Uusitalo, W. Walters, I. Ahmad, J. Blomqvist, M. Carpenter, J. Cizewski, S. Fischer, H. Grawe, G. Hackman, M. Huhta, C. Lister, D. Nisius, G. Poli, P. Reiter, J. Ressler, J. Schwartz, A. Sonzogni, E2 polarization charge in ^{102}Sn, Phys. Lett. B 440 (3) (1998) 246–250, https://doi.org/10.1016/S0370-2693(98)01178-2.

[23] M. Lipoglavšek, C. Baktash, J. Blomqvist, M.P. Carpenter, D.J. Dean, T. Engeland, C. Fahlander, M. Hjorth-Jensen, R.V.F. Janssens, A. Likar, J. Nyberg, E. Osnes, S.D. Paul, A. Piechaczek, D.C. Radford, D. Rudolph, D. Seweryniak, D.G. Sarantites, M. Vencelj, C.-H. Yu, Breakup of the doubly magic ^{100}Sn core, Phys. Rev. C 66 (2002) 011302, https://doi.org/10.1103/PhysRevC.66.011302.

[24] M. Lipoglavšek, M. Vencelj, C. Baktash, P. Fallon, P.A. Hausladen, A. Likar, C.-H. Yu, ^{100}Sn core excitations in ^{97}Ag, Phys. Rev. C 72 (2005) 061304, https://doi.org/10.1103/PhysRevC.72.061304.

[25] H. Grawe, A. Blazhev, M. Górska, R. Grzywacz, H. Mach, I. Mukha, Nuclear structure far off stability –implications for nuclear astrophysics, Eur. Phys. J. A 27 (1) (2006) 257–267, https://doi.org/10.1140/epja/i2006-08-040-7.

[26] F. Nowacki, Shell model description of correlations in ^{56}Ni and ^{100}Sn, in: RIKEN Symposium Shell Model 2000, Nucl. Phys. A 704 (1) (2002) 223–231, https://doi.org/10.1016/S0375-9474(02)00782-0.

[27] T. Faestermann, M. Górska, H. Grawe, The structure of ^{100}Sn and neighbouring nuclei, Prog. Part. Nucl. Phys. 69 (2013) 85–130, https://doi.org/10.1016/j.ppnp.2012.10.002.

[28] R.D.O. Llewellyn, M.A. Bentley, R. Wadsworth, H. Iwasaki, J. Dobaczewski, G. de Angelis, J. Ash, D. Bazin, P.C. Bender, B. Cederwall, B.P. Crider, M. Doncel, R. Elder, B. Elman, A. Gade, M. Grinder, T. Haylett, D.G. Jenkins, I.Y. Lee, B. Longfellow, E. Lunderberg, T. Mijatović, S.A. Milne, D. Muir, A. Pastore, D. Rhodes, D. Weisshaar, Establishing the maximum collectivity in highly deformed $N = Z$ nuclei, Phys. Rev. Lett. 124 (2020) 152501, https://doi.org/10.1103/PhysRevLett.124.152501.

[29] K. Arnswald, T. Braunroth, M. Seidlitz, L. Coraggio, P. Reiter, B. Birkenbach, A. Blazhev, A. Dewald, C. Fransen, B. Fu, A. Gargano, H. Hess, R. Hirsch, N. Itaco, S. Lenzi, L. Lewandowski, J. Litzinger, C. Müller-Gatermann, M. Queiser, D. Rosiak, D. Schneiders, B. Siebeck, T. Steinbach, A. Vogt, K. Wolf, K. Zell, Enhanced collectivity along the $N = Z$ line: lifetime measurements in ^{44}Ti, ^{48}Cr, and ^{52}Fe, Phys. Lett. B 772 (2017) 599–606, https://doi.org/10.1016/j.physletb.2017.07.032.

[30] K. Kaneko, Y. Sun, G. de Angelis, Enhancement of high-spin collectivity in $N = Z$ nuclei by the isoscalar neutron-proton pairing, Nucl. Phys. A 957 (2017) 144–153, https://doi.org/10.1016/j.nuclphysa.2016.08.007.

[31] P. Petkov, C. Müller-Gatermann, D. Werner, A. Dewald, A. Blazhev, C. Fransen, J. Jolie, S. Ohkubo, K.O. Zell, New lifetime measurements for the lowest quadrupole states in ^{20,22}Ne and possible explanations of the high collectivity of the depopulating $E2$ transitions, Phys. Rev. C 100 (2019) 024312, https://doi.org/10.1103/PhysRevC.100.024312.

[32] C.A. Ur, D. Bucurescu, S.M. Lenzi, G. Martínez-Pinedo, D.R. Napoli, D. Bazzacco, F. Brandolini, D.M. Brink, J.A. Cameron, E. Caurier, G. de Angelis, M. De Poli, A. Gadea, S. Lunardi, N. Mărginean, M.A. Nagarajan, P. Pavan, C. Rossi Alvarez, C.E. Svensson, Excited states in ^{52}Fe and the origin of the yrast trap at $I^{\pi} = 12^{+}$, Phys. Rev. C 58 (1998) 3163–3170, https://doi.org/10.1103/PhysRevC.58.3163, https://link.aps.org/doi/10.1103/PhysRevC.58.3163.

[33] Evaluated Nuclear Structure Data File (ENSDF), http://www.nndc.bnl.gov/ensdf, http://www.nndc.bnl.gov/ensdf.

[34] A. Dewald, O. Möller, P. Petkov, Developing the recoil distance Doppler-shift technique towards a versatile tool for lifetime measurements of excited nuclear states, Prog. Part. Nucl. Phys. 67 (3) (2012) 786–839, https://doi.org/10.1016/j.ppnp.2012.03.003.

[35] N. Saed-Samii, Diplomarbeit Universität zu Köln, 2013, unpublished.

[36] J. Theuerkauf, S. Esser, S. Krink, M. Luig, N. Nicolay, O. Stuch, H. Wolters, Program TV, Institute for Nuclear Physics, University of Cologne, Cologne, Germany.

[37] P. Petkov, D. Tonev, J. Gableske, A. Dewald, T. Klemme, P. von Brentano, On the line-shape and lifetime determination in recoil distance Doppler-shift measurements, Nucl. Instrum. Methods Phys. Res. A 431 (1) (1999) 208–223, https://doi.org/10.1016/S0168-9002(99)00276-4.

[38] G. Winter, The application of lineshape analysis in plunger measurements, Nucl. Instrum. Methods Phys. Res. 214 (2) (1983) 537–539, https://doi.org/10.1016/0167-5087(83)90629-4.

[39] G. Winter, ZfK Rossendorf Report ZfK-497, 1983.

[40] L. Northcliffe, R. Schilling, Range and stopping-power tables for heavy ions, At. Data Nucl. Data Tables 7 (3) (1970) 233–463, https://doi.org/10.1016/S0092-640X(70)80016-X.

[41] J. Lindhard, M. Scharff, H.E. Schiøtt, Range concepts and heavy ion ranges, Kgl. Dan. Vid. Selsk. Mat. Fys. Medd. 33 (14) (1963), http://gymarkiv.sdu.dk/MFM/kdvs/mfm%2030-39/mfm-33-14.pdf.

[42] W. Currie, A Monte Carlo programme for Doppler shift analysis, Nucl. Instrum. Methods 73 (2) (1969) 173–185, https://doi.org/10.1016/0029-554X(69)90203-1.

[43] J. Keinonen, Use of capture reactions to measure short lifetimes by the DSA method, AIP Conf. Proc. 125 (1985) 557, https://doi.org/10.1063/1.35144.

[44] J.F. Ziegler, J.P. Biersack, The Stopping and Range of Ions in Matter, Springer US, Boston, MA, 1985, pp. 93–129.

[45] J. Keinonen, Reliability of short lifetimes measured by the Doppler shift attenuation method, AIP Conf. Proc. 238 (1) (1991) 383–392, https://doi.org/10.1063/1.41288.

[46] T.K. Alexander, J.S. Forster, Lifetime Measurements of Excited Nuclear Levels by Doppler-Shift Methods, Springer US, Boston, MA, 1978, pp. 197–331.

[47] P. Petkov, D. Tonev, J. Gableske, A. Dewald, P. von Brentano, Lifetime analysis using the Doppler-shift attenuation method with a gate on feeding transition, Nucl. Instrum. Methods Phys. Res. A 437 (2) (1999) 274–281, https://doi.org/10.1016/S0168-9002(99)00771-8.

[48] R. Ernst, K.-H. Speidel, O. Kenn, U. Nachum, J. Gerber, P. Maier-Komor, N. Benczer-Koller, G. Jakob, G. Kumbartzki, L. Zamick, F. Nowacki, Stringent tests of shell model calculations in fp shell nuclei ^{46,48}Ti and ^{50,52}Cr from measurements of g factors and $B(E2)$ values, Phys. Rev. Lett. 84 (2000) 416–419, https://doi.org/10.1103/PhysRevLett.84.416.

[49] N. Shimizu, T. Mizusaki, Y. Utsuno, Y. Tsunoda, Thick-restart block lanczos method for large-scale shell-model calculations, Comput. Phys. Commun. 244 (2019) 372–384, https://doi.org/10.1016/j.cpc.2019.06.011.

[50] E. Caurier, G. Martinez-Pinedo, F. Nowacki, A. Poves, A.P. Zuker, The shell model as unified view of nuclear structure, Rev. Mod. Phys. 77 (2005) 427–488, https://doi.org/10.1103/RevModPhys.77.427.

[51] E. Caurier, F. Nowacki, Present status of shell model techniques, Acta Phys. Pol. B 30 (1999) 705–714.

[52] A. Poves, J. Sánchez-Solano, E. Caurier, F. Nowacki, Shell model study of the isobaric chains $A = 50$, $A = 51$ and $A = 52$, Nucl. Phys. A 694 (1–2) (2001) 157–198, https://doi.org/10.1016/S0375-9474(01)00967-8.

[53] J.M. Allmond, B.A. Brown, A.E. Stuchbery, A. Galindo-Uribarri, E. Padilla-Rodal, D.C. Radford, J.C. Batchelder, M.E. Howard, J.F. Liang, B. Manning, R.L. Varner, C.-H. Yu, High-precision $B(E2)$ measurements of semi-magic ^{58,60,62,64}Ni by Coulomb excitation, Phys. Rev. C 90 (2014) 034309, https://doi.org/10.1103/PhysRevC.90.034309.

[54] C. Loelius, H. Iwasaki, B.A. Brown, M. Honma, V.M. Bader, T. Baugher, D. Bazin, J.S. Berryman, T. Braunroth, C.M. Campbell, A. Dewald, A. Gade, N. Kobayashi, C. Langer, I.Y. Lee, A. Lemasson, E. Lunderberg, C. Morse, F. Recchia, D. Smalley, S.R. Stroberg, R. Wadsworth, C. Walz, D. Weisshaar, A. Westerberg, K. Whitmore, K. Wimmer, Lifetime measurement of the 4_1^+ state of ^{58}Ni with the recoil distance method, Phys. Rev. C 94 (2016) 024340, https://doi.org/10.1103/PhysRevC.94.024340.

[55] V.I. Isakov, K.I. Erokhina, Nuclear masses and properties of nuclei in the vicinity of the remote magic nucleus ^{100}Sn, Phys. At. Nucl. 65 (8) (2002) 1431–1443, https://doi.org/10.1134/1.1501655.

[56] V.R. Pandharipande, I. Sick, P.K.A.d. Huberts, Independent particle motion and correlations in fermion systems, Rev. Mod. Phys. 69 (1997) 981–991, https://doi.org/10.1103/RevModPhys.69.981.

[57] C. Barbieri, Role of long-range correlations on the quenching of spectroscopic factors, Phys. Rev. Lett. 103 (2009) 202502, https://doi.org/10.1103/PhysRevLett.103.202502.

[58] M. Hjorth-Jensen, T.T.S. Kuo, E. Osnes, Realistic effective interactions for nuclear systems, Phys. Rep. 261 (1995) 125–270, https://doi.org/10.1016/0370-1573(95)00012-6.

[59] H. Grawe, et al., Phys. Lett. B (2021), https://doi.org/10.1016/j.physletb.2021.136591, in press.

[60] J. Park, R. Krücken, D. Lubos, R. Gernhäuser, M. Lewitowicz, S. Nishimura, D.S. Ahn, H. Baba, B. Blank, A. Blazhev, P. Boutachkov, F. Browne, I. Čeliković, G. de France, P. Doornenbal, T. Faestermann, Y. Fang, N. Fukuda, J. Giovinazzo, N. Goel, M. Górska, H. Grawe, S. Ilieva, N. Inabe, T. Isobe, A. Jungclaus, D. Kameda, G.D. Kim, Y.-K. Kim, I. Kojouharov, T. Kubo, N. Kurz, G. Lorusso, K. Moschner, D. Murai, I. Nishizuka, Z. Patel, M.M. Rajabali, S. Rice, H. Sakurai, H. Schaffner, Y. Shimizu, L. Sinclair, P.-A. Söderström, K. Steiger, T. Sumikama, H. Suzuki, H. Takeda, Z. Wang, H. Watanabe, J. Wu, Z.Y. Xu, Properties of γ-decaying isomers and isomeric ratios in the ^{100}Sn region, Phys. Rev. C 96 (2017) 044311, https://doi.org/10.1103/PhysRevC.96.044311.

[61] F. Nowacki, A. Obertelli, A. Poves, The neutron-rich edge of the nuclear landscape: experiment and theory, Prog. Part. Nucl. Phys. (2021) 103866, https://doi.org/10.1016/j.ppnp.2021.103866.

Discussion and conclusions

The aim of this thesis was the investigation of collective properties in even-even $N = Z$ nuclei within the pf shell. In total, six lifetime experiments were performed using two different methods which utilize the Doppler-shifted energy lineshapes of emitted γ rays from recoiling nuclei during their stopping processes. The measured lifetimes are converted into $B(\sigma\lambda)$ values which are confronted with results from modern shell-model calculations. In the following, the content of the three publications is summarized.

In the first publication "Enhanced collectivity along the $N = Z$ line: Lifetime measurements in ^{44}Ti, ^{48}Cr, and ^{52}Fe" [16] the three mentioned self-conjugate even-even nuclei are studied which are located between the doubly-magic shell-closures ^{40}Ca and ^{56}Ni in the $0f1p$ shell. In this region, the nuclear shell-model is the major framework for theoretical calculations of nuclear properties. Well established GXPF1A [18], KB3G [21], and FPD6 [14] interactions are available for the pf model space and provide results which are in excellent agreement with experimental data on excitation energies and reduced transition strengths for the lower pf shell nuclei [73]. Although these nuclei can be populated with various fusion-evaporation reactions, 2_1^+ lifetime values in ^{44}Ti, ^{48}Cr, and ^{52}Fe were only known with considerable uncertainties. Precise lifetime values are crucial to further test the shell-model predictions. Therefore, refined lifetime experiments were performed employing the Cologne coincidence-plunger setup at the FN tandem accelerator at the Institute for Nuclear Physics, University of Cologne, Germany. The lifetime analysis yielded increased $B(E2; 2^+ \rightarrow 0^+_{\text{g.s.}})$ values for ^{44}Ti and ^{52}Fe indicating a more collective behavior for both nuclei. Applying the new results, a unified evolution of $B(E2)$ strengths is obtained along the three chains of isotopes with minima at the (sub-)shell closures $N = 20, 28$ as well as $N = 32$ (for the Cr isotopes) and increased $B(E2)$ values towards mid shell. In particular, the increased $B(E2)$ value in ^{44}Ti solves the conundrum of a local minimum at $N = 22$. The employed shell-model interactions reproduce the trend of $B(E2)$ values along the chromium and iron isotopes. For ^{48}Cr, experiment and theory are in a good agreement; for ^{52}Fe, the experimental value is reproduced by the FPD6 interaction and the realistic Hamiltonian from Coraggio *et al.* while the values from the GXPF1A and KB3G interactions are lower. Merely, the evolution along the titanium isotopes could not be reproduced by the different shell-model interactions. This is indicated by the rising impact of multi-particle multi-hole cross-shell excitations from the sd shell. In addition to the single $B(E2)$ values, also the $B_{4/2}$ ratios were obtained for the three nuclei. The ratios, build of the new values and adopted $B(E2; 4^+ \rightarrow 2_1^+)$ values, give $1.36^{+0.29}_{-0.22}$, $1.00^{+0.11}_{-0.08}$, and $1.14^{+0.32}_{-0.22}$ for ^{44}Ti, ^{48}Cr, and ^{52}Fe, respectively. These values are interpreted as non-collective excitations with tendencies of rotor-like behavior for ^{44}Ti. The corresponding ratios of excitation energies $E(4^+)/E(2^+)$ are settled between 2 and 3, predicting a transition from vibrational

to rotational character. The inconsistent description of both ratios could not be addressed within this work but might be traced back to the limited precision of the $B_{4/2}$ ratios originating from the $B(E2; 4_1^+ \rightarrow 2_1^+)$ values which are partly known only with considerable uncertainties. Thus, future precise lifetime measurements of 4_1^+ states in the three $N = Z$ nuclei are needed to further reduce the experimental uncertainties and to pin down the evolution of the $B_{4/2}$ ratios.

The second part of this thesis "Lifetime measurements in ^{44}Ti" [17] deals with the even-even $N = Z$ nucleus ^{44}Ti which is located in the lower pf shell only one α particle away from doubly-magic ^{40}Ca. For this reason, ^{44}Ti has been subject of different theoretical approaches using the α-cluster model [58–63]. As discussed in the preceding publication, the pf shell-model interactions do not provide an adequate description of the titanium isotopes in terms of the $B(E2; 2^+ \rightarrow 0^+_{\text{g.s.}})$ values – especially, for the neutron-deficient isotopes. Multi-particle multi-hole cross-shell configurations were identified to arise around the $Z = 20$ shell closure and are included in the novel ZBM2 [29] and ZBM2M [31] shell-model interactions. Moreover, the addition of positive-parity s and d orbitals to the fp model space, also allows for the calculation of negative-parity states in ^{44}Ti. This nucleus offers an excellent study ground for modern shell-model calculations in order to investigate the impact of core excitations and to test the predictions in terms of negative-parity states. For these states only scarce and contradictory lifetime information was available. Therefore, precise lifetime measurements were performed utilizing both the recoil-distance Doppler-shift technique and the Doppler-shift attenuation method in order to cover a broad range of lifetimes between several hundreds of femtoseconds and a few hundreds picoseconds. The determined lifetimes for the 4_1^+ and 6_1^+ states are in a good agreement with results from previous measurements whereas the experimental uncertainty could be slightly reduced. Furthermore, precise lifetimes for the 3_1^- and 4_1^- states could be deduced which for the latter one considerably deviates from a previous value. However, the increased lifetime value of 110(8) ps is now in agreement with predictions from Dixon *et al.* who discussed a lower lifetime limit of $\tau > 50$ ps [74]. The new lifetime value for the 3_1^- state is in a fair agreement with a preliminary result from Michelagnoli *et al.* [75]. The deduced reduced transition probabilities were compared with results from the novel ZBM2M shell-model interaction as well as the GXPF1A, KB3G, and FPD6 interactions along the yrast band. The ZBM2M interaction reproduces the 2_1^+ and 4_1^+ states very well which are dominated by core-excited configurations and cannot be reproduced by the pf-shell interactions. With increasing J, the states of the ground-state band are in a better agreement with the GXPF1A, KB3G, and FPD6 interactions, which show a similar evolution, indicating a minor impact of cross-shell configurations at higher-spin states. Moreover, the overall trend of $B(E2)$ values along the ground-state band is well reproduced by results from the $^{40}\text{Ca} + \alpha$ calculations from Ref. [62]. For the $8_1^+ \rightarrow 6_1^+$ transition, the ZBM2M interaction and the results from the α-cluster model predict higher $B(E2)$ values than derived from the three pf shell interactions. This deviation could not be solved as from previous experiments only a lower limit of > 1.5 W.u. could be obtained [76]. Excitation energies and $B(E2)$ values from negative-parity states in ^{44}Ti were compared with results from shell-model calculations for the first time. The experimentally deduced finite $B(E1)$ value of the $3_1^- \rightarrow 2_1^+$ transition indicates isospin-symmetry breaking, as the isovector character of the $E1$ transition operator does not allow transitions between $T = 0$ states. Within the ZBM2M interaction

the isospin symmetry is conserved resulting in $B(E1; 3_1^- \rightarrow 2_1^+) = 0$. For the $4_1^- \rightarrow 3_1^-$ transition, results from the ZBM2M interaction show the same trend to lower $B(\sigma\lambda)$ values, but even underestimate the experimental values by a factor of two orders of magnitude. To investigate these deviations between experiment and theory, the untruncated $sdpf$ model space can be employed in order to obtain comprehensive shell-model results. Moreover, future measurements of the 8_1^+ level lifetime can close the gap of available $B(E2)$ values along the yrast band and can give insights to the different theoretical results.

In the third publication "Enhanced quadrupole collectivity in doubly-magic ^{56}Ni: Lifetime measurements of the 4_1^+ and 6_1^+ states" [20], the shell-closure nucleus ^{56}Ni is investigated. This shell closure within the pf shell is caused by the spin-orbit splitting of the $f_{7/2}$ orbital from the remaining three orbitals. Unlike other (harmonic-oscillator) shell closures, spin-orbit shell closures exhibit enhanced $E2$ strengths for the $2_1^+ \rightarrow 0_{\text{g.s.}}^+$ transition as the 2^+ state is a direct quadrupole excitation of the doubly-magic core. This feature has been considered as a softness of the shell closure at ^{56}Ni [13, 77]. Experimental observations from Coulomb excitation [46, 78] and pioneering lifetime measurements [79] confirm such enhanced $B(E2)$ values. However, for the higher-lying yrast states in ^{56}Ni no lifetime values except for lower limits are known. These are of particular interest as they would shed light on whether the enhanced collectivity is restricted to the 2_1^+ state or can be found in further members of the yrast band. Lifetime measurements were performed utilizing the Doppler-shift attenuation method at the University of Cologne. Results were obtained for the 4_1^+ and 6_1^+ states exhibiting highest $B(E2)$ values with respect to the neighboring $N = 28$ isotones between ^{48}Ca and ^{58}Zn. State-of-the-art shell-model calculations were performed using the GXPF1A and PFSDG-U interactions as well as valence ab-initio calculations starting from a realistic Hamiltonian derived from chiral perturbation theory including three-body potential contributions. The calculated excitation energies and $B(E2)$ values showed a good agreement with the experimental findings. An inspection of the wavefunctions of the yrast states up to the 6_1^+ state in ^{56}Ni yielded dominant $1p1h$, $2p2h$, and $3p3h$ contributions. Such deviations from the independent-particle model indicate that the softness of the shell closure in ^{56}Ni, which was deduced from the $B(E2)$ value of the $2_1^+ \rightarrow 0_{\text{g.s.}}^+$, is also present in higher-lying members of the yrast band. The new $B(E2)$ values of ^{56}Ni are consequently used for a comparison with doubly-magic ^{100}Sn. Such a comparison is justified as both nuclei are doubly magic and are ℓs-open shell cores with similar single-particle and single-hole energies. Since γ-ray transitions from excited states in ^{100}Sn have not been measured up to now, the comparison is based on gds large-scale shell-model calculations as well as on results from Hartree-Fock random-phase approximation [72]. For the 6_1^+ state in ^{100}Sn, the possible existence of $E2$ isomerism has been proposed and discussed by Refs. [66, 80]. The theoretical calculations yielded $B(E2)$ values of ≈ 1 W.u. at transition energies of 58 keV to 297 keV. For the gds LSSM calculations, this corresponds to a lifetime value of 2.5 µs which could not be corroborated by latest experiments [70, 71]. Assuming a higher $B(E2)$ value of approximately 5 W.u., like in ^{56}Ni, the corresponding lifetime would drop to 3 ns or 700 ns depending on the transition-energy predictions of the HF-RPA and gds LSSM calculations, respectively. A smaller lifetime of the 6_1^+ state could be an explanation for the absence of time-delayed γ rays in a previous experiment with detection capabilities of 300 ns [71]. The newly determined lifetimes in ^{56}Ni draw

again attention to the even-even neighbor ^{60}Zn, which is the only nuclide along the $N = Z$ line of even-even nuclei between ^{4}He and ^{80}Zr with no experimental values on excited states' lifetimes available (see Ref. [39]).

Within the scope of this thesis a total of ten nuclear-level lifetimes in the range of 610 fs to 110 ps were determined along the $N = Z$ line. The corresponding reduced $E2$, $E2/M1$, and $E1$ transition strengths showed enhanced values with respect to the isotopic and isotonic systematics. The results from ground-state band decays are summarized in Figs. 8(b,d,f). The evolution of collectivity is shown along the $N = Z$ line. For comparison, the corresponding excitation energies are given in Figs. 8(a,c,e). The experimental results are confronted with shell-model results using the well-established GXPF1A interaction. For the calculation of $B(E2)$ values, effective charges of $e_\pi = 1.31$ and $e_\nu = 0.46$ were used for protons and neutrons, respectively. These were microscopically deduced in Ref. [11] and are generally not restricted to a specific region.

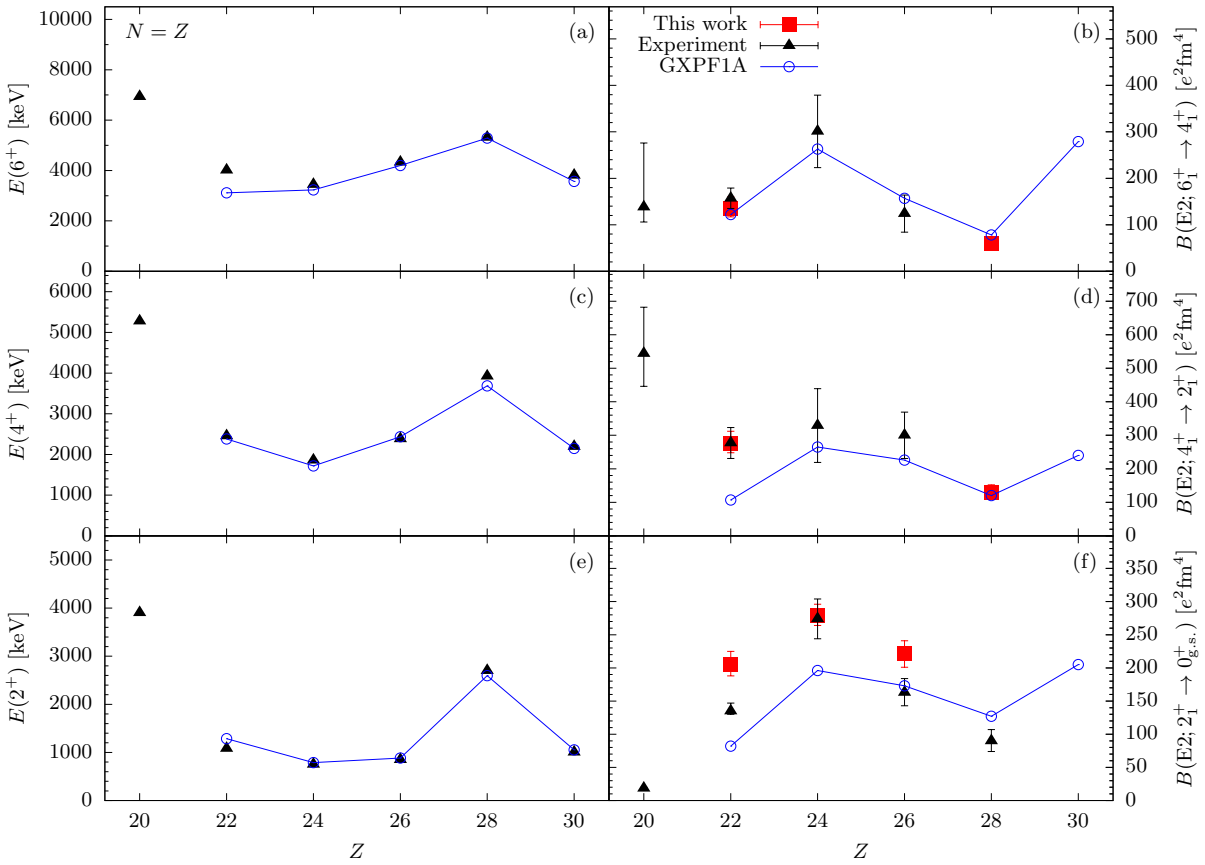

Figure 8: Excitation energies of the (e) 2_1^+, (c) 4_1^+, and (a) 6_1^+ states, as well as $B(E2)$ values for the (f) $2_1^+ \rightarrow 0_{\text{g.s.}}^+$, (d) $4_1^+ \rightarrow 2_1^+$, and (b) $6_1^+ \rightarrow 4_1^+$ transitions are plotted for $N = Z$ nuclei between $^{40}_{20}$Ca and $^{60}_{30}$Zn. Results obtained in this work are given as red filled squares, values obtained from Refs. [38, 39, 81, 82] are given as black filled triangles. For comparison, shell-model results from the GXPF1A interaction are shown as blue open circles. See text for details.

The adopted excitation-energy values are well reproduced by the GXPF1A interaction which only underestimates the 6_1^+ state in ^{44}Ti. The $B(E2)$ values of the $2_1^+ \rightarrow 0_{\text{g.s.}}^+$ and $4_1^+ \rightarrow 2_1^+$ in ^{44}Ti ($Z = 22$) are considerably underestimated by the GXPF1A interaction which has been discussed in detail in the second publication of this thesis and was explained by additional contributions of particle-hole excitations caused by sd-fp cross-shell excitations. While the values for the 6_1^+ and 4_1^+ decays are in agreement with previous results, the new $B(E2)$ value of the $2_1^+ \rightarrow 0_{\text{g.s.}}^+$ transition overpredicts the adopted value. Above $Z = 22$, the GXPF1A interaction provides a good description of the $B(E2)$ values of the 6_1^+ and 4_1^+ decays. However, for the $2_1^+ \rightarrow 0_{\text{g.s.}}^+$ transitions in ^{48}Cr and ^{52}Fe, the shell model underestimates the present values. The new values for the spin-orbit shell closure at ^{56}Ni are in good agreement with the calculation.

Future experiments along the $N = Z$ line

The $N = Z$ line will remain in future a fertile testing ground for modern shell-model interactions. Above ^{56}Ni, it offers the possibility to study the evolution of nuclear ground-state shapes which are predicted to change with increasing mass from spherical ($^{56}_{28}$Ni) to triaxial ($^{64}_{32}$Ge [83]), oblate ($^{72}_{36}$Kr [84]), prolate ($^{76}_{38}$Sr [85]), and back again to spherical towards $^{100}_{50}$Sn (see Ref. [86] for more details). For $^{60}_{30}$Zn, which is located two protons and two neutrons above doubly-magic ^{56}Ni and below ^{64}Ge, calculations based on the Hartree-Fock-Bogoliubov (HFB) formalism, utilizing the finite-range Gogny D1S effective nucleon-nucleon interaction, predict a moderately prolate-deformed shape (see Fig. 5 in Ref. [87]). An investigation of $B(E2)$ values of the ground-state band will give insights to the structure and the shape of ^{60}Zn. From the intrinsic quadrupole moment, the quadrupole deformation parameter β_2 can be obtained and compared with the calculations from Ref. [87]. Moreover, reduced transition strengths along the ground-state band are of particular interest as this band is predicted to show contributions of an α-cluster component [88].

However, until now, no experimental $B(E2)$ values are available for this nucleus. Previous lifetime experiments with stable beams were challenged by a large number of different reaction channels contributing to the γ-ray background and by insufficient production yields, e.g. for the promising 2np exit channel, which was already used for lifetime measurements in ^{44}Ti, ^{52}Fe, and ^{56}Ni within this work, a theoretical cross section of $\sigma_{\text{theo.}} = 4$ mb was obtained with the computer code CASCADE [89]. Within the scope of this thesis, a commissioning experiment employing the Cologne coincidence plunger setup combined with twelve HPGe detectors was performed at the FN tandem accelerator at the Institute for Nuclear Physics (University of Cologne) utilizing a ^{40}Ca(^{23}Na, 2np)^{60}Zn fusion-evaporation reaction at 62 MeV beam energy. Within a $\gamma\gamma$ analysis the first excited 2^+ and 4^+ states were identified in a γ-gated energy spectrum summed over all target-to-stopper distances. An exemplary γ-ray spectrum is shown in Fig. 9. However, a lifetime analysis was not practicable as the statistics in the spectra of single distances were insufficient.

Refined experiments have to be considered in order to determine lifetimes in the ground-state band of ^{60}Zn. Today, high-efficiency high-resolution γ-ray spectrometer, such as the Advanced GAmma Tracking Array (AGATA) [90] or the GALILEO spectrometer [91] can be coupled to powerful ancillary-

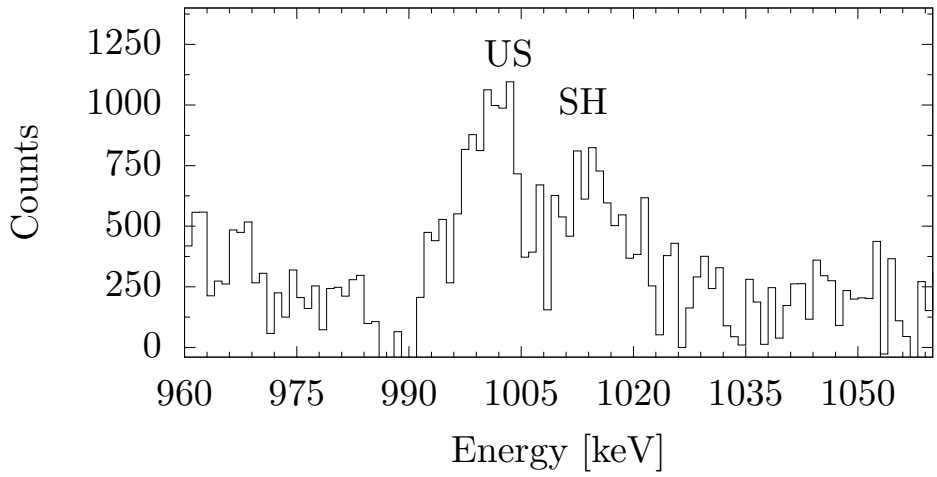

Figure 9: γ-ray spectrum of the $2_1^+ \rightarrow 0_{g.s.}^+$ transition at 1004 keV in ^{60}Zn after ^{40}Ca + ^{23}Na fusion-evaporation reactions at 62 MeV beam energy. The spectrum is produced by a γ gate onto the complete $4_1^+ \rightarrow 2_1^+$ transition including the Doppler-shifted components of all distances. The Doppler-shifted (SH) and unshifted (US) components are labeled.

detector systems such as the NEutron Detector Array NEDA [92] or the 4π charged-particle detector EUCLIDES [93] to track down most elusive reaction channels.

Alternatively, the $B(E2)$ values for the $2_1^+ \rightarrow 0_{g.s.}^+$ and, eventually, the $4_1^+ \rightarrow 2_1^+$ transitions can be directly extracted from Coulomb excitation measurements with a radioactive-ion beam. Therefore, the MINIBALL [94] setup at HIE-ISOLDE (CERN) [95] could be an option for a future experiment in which ^{60}Zn ions can be extracted from a ZrO_2 felt with yields up to $2.1 \cdot 10^5$ ions/μC [96]. Similar experiments were performed for neutron-rich zinc isotopes at REX-ISOLDE in the past [97].

Further studies along the $N = Z$ line towards doubly-magic ^{100}Sn require large particle accelerators providing high beam energies and sophisticated measuring instruments. Vigorous effort is made at radioactive ion-beam facilities [98] around the world – such as the Rikagaku Kenkyūjo (RIKEN, Japan) employing the BigRIPS fragement separator [99], the Facility for Rare Isotope Beams (FRIB) and the National Superconducting Cyclotron Laboratory (NSCL, United States) [100], the Gesellschaft für Schwerionenforschung (GSI, Germany) employing the projectile fragment separator (FRS) [101], the SPIRAL2 accelerator at the Grand Accélérateur National d'Ions Lourds (GANIL, France) [102], and the HIE-ISOLDE facility [95] at the Conseil Européen pour la Recherche Nucléaire (CERN, Switzerland/France) – pushing the frontiers to exotic nuclei far from stability and filling the blank on the nuclide chart. At these facilities experiments can be conceived to investigate basic properties of highly-exotic nuclear systems and to benchmark fundamental nuclear models.

Bibliography

[1] M. G. Mayer. "On Closed Shells in Nuclei. II." *Phys. Rev.* 75 (June 1949), pp. 1969–1970 (cit. on pp. 7–8).

[2] O. Haxel, J. H. D. Jensen and H. E. Suess. "On the "Magic Numbers" in Nuclear Structure." *Phys. Rev.* 75 (June 1949), pp. 1766–1766 (cit. on pp. 7–8).

[3] T. Otsuka, M. Honma, T. Mizusaki, N. Shimizu and Y. Utsuno. "Monte Carlo shell model for atomic nuclei." *Prog. Part. Nucl. Phys.* 47.1 (2001), pp. 319–400 (cit. on p. 7).

[4] E. Caurier, G. Martínez-Pinedo, F. Nowacki, A. Poves and A. P. Zuker. "The shell model as a unified view of nuclear structure." *Rev. Mod. Phys.* 77 (June 2005), pp. 427–488 (cit. on pp. 7, 13).

[5] Y. Z. Ma, L. Coraggio, L. De Angelis, T. Fukui, A. Gargano, N. Itaco and F. R. Xu. "Contribution of chiral three-body forces to the monopole component of the effective shell-model Hamiltonian." *Phys. Rev. C* 100.3 (2019), p. 034324 (cit. on pp. 7, 12).

[6] R. F. Casten. Nuclear Structure from a Simple Perspective. 2nd ed. Oxford University Press, 2000 (cit. on pp. 8, 13–14, 18–19).

[7] K. Arnswald. "Lifetime measurements in self-conjugate nuclei ^{44}Ti, ^{48}Cr, and ^{52}Fe," MA thesis. Institut für Kernphysik, Universität zu Köln, 2016 (cit. on pp. 8, 22).

[8] K. Heyde. The Nuclear Shell Model. Second Corrected and Enlarged Edition. Springer-Verlag, 1994 (cit. on pp. 9–10, 18).

[9] M. Seidlitz. "Nuclear shell effects in neutron-roch nuclei around $N = 20$ and $N = 32, 34$." PhD thesis. Universität zu Köln, 2012 (cit. on p. 9).

[10] T. Kuo and G. Brown. "Structure of finite nuclei and the free nucleon-nucleon interaction: An application to ^{18}O and ^{18}F." *Nucl. Phys.* 85.1 (1966), pp. 40–86 (cit. on p. 10).

[11] M. Dufour and A. P. Zuker. "Realistic collective nuclear Hamiltonian." *Phys. Rev. C* 54 (Oct. 1996), pp. 1641–1660 (cit. on pp. 10, 60).

[12] M. Hjorth-Jensen, T. T. S. Kuo and E. Osnes. "Realistic effective interactions for nuclear systems." *Phys. Rep.* 261 (1995), pp. 125–270 (cit. on pp. 10, 21).

[13] M. Honma, T. Otsuka, B. A. Brown and T. Mizusaki. "New effective interaction for pf-shell nuclei and its implications for the stability of the $N = Z = 28$ closed core." *Phys. Rev. C* 69 (Mar. 2004), p. 034335 (cit. on pp. 10–12, 59).

[14] W. A. Richter, M. G. Van Der Merwe, R. E. Julies and B. A. Brown. "New effective interactions for the 0f1p shell." *Nucl. Phys. A* 523.2 (1991), pp. 325–353 (cit. on pp. 10, 57).

[15] E. Caurier, G. Martínez-Pinedo, A. Poves and A. P. Zuker. "Gamow-Teller strength in ^{54}Fe and ^{56}Fe." *Phys. Rev. C* 52 (Oct. 1995), R1736–R1740 (cit. on p. 10).

[16] K. Arnswald, T. Braunroth, M. Seidlitz, L. Coraggio, P. Reiter, B. Birkenbach, A. Blazhev, A. Dewald, C. Fransen, B. Fu, A. Gargano, H. Hess, R. Hirsch, N. Itaco, S. Lenzi, L. Lewandowski,

J. Litzinger, C. Müller-Gatermann, M. Queiser, D. Rosiak, D. Schneiders, B. Siebeck, T. Steinbach, A. Vogt, K. Wolf and K. Zell. "Enhanced collectivity along the $N = Z$ line: Lifetime measurements in ^{44}Ti, ^{48}Cr, and ^{52}Fe." *Phys. Lett. B* 772 (2017), pp. 599–606 (cit. on pp. 10, 12–13, 16, 18, 20, 22, 57).

[17] K. Arnswald, P. Reiter, A. Blazhev, T. Braunroth, A. Dewald, M. Droste, C. Fransen, A. Goldkuhle, R. Hetzenegger, R. Hirsch, E. Hoemann, L. Kaya, L. Lewandowski, C. Müller-Gatermann, P. Petkov, D. Rosiak, M. Seidlitz, B. Siebeck, A. Vogt, D. Werner, K. Wolf and K.-O. Zell. "Lifetime measurements in ^{44}Ti." *Phys. Rev. C* 102 (Nov. 2020), p. 054302 (cit. on pp. 10, 12–13, 20, 22, 58).

[18] M. Honma, T. Otsuka, B. A. Brown and T. Mizusaki. "Shell-model description of neutron-rich pf-shell nuclei with a new effective interaction GXPF1." *Eur. Phys. J. A* 25.1 (2005), pp. 499–502 (cit. on pp. 10, 57).

[19] K. Jha, P. Kumar, S. Sarkar, P. Raina and S. Aydin. "A way forward towards the improvement of tensor force in pf-shell." *Nucl. Phys. A* 1004 (2020), p. 122038 (cit. on p. 11).

[20] K. Arnswald, A. Blazhev, F. Nowacki, P. Petkov, P. Reiter, T. Braunroth, A. Dewald, M. Droste, C. Fransen, R. Hirsch, V. Karayonchev, L. Kaya, L. Lewandowski, C. Müller-Gatermann, M. Seidlitz, B. Siebeck, A. Vogt, D. Werner and K. Zell. "Enhanced quadrupole collectivity in doubly-magic ^{56}Ni: Lifetime measurements of the 4_1^+ and 6_1^+ states." *Phys. Lett. B* 820 (2021), p. 136592 (cit. on pp. 11–12, 16, 21, 23, 59).

[21] A. Poves, J. Sánchez-Solano, E. Caurier and F. Nowacki. "Shell model study of the isobaric chains $A = 50$, $A = 51$ and $A = 52$." *Nucl. Phys. A* 694.1-2 (2001), pp. 157–198 (cit. on pp. 11, 57).

[22] A. Poves and A. Zuker. "Theoretical spectroscopy and the *f p* shell." *Phys. Rep.* 70.4 (1981), pp. 235–314 (cit. on p. 11).

[23] T. Kuo and G. Brown. "Reaction matrix elements for the 0f-1p shell nuclei." *Nucl. Phys. A* 114.2 (1968), pp. 241–279 (cit. on p. 11).

[24] F. Nowacki, A. Poves, E. Caurier and B. Bounthong. "Shape Coexistence in ^{78}Ni as the Portal to the Fifth Island of Inversion." *Phys. Rev. Lett.* 117 (Dec. 2016), p. 272501 (cit. on p. 12).

[25] R. Taniuchi, C. Santamaria, P. Doornenbal, A. Obertelli, K. Yoneda, G. Authelet, H. Baba, D. Calvet, F. Château, A. Corsi, A. Delbart, J.-M. Gheller, A. Gillibert, J. D. Holt, T. Isobe, V. Lapoux, M. Matsushita, J. Menéndez, S. Momiyama, T. Motobayashi, M. Niikura, F. Nowacki, K. Ogata, H. Otsu, T. Otsuka, C. Péron, S. Péru, A. Peyaud, E. C. Pollacco, A. Poves, J.-Y. Roussé, H. Sakurai, A. Schwenk, Y. Shiga, J. Simonis, S. R. Stroberg, S. Takeuchi, Y. Tsunoda, T. Uesaka, H. Wang, F. Browne, L. X. Chung, Z. Dombradi, S. Franchoo, F. Giacoppo, A. Gottardo, K. Hadyńska-Klęk, Z. Korkulu, S. Koyama, Y. Kubota, J. Lee, M. Lettmann, C. Louchart, R. Lozeva, K. Matsui, T. Miyazaki, S. Nishimura, L. Olivier, S. Ota, Z. Patel, E. Şahin, C. Shand, P.-A. Söderström, I. Stefan, D. Steppenbeck, T. Sumikama, D. Suzuki, Z. Vajta, V. Werner, J. Wu and Z. Y. Xu. "^{78}Ni revealed as a doubly magic stronghold against nuclear deformation." *Nature* 569.7754 (May 2019), pp. 53–58 (cit. on p. 12).

[26] L. Coraggio, A. Covello, A. Gargano, N. Itaco and T. T. S. Kuo. "Effective shell-model hamiltonians from realistic nucleon-nucleon potentials within a perturbative approach." *Ann. Phys.* 327.9 (2012), pp. 2125–2151 (cit. on p. 12).

[27] R. Machleidt. "High-precision, charge-dependent Bonn nucleon-nucleon potential." *Phys. Rev. C* 63 (Jan. 2001), p. 024001 (cit. on p. 12).

[28] K. Sieja and F. Nowacki. "Three-body forces and persistence of spin-orbit shell gaps in medium-mass nuclei: Toward the doubly magic ^{78}Ni." *Phys. Rev. C* 85 (May 2012), p. 051301 (cit. on p. 12).

[29] E. Caurier, K. Langanke, G. Martínez-Pinedo, F. Nowacki and P. Vogel. "Shell model description of isotope shifts in calcium." *Phys. Lett. B* 522.3 (2001), pp. 240–244 (cit. on pp. 12, 58).

[30] H. Hasper. "Large scale shell-model calculations in the upper part of the sd shell: General description and energy levels for $A = 36 - 39$." *Phys. Rev. C* 19 (Apr. 1979), pp. 1482–1497 (cit. on p. 12).

[31] M. L. Bissell, J. Papuga, H. Naïdja, K. Kreim, K. Blaum, M. De Rydt, R. F. Garcia Ruiz, H. Heylen, M. Kowalska, R. Neugart, G. Neyens, W. Nörtershäuser, F. Nowacki, M. M. Rajabali, R. Sanchez, K. Sieja and D. T. Yordanov. "Proton-Neutron Pairing Correlations in the Self-Conjugate Nucleus ^{38}K Probed via a Direct Measurement of the Isomer Shift." *Phys. Rev. Lett.* 113 (July 2014), p. 052502 (cit. on pp. 12, 58).

[32] B. A. Brown and W. D. M. Rae. "The Shell-Model Code NuShellX@MSU." *Nucl. Data Sheets* 120 (2014), pp. 115–118 (cit. on p. 13).

[33] N. Shimizu. Nuclear shell-model code for massive parallel computation, "KSHELL". 2013 (cit. on p. 13).

[34] N. Shimizu, T. Mizusaki, Y. Utsuno and Y. Tsunoda. "Thick-restart block Lanczos method for large-scale shell-model calculations." *Comput. Phys. Commun.* 244 (2019), pp. 372–384 (cit. on p. 13).

[35] A. Vogt. "Multinucleon-Transfer Reactions as a Gateway to Neutron-Rich Actinides and Nuclei near the $N = 82$ and $Z = 50$ Shell Closures." PhD thesis. Institut für Kernphysik, Universität zu Köln, 2017 (cit. on p. 13).

[36] K. Alder, A. Bohr, T. Huus, B. Mottelson and A. Winther. "Study of Nuclear Structure by Electromagnetic Excitation with Accelerated Ions." *Rev. Mod. Phys.* 28 (Oct. 1956), pp. 432–542 (cit. on p. 14).

[37] S. Raman, C. Nestor and P. Tikkanen. "Transition probability from the ground to the first-excited 2^+ state of even-even nuclides." *At. Data Nucl. Data Tables* 78.1 (2001), pp. 1–128 (cit. on p. 14).

[38] B. Pritychenko, M. Birch, B. Singh and M. Horoi. "Tables of E2 transition probabilities from the first 2^+ states in even-even nuclei." *At. Data Nucl. Data Tables* 107 (2016), pp. 1–139 (cit. on pp. 15, 60).

[39] Evaluated Nuclear Structure Data File (ENSDF). URL: `http://www.nndc.bnl.gov/ensdf` (cit. on pp. 15–17, 60).

[40] M. Seidlitz, P. Reiter, A. Dewald, O. Möller, B. Bruyneel, S. Christen, F. Finke, C. Fransen, M. Górska, H. Grawe, A. Holler, G. Ilie, T. Kotthaus, P. Kudejová, S. M. Lenzi, S. Mandal, B. Melon, D. Mücher, J.-M. Regis, B. Saha, P. von Brentano, A. Wiens and K. O. Zell. "Precision lifetime measurements of the first 2^+ and 4^+ states in ^{56}Cr at the $N = 32$ subshell closure." *Phys. Rev. C* 84 (Sept. 2011), p. 034318 (cit. on pp. 15–16).

[41] A. Goldkuhle, C. Fransen, A. Blazhev, M. Beckers, B. Birkenbach, T. Braunroth, E. Clément, A. Dewald, J. Dudouet, J. Eberth, H. Hess, B. Jacquot, J. Jolie, Y.-H. Kim, A. Lemasson, S. M. Lenzi, H. J. Li, J. Litzinger, C. Michelagnoli, C. Müller-Gatermann, B. S. Nara Singh, R. M. Pérez-Vidal, D. Ralet, P. Reiter, A. Vogt, N. Warr, K. O. Zell, A. Ataç, D. Barrientos,

C. Barthe-Dejean, G. Benzoni, A. J. Boston, H. C. Boston, P. Bourgault, I. Burrows, J. Cacitti, B. Cederwall, M. Ciemala, D. M. Cullen, G. De France, C. Domingo-Pardo, J.-L. Foucher, G. Fremont, A. Gadea, P. Gangnant, V. González, J. Goupil, C. Henrich, C. Houarner, M. Jean, D. S. Judson, A. Korichi, W. Korten, M. Labiche, A. Lefevre, L. Legeard, F. Legruel, S. Leoni, J. Ljungvall, A. Maj, C. Maugeais, L. Ménager, N. Ménard, R. Menegazzo, D. Mengoni, B. Million, H. Munoz, D. R. Napoli, A. Navin, J. Nyberg, M. Ozille, Z. Podolyak, A. Pullia, B. Raine, F. Recchia, J. Ropert, F. Saillant, M. D. Salsac, E. Sanchis, C. Schmitt, J. Simpson, C. Spitaels, O. Stezowski, C. Theisen, M. Toulemonde, M. Tripon, J.-J. Valiente Dobón, G. Voltolini and M. Zielińska. "Lifetime measurements in ^{52,54}Ti to study shell evolution toward $N = 32$." *Phys. Rev. C* 100 (Nov. 2019), p. 054317 (cit. on pp. 15–17).

[42] C. Loelius, H. Iwasaki, B. A. Brown, M. Honma, V. M. Bader, T. Baugher, D. Bazin, J. S. Berryman, T. Braunroth, C. M. Campbell, A. Dewald, A. Gade, N. Kobayashi, C. Langer, I. Y. Lee, A. Lemasson, E. Lunderberg, C. Morse, F. Recchia, D. Smalley, S. R. Stroberg, R. Wadsworth, C. Walz, D. Weisshaar, A. Westerberg, K. Whitmore and K. Wimmer. "Lifetime measurement of the 4_1^+ state of ^{58}Ni with the recoil distance method." *Phys. Rev. C* 94 (Aug. 2016), p. 024340 (cit. on pp. 15, 17).

[43] R. Ernst, K.-H. Speidel, O. Kenn, U. Nachum, J. Gerber, P. Maier-Komor, N. Benczer-Koller, G. Jakob, G. Kumbartzki, L. Zamick and F. Nowacki. "Stringent Tests of Shell Model Calculations in *fp* Shell Nuclei ^{46,48}Ti and ^{50,52}Cr from Measurements of g Factors and $B(E2)$ Values." *Phys. Rev. Lett.* 84 (Jan. 2000), pp. 416–419 (cit. on p. 15).

[44] R. Janssens, B. Fornal, P. Mantica, B. Brown, R. Broda, P. Bhattacharyya, M. Carpenter, M. Cinausero, P. Daly, A. Davies, T. Glasmacher, Z. Grabowski, D. Groh, M. Honma, F. Kondev, W. Królas, T. Lauritsen, S. Liddick, S. Lunardi, N. Marginean, T. Mizusaki, D. Morrissey, A. Morton, W. Mueller, T. Otsuka, T. Pawlat, D. Seweryniak, H. Schatz, A. Stolz, S. Tabor, C. Ur, G. Viesti, I. Wiedenhöver and J. Wrzesiński. "Structure of ^{52,54}Ti and shell closures in neutron-rich nuclei above 48Ca." *Phys. Lett. B* 546.1 (2002), pp. 55–62 (cit. on p. 14).

[45] J. Prisciandaro, P. Mantica, B. Brown, D. Anthony, M. Cooper, A. Garcia, D. Groh, A. Komives, W. Kumarasiri, P. Lofy, A. Oros-Peusquens, S. Tabor and M. Wiedeking. "New evidence for a subshell gap at $N = 32$." *Phys. Lett. B* 510.1 (2001), pp. 17–23 (cit. on p. 14).

[46] K. L. Yurkewicz, D. Bazin, B. A. Brown, C. M. Campbell, J. A. Church, D. C. Dinca, A. Gade, T. Glasmacher, M. Honma, T. Mizusaki, W. F. Mueller, H. Olliver, T. Otsuka, L. A. Riley and J. R. Terry. "Nuclear structure in the vicinity of $N = Z = 28$ ^{56}Ni." *Phys. Rev. C* 70 (Nov. 2004), p. 054319 (cit. on pp. 16, 59).

[47] A. Bohr and B. R. Mottelson. Nuclear Structure. 2nd ed. Vol. 2. World Scientific Publishing Co. Pte. Ltd., 1998 (cit. on p. 17).

[48] R. B. Cakirli, R. F. Casten, J. Jolie and N. Warr. "Highly anomalous yrast $B(E2)$ values and vibrational collectivity." *Phys. Rev. C* 70 (Oct. 2004), p. 047302 (cit. on pp. 17–18).

[49] R. Broda, B. Fornal, W. Królas, T. Pawłat, J. Wrzesiński, D. Bazzacco, S. Lunardi, G. De Angelis, A. Gadea, C. Ur, N. Marginean, R. Janssens, M. Carpenter, S. Freeman, N. Hammond, T. Lauritsen, C. Lister, F. Moore, D. Seweryniak, P. Daly, Z. Grabowski, B. Brown and M. Honma. "Yrast states in $N = 30$ ^{50}Ca and ^{51}Sc isotones studied with deep-inelastic heavy ion reactions." *Acta Phys. Pol. B* 36 (2005), pp. 1343–1350 (cit. on p. 17).

[50] E. Ideguchi, D. G. Sarantites, W. Reviol, A. V. Afanasjev, M. Devlin, C. Baktash, R. V. F. Janssens, D. Rudolph, A. Axelsson, M. P. Carpenter, A. Galindo-Uribarri, D. R. LaFosse, T. Lauritsen, F. Lerma, C. J. Lister, P. Reiter, D. Seweryniak, M. Weiszflog and J. N. Wilson. "Superdeformation

in the Doubly Magic Nucleus $^{40}_{20}Ca_{20}$." *Phys. Rev. Lett.* 87 (Nov. 2001), p. 222501 (cit. on p. 18).

[51] D. Hertz-Kintish, L. Zamick and S. J. Q. Robinson. "$B(E2, 4 \to 2)/B(E2, 2 \to 0)$ ratio in even-even nuclei: Apparent anomalous behavior of the chromium isotopes." *Phys. Rev. C* 90 (Sept. 2014), p. 034307 (cit. on p. 18).

[52] R. D. O. Llewellyn, M. A. Bentley, R. Wadsworth, H. Iwasaki, J. Dobaczewski, G. de Angelis, J. Ash, D. Bazin, P. C. Bender, B. Cederwall, B. P. Crider, M. Doncel, R. Elder, B. Elman, A. Gade, M. Grinder, T. Haylett, D. G. Jenkins, I. Y. Lee, B. Longfellow, E. Lunderberg, T. Mijatović, S. A. Milne, D. Muir, A. Pastore, D. Rhodes and D. Weisshaar. "Establishing the Maximum Collectivity in Highly Deformed $N = Z$ Nuclei." *Phys. Rev. Lett.* 124 (Apr. 2020), p. 152501 (cit. on p. 19).

[53] P. Petkov, C. Müller-Gatermann, D. Werner, A. Dewald, A. Blazhev, C. Fransen, J. Jolie, S. Ohkubo and K. O. Zell. "New lifetime measurements for the lowest quadrupole states in ^{20,22}Ne and possible explanations of the high collectivity of the depopulating $E2$ transitions." *Phys. Rev. C* 100 (Aug. 2019), p. 024312 (cit. on p. 19).

[54] K. Kaneko, Y. Sun and G. de Angelis. "Enhancement of high-spin collectivity in $N = Z$ nuclei by the isoscalar neutron-proton pairing." *Nucl. Phys. A* 957 (2017), pp. 144–153 (cit. on p. 19).

[55] D. A. Bromley. "Clustering Phenomena in the Nuclear Many-Body System." *Clustering Aspects of Nuclear Structure: Invited Papers presented at the 4th International Conference on Clustering Aspects of Nuclear Structure and Nuclear Reactions, Chester, United Kingdom, 23–27 July, 1984*. Ed. by J. S. Lilley and M. A. Nagarajan. Dordrecht: Springer Netherlands, 1985, pp. 1–32 (cit. on p. 20).

[56] H. Horiuchi and K. Ikeda. "A Molecule-like Structure in Atomic Nuclei of 16O* and 10Ne." *Prog. Theor. Phys.* 40.2 (Aug. 1968), pp. 277–287 (cit. on p. 20).

[57] H. Horiuchi. "Microscopic Study of the Dependence of the Light Ion Potential on the Projectile Mass Number." *Prog. Theor. Phys.* 73.5 (May 1985), pp. 1172–1190 (cit. on p. 20).

[58] T. Yamaya, S. Oh-ami, M. Fujiwara, T. Itahashi, K. Katori, M. Tosaki, S. Kato, S. Hatori and S. Ohkubo. "Existence of α-cluster structure in ^{44}Ti via the (^{6}Li,d) reaction." *Phys. Rev. C* 42 (Nov. 1990), pp. 1935–1944 (cit. on pp. 20, 58).

[59] T. Yamaya, M. Saito, M. Fujiwara, T. Itahashi, K. Katori, T. Suehiro, S. Kato, S. Hatori and S. Ohkubo. "Alpha-cluster bands in ^{40}Ca observed via the (^{6}Li, d) reaction." *Phys. Lett. B* 306.1 (1993), pp. 1–5 (cit. on pp. 20, 58).

[60] T. Yamaya, M. Saitoh, M. Fujiwara, T. Itahashi, K. Katori, T. Suehiro, S. Kato, S. Hatori and S. Ohkubo. "Cluster structure in ^{40}Ca via the α-transfer reaction." *Nucl. Phys. A* 573.1 (1994), pp. 154–172 (cit. on pp. 20, 58).

[61] T. Yamaya, K. Ishigaki, H. Ishiyama, T. Suehiro, S. Kato, M. Fujiwara, K. Katori, M. H. Tanaka, S. Kubono, V. Guimaraes and S. Ohkubo. "α-cluster states above the threshold energy in ^{44}Ti." *Phys. Rev. C* 53 (Jan. 1996), pp. 131–136 (cit. on pp. 20, 58).

[62] S. Ohkubo, Y. Hirabayashi and T. Sakuda. "α-cluster structure of ^{44}Ti in core-excited α+^{40}Ca model." *Phys. Rev. C* 57 (May 1998), pp. 2760–2762 (cit. on pp. 20, 58).

[63] M. Kimura and H. Horiuchi. "Coexistence of cluster structure and superdeformation in ^{44}Ti." *Nucl. Phys. A* 767 (2006), pp. 58–80 (cit. on pp. 20, 58).

[64] J. Erler, N. Birge, M. Kortelainen, W. Nazarewicz, E. Olsen, A. M. Perhac and M. Stoitsov. "The limits of the nuclear landscape." *Nature* 486.7404 (June 2012), pp. 509–512 (cit. on p. 20).

[65] H. Schatz and K. Rehm. "X-ray binaries." *Nucl. Phys. A* 777 (2006). Special Issue on Nuclear Astrophysics, pp. 601–622 (cit. on p. 21).

[66] T. Faestermann, M. Górska and H. Grawe. "The structure of ^{100}Sn and neighbouring nuclei." *Prog. Part. Nucl. Phys.* 69 (2013), pp. 85–130 (cit. on pp. 21–22, 59).

[67] H. Schatz, A. Aprahamian, V. Barnard, L. Bildsten, A. Cumming, M. Ouellette, T. Rauscher, F.-K. Thielemann and M. Wiescher. "End Point of the *rp* Process on Accreting Neutron Stars." *Phys. Rev. Lett.* 86 (Apr. 2001), pp. 3471–3474 (cit. on p. 21).

[68] H. Schatz and A. Aprahamian and J. Görres and M. Wiescher and T. Rauscher and J.F. Rembges and F.-K. Thielemann and B. Pfeiffer and P. Möller and K.-L. Kratz and H. Herndl and B.A. Brown and H. Rebel. "rp-process nucleosynthesis at extreme temperature and density conditions." *Phys. Rep.* 294.4 (1998), pp. 167–263 (cit. on p. 21).

[69] B. A. Brown, R. R. C. Clement, H. Schatz, A. Volya and W. A. Richter. "Proton drip-line calculations and the rp process." *Phys. Rev. C* 65 (Mar. 2002), p. 045802 (cit. on p. 21).

[70] C. B. Hinke, M. Böhmer, P. Boutachkov, T. Faestermann, H. Geissel, J. Gerl, R. Gernhäuser, M. Górska, A. Gottardo, H. Grawe, J. L. Grębosz, R. Krücken, N. Kurz, Z. Liu, L. Maier, F. Nowacki, S. Pietri, Z. Podolyák, K. Sieja, K. Steiger, K. Straub, H. Weick, H.-J. Wollersheim, P. J. Woods, N. Al-Dahan, N. Alkhomashi, A. Ataç, A. Blazhev, N. F. Braun, I. T. Čeliković, T. Davinson, I. Dillmann, C. Domingo-Pardo, P. C. Doornenbal, G. de France, G. F. Farrelly, F. Farinon, N. Goel, T. C. Habermann, R. Hoischen, R. Janik, M. Karny, A. Kaşkaş, I. M. Kojouharov, T. Kröll, Y. Litvinov, S. Myalski, F. Nebel, S. Nishimura, C. Nociforo, J. Nyberg, A. R. Parikh, A. Procházka, P. H. Regan, C. Rigollet, H. Schaffner, C. Scheidenberger, S. Schwertel, P.-A. Söderström, S. J. Steer, A. Stolz and P. Strmeň. "Superallowed Gamow–Teller decay of the doubly magic nucleus ^{100}Sn." *Nature* 486.7403 (June 2012), pp. 341–345 (cit. on pp. 21, 59).

[71] J. Park, R. Krücken, D. Lubos, R. Gernhäuser, M. Lewitowicz, S. Nishimura, D. S. Ahn, H. Baba, B. Blank, A. Blazhev, P. Boutachkov, F. Browne, I. Čeliković, G. de France, P. Doornenbal, T. Faestermann, Y. Fang, N. Fukuda, J. Giovinazzo, N. Goel, M. Górska, H. Grawe, S. Ilieva, N. Inabe, T. Isobe, A. Jungclaus, D. Kameda, G. D. Kim, Y.-K. Kim, I. Kojouharov, T. Kubo, N. Kurz, G. Lorusso, K. Moschner, D. Murai, I. Nishizuka, Z. Patel, M. M. Rajabali, S. Rice, H. Sakurai, H. Schaffner, Y. Shimizu, L. Sinclair, P.-A. Söderström, K. Steiger, T. Sumikama, H. Suzuki, H. Takeda, Z. Wang, H. Watanabe, J. Wu and Z. Y. Xu. "Properties of γ-decaying isomers and isomeric ratios in the ^{100}Sn region." *Phys. Rev. C* 96 (Oct. 2017), p. 044311 (cit. on pp. 21, 59).

[72] V. I. Isakov and K. I. Erokhina. "Nuclear masses and properties of nuclei in the vicinity of the remote magic nucleus ^{100}Sn." *Phys. At. Nucl.* 65.8 (Aug. 2002), pp. 1431–1443 (cit. on pp. 22, 59).

[73] H. Grawe. "Shell Model from a Practitioner's Point of View." *The Euroschool Lectures on Physics with Exotic Beams, Vol. I*. Ed. by J. Al-Khalili and E. Roeckl. Berlin, Heidelberg: Springer Berlin Heidelberg, 2004, pp. 33–75 (cit. on p. 57).

[74] W. R. Dixon, R. S. Storey and J. J. Simpson. "Levels of ^{44}Ti from the ^{40}Ca$(\alpha,\gamma)^{44}$Ti reaction." *Phys. Rev. C* 15 (May 1977), pp. 1896–1910 (cit. on p. 58).

[75] C. Michelagnoli, C. A. Ur, E. Farnea, S. M. Lenzi, S. Lunardi, F. Recchia, N. Marginean, D. Bucurescu, G. Cata-Danil, D. Delenau, D. Filipescu, D. Ghita, T. Glodariu, R. Marginean, C. Mihai, A. Negret, S. Pascu, T. Sava, L. Stroe and G. Suliman. "Lifetime Measurement in $N = Z$ Nucleus ^{44}Ti." *Acta. Phys. Pol. B* 42.3 (2011), pp. 825–828 (cit. on p. 58).

[76] J. J. Simpson, W. Dünnweber, J. P. Wurm, P. W. Green, J. A. Kuehner, W. R. Dixon and R. S. Storey. "Yrast levels in ^{44}Ti." *Phys. Rev. C* 12 (Aug. 1975), pp. 468–473 (cit. on p. 58).

[77] T. Otsuka, M. Honma and T. Mizusaki. "Structure of the $N = Z = 28$ Closed Shell Studied by Monte Carlo Shell Model Calculation." *Phys. Rev. Lett.* 81 (Aug. 1998), pp. 1588–1591 (cit. on p. 59).

[78] G. Kraus, P. Egelhof, C. Fischer, H. Geissel, A. Himmler, F. Nickel, G. Münzenberg, W. Schwab, A. Weiss, J. Friese, A. Gillitzer, H. J. Körner, M. Peter, W. F. Henning, J. P. Schiffer, J. V. Kratz, L. Chulkov, M. Golovkov, A. Ogloblin and B. A. Brown. "Proton Inelastic Scattering on ^{56}Ni in Inverse Kinematics." *Phys. Rev. Lett.* 73 (Sept. 1994), pp. 1773–1776 (cit. on p. 59).

[79] N. Schulz, J. Chevallier, B. Haas, J. Richert and M. Toulemonde. "Electromagnetic Transition Rates in ^{56}Ni." *Phys. Rev. C* 8 (Nov. 1973), pp. 1779–1781 (cit. on p. 59).

[80] H. Grawe, A. Blazhev, M. Górska, R. Grzywacz, H. Mach and I. Mukha. "Nuclear structure far off stability –Implications for nuclear astrophysics." *Eur. Phys. J. A* 27.1 (Mar. 2006), pp. 257–267 (cit. on p. 59).

[81] F. Brandolini, S. Lenzi, D. Napoli, R. Ribas, H. Somacal, C. Ur, D. Bazzacco, J. Cameron, G. de Angelis, M. De Poli, C. Fahlander, A. Gadea, S. Lunardi, G. Martínez-Pinedo, N. Medina, C. Rossi Alvarez, J. Sánchez-Solano and C. Svensson. "Precise DSAM lifetime measurements in ^{48}Cr and ^{50}Cr as a test of large scale shell model calculations." *Nucl. Phys. A* 642.3 (1998), pp. 387–406 (cit. on p. 60).

[82] C. A. Ur, D. Bucurescu, S. M. Lenzi, G. Martínez-Pinedo, D. R. Napoli, D. Bazzacco, F. Brandolini, D. M. Brink, J. A. Cameron, E. Caurier, G. de Angelis, M. De Poli, A. Gadea, S. Lunardi, N. Mărginean, M. A. Nagarajan, P. Pavan, C. Rossi Alvarez and C. E. Svensson. "Excited states in ^{52}Fe and the origin of the yrast trap at $I^{\pi} = 12^{+}$." *Phys. Rev. C* 58 (Dec. 1998), pp. 3163–3170 (cit. on p. 60).

[83] K. Starosta, A. Dewald, A. Dunomes, P. Adrich, A. M. Amthor, T. Baumann, D. Bazin, M. Bowen, B. A. Brown, A. Chester, A. Gade, D. Galaviz, T. Glasmacher, T. Ginter, M. Hausmann, M. Horoi, J. Jolie, B. Melon, D. Miller, V. Moeller, R. P. Norris, T. Pissulla, M. Portillo, W. Rother, Y. Shimbara, A. Stolz, C. Vaman, P. Voss, D. Weisshaar and V. Zelevinsky. "Shape and Structure of $N = Z$ ^{64}Ge: Electromagnetic Transition Rates from the Application of the Recoil Distance Method to a Knockout Reaction." *Phys. Rev. Lett.* 99 (July 2007), p. 042503 (cit. on p. 61).

[84] A. Gade, D. Bazin, A. Becerril, C. M. Campbell, J. M. Cook, D. J. Dean, D.-C. Dinca, T. Glasmacher, G. W. Hitt, M. E. Howard, W. F. Mueller, H. Olliver, J. R. Terry and K. Yoneda. "Quadrupole Deformation of the Self-Conjugate Nucleus ^{72}Kr." *Phys. Rev. Lett.* 95 (July 2005), p. 022502 (cit. on p. 61).

[85] A. Lemasson, H. Iwasaki, C. Morse, D. Bazin, T. Baugher, J. S. Berryman, A. Dewald, C. Fransen, A. Gade, S. McDaniel, A. Nichols, A. Ratkiewicz, S. Stroberg, P. Voss, R. Wadsworth, D. Weisshaar, K. Wimmer and R. Winkler. "Observation of mutually enhanced collectivity in self-conjugate $^{76}_{38}\mathrm{Sr}_{38}$." *Phys. Rev. C* 85 (Apr. 2012), p. 041303 (cit. on p. 61).

[86] W. Nazarewicz, J. Dudek, R. Bengtsson, T. Bengtsson and I. Ragnarsson. “Microscopic study of the high-spin behaviour in selected $A \simeq 80$ nuclei.” *Nucl. Phys. A* 435.2 (1985), pp. 397–447 (cit. on p. 61).

[87] A. Obertelli, T. Baugher, D. Bazin, J.-P. Delaroche, F. Flavigny, A. Gade, M. Girod, T. Glasmacher, A. Goergen, G. F. Grinyer, W. Korten, J. Ljungvall, S. McDaniel, A. Ratkiewicz, B. Sulignano and D. Weisshaar. “Shape evolution in self-conjugate nuclei, and the transitional nucleus ^{68}Se.” *Phys. Rev. C* 80 (Sept. 2009), p. 031304 (cit. on p. 61).

[88] G. G. Adamian, N. V. Antonenko, R. V. Jolos, Y. V. Palchikov and W. Scheid. “Cluster effects in the structure of the ground state and superdeformed bands of ^{60}Zn.” *Phys. Rev. C* 67 (May 2003), p. 054303 (cit. on p. 61).

[89] F. Pühlhofer. “On the interpretation of evaporation residue mass distributions in heavy-ion induced fusion reactions.” *Nucl. Phys. A* 280.1 (1977), pp. 267–284 (cit. on p. 61).

[90] S. Akkoyun, A. Algora, B. Alikhani, F. Ameil, G. de Angelis, L. Arnold, A. Astier, A. Ataç, Y. Aubert, C. Aufranc, A. Austin, S. Aydin, F. Azaiez, S. Badoer, D. Balabanski, D. Barrientos, G. Baulieu, R. Baumann, D. Bazzacco, F. Beck, T. Beck, P. Bednarczyk, M. Bellato, M. Bentley, G. Benzoni, R. Berthier, L. Berti, R. Beunard, G. Lo Bianco, B. Birkenbach, P. Bizzeti, A. Bizzeti-Sona, F. Le Blanc, J. Blasco, N. Blasi, D. Bloor, C. Boiano, M. Borsato, D. Bortolato, A. Boston, H. Boston, P. Bourgault, P. Boutachkov, A. Bouty, A. Bracco, S. Brambilla, I. Brawn, A. Brondi, S. Broussard, B. Bruyneel, D. Bucurescu, I. Burrows, A. Bürger, S. Cabaret, B. Cahan, E. Calore, F. Camera, A. Capsoni, F. Carrió, G. Casati, M. Castoldi, B. Cederwall, J.-L. Cercus, V. Chambert, M. El Chambit, R. Chapman, L. Charles, J. Chavas, E. Clément, P. Cocconi, S. Coelli, P. Coleman-Smith, A. Colombo, S. Colosimo, C. Commeaux, D. Conventi, R. Cooper, A. Corsi, A. Cortesi, L. Costa, F. Crespi, J. Cresswell, D. Cullen, D. Curien, A. Czermak, D. Delbourg, R. Depalo, T. Descombes, P. Désesquelles, P. Detistov, C. Diarra, F. Didierjean, M. Dimmock, Q. Doan, C. Domingo-Pardo, M. Doncel, F. Dorangeville, N. Dosme, Y. Drouen, G. Duchêne, B. Dulny, J. Eberth, P. Edelbruck, J. Egea, T. Engert, M. Erduran, S. Ertürk, C. Fanin, S. Fantinel, E. Farnea, T. Faul, M. Filliger, F. Filmer, C. Finck, G. de France, A. Gadea, W. Gast, A. Geraci, J. Gerl, R. Gernhäuser, A. Giannatiempo, A. Giaz, L. Gibelin, A. Givechev, N. Goel, V. González, A. Gottardo, X. Grave, J. Gre¸bosz, R. Griffiths, A. Grint, P. Gros, L. Guevara, M. Gulmini, A. Görgen, H. Ha, T. Habermann, L. Harkness, H. Harroch, K. Hauschild, C. He, A. Hernández-Prieto, B. Hervieu, H. Hess, T. Hüyük, E. Ince, R. Isocrate, G. Jaworski, A. Johnson, J. Jolie, P. Jones, B. Jonson, P. Joshi, D. Judson, A. Jungclaus, M. Kaci, N. Karkour, M. Karolak, A. Kaşkaş, M. Kebbiri, R. Kempley, A. Khaplanov, S. Klupp, M. Kogimtzis, I. Kojouharov, A. Korichi, W. Korten, T. Kröll, R. Krücken, N. Kurz, B. Ky, M. Labiche, X. Lafay, L. Lavergne, I. Lazarus, S. Leboutelier, F. Lefebvre, E. Legay, L. Legeard, F. Lelli, S. Lenzi, S. Leoni, A. Lermitage, D. Lersch, J. Leske, S. Letts, S. Lhenoret, R. Lieder, D. Linget, J. Ljungvall, A. Lopez-Martens, A. Lotodé, S. Lunardi, A. Maj, J. van der Marel, Y. Mariette, N. Marginean, R. Marginean, G. Maron, A. Mather, W. Me¸czyński, V. Mendéz, P. Medina, B. Melon, R. Menegazzo, D. Mengoni, E. Merchan, L. Mihailescu, C. Michelagnoli, J. Mierzejewski, L. Milechina, B. Million, K. Mitev, P. Molini, D. Montanari, S. Moon, F. Morbiducci, R. Moro, P. Morrall, O. Möller, A. Nannini, D. Napoli, L. Nelson, M. Nespolo, V. Ngo, M. Nicoletto, R. Nicolini, Y. Le Noa, P. Nolan, M. Norman, J. Nyberg, A. Obertelli, A. Olariu, R. Orlandi, D. Oxley, C. Özben, M. Ozille, C. Oziol, E. Pachoud, M. Palacz, J. Palin, J. Pancin, C. Parisel, P. Pariset, G. Pascovici, R. Peghin, L. Pellegri, A. Perego, S. Perrier, M. Petcu, P. Petkov, C. Petrache, E. Pierre, N. Pietralla, S. Pietri, M. Pignanelli, I. Piqueras, Z. Podolyak, P. Le Pouhalec, J. Pouthas, D. Pugnére, V. Pucknell, A. Pullia, B. Quintana, R. Raine, G. Rainovski, L. Ramina, G. Rampazzo, G. La Rana, M. Rebeschini, F. Recchia, N. Redon, M. Reese, P. Reiter, P. Regan, S. Riboldi, M. Richer, M. Rigato,

S. Rigby, G. Ripamonti, A. Robinson, J. Robin, J. Roccaz, J.-A. Ropert, B. Rossé, C. Rossi Alvarez, D. Rosso, B. Rubio, D. Rudolph, F. Saillant, E. Şahin, F. Salomon, M.-D. Salsac, J. Salt, G. Salvato, J. Sampson, E. Sanchis, C. Santos, H. Schaffner, M. Schlarb, D. Scraggs, D. Seddon, M. Şenyiğit, M.-H. Sigward, G. Simpson, J. Simpson, M. Slee, J. Smith, P. Sona, B. Sowicki, P. Spolaore, C. Stahl, T. Stanios, E. Stefanova, O. Stézowski, J. Strachan, G. Suliman, P.-A. Söderström, J. Tain, S. Tanguy, S. Tashenov, C. Theisen, J. Thornhill, F. Tomasi, N. Toniolo, R. Touzery, B. Travers, A. Triossi, M. Tripon, K. Tun-Lanoë, M. Turcato, C. Unsworth, C. Ur, J. Valiente-Dobon, V. Vandone, E. Vardaci, R. Venturelli, F. Veronese, C. Veyssiere, E. Viscione, R. Wadsworth, P. Walker, N. Warr, C. Weber, D. Weisshaar, D. Wells, O. Wieland, A. Wiens, G. Wittwer, H. Wollersheim, F. Zocca, N. Zamfir, M. Zie¸bliński and A. Zucchiatti. "AGATA—Advanced GAmma Tracking Array." *Nucl. Instrum. Methods Phys. Res. A* 668 (2012), pp. 26–58 (cit. on p. 61).

[91] C. A. Ur. "Perspectives for the gamma-ray spectroscopy at LNL: the GALILEO project." *J. Phys. Conf. Ser.* 366 (May 2012), p. 012044 (cit. on p. 61).

[92] J. Valiente-Dobón, G. Jaworski, A. Goasduff, F. Egea, V. Modamio, T. Hüyük, A. Triossi, M. Jastrząb, P. Söderström, A. Di Nitto, G. de Angelis, G. de France, N. Erduran, A. Gadea, M. Moszyński, J. Nyberg, M. Palacz, R. Wadsworth, R. Aliaga, C. Aufranc, M. Bézard, G. Baulieu, E. Bissiato, A. Boujrad, I. Burrows, S. Carturan, P. Cocconi, G. Colucci, D. Conventi, M. Cordwell, S. Coudert, J. Deltoro, L. Ducroux, T. Dupasquier, S. Ertürk, X. Fabian, V. González, A. Grant, K. Hadyńska-Klęk, A. Illana, M. Jurado-Gomez, M. Kogimtzis, I. Lazarus, L. Legeard, J. Ljungvall, G. Pasqualato, R. Pérez-Vidal, A. Raggio, D. Ralet, N. Redon, F. Saillant, B. Sayğı, E. Sanchis, M. Scarcioffolo, M. Siciliano, D. Testov, O. Stezowski, M. Tripon and I. Zanon. "NEDA—NEutron Detector Array." *Nucl. Instrum. Methods Phys. Res. A* 927 (2019), pp. 81–86 (cit. on p. 62).

[93] D. Testov, D. Mengoni, A. Goasduff, A. Gadea, R. Isocrate, P. R. John, G. de Angelis, D. Bazzacco, C. Boiano, A. Boso, P. Cocconi, J. A. Dueñas, F. J. Egea Canet, L. Grassi, K. Hadyńska-Klek, G. Jaworski, S. Lunardi, R. Menegazzo, D. R. Napoli, F. Recchia, M. Siciliano and J. J. Valiente-Dobón. "The 4π highly-efficient light-charged-particle detector EUCLIDES, installed at the GALILEO array for in-beam γ-ray spectroscopy." *Eur. Phys. J. A* 55.4 (Apr. 2019), p. 47 (cit. on p. 62).

[94] N. Warr, J. Van de Walle, M. Albers, F. Ames, B. Bastin, C. Bauer, V. Bildstein, A. Blazhev, S. Bönig, N. Bree, B. Bruyneel, P. A. Butler, J. Cederkäll, E. Clément, T. E. Cocolios, T. Davinson, H. De Witte, P. Delahaye, D. D. DiJulio, J. Diriken, J. Eberth, A. Ekström, J. Elseviers, S. Emhofer, D. V. Fedorov, V. N. Fedosseev, S. Franchoo, C. Fransen, L. P. Gaffney, J. Gerl, G. Georgiev, R. Gernhäuser, T. Grahn, D. Habs, H. Hess, A. M. Hurst, M. Huyse, O. Ivanov, J. Iwanicki, D. G. Jenkins, J. Jolie, N. Kesteloot, O. Kester, U. Köster, M. Krauth, T. Kröll, R. Krücken, M. Lauer, J. Leske, K. P. Lieb, R. Lutter, L. Maier, B. A. Marsh, D. Mücher, M. Münch, O. Niedermaier, J. Pakarinen, M. Pantea, G. Pascovici, N. Patronis, D. Pauwels, A. Petts, N. Pietralla, R. Raabe, E. Rapisarda, P. Reiter, A. Richter, O. Schaile, M. Scheck, H. Scheit, G. Schrieder, D. Schwalm, M. Seidlitz, M. Seliverstov, T. Sieber, H. Simon, K.-H. Speidel, C. Stahl, I. Stefanescu, P. G. Thirolf, H.-G. Thomas, M. Thürauf, P. Van Duppen, D. Voulot, R. Wadsworth, G. Walter, D. Weißhaar, F. Wenander, A. Wiens, K. Wimmer, B. H. Wolf, P. J. Woods, K. Wrzosek-Lipska and K. O. Zell. "The Miniball spectrometer." *Eur. Phys. J. A* 49.3 (Mar. 2013), p. 40 (cit. on p. 62).

[95] M. Lindroos, P. Butler, M. Huyse and K. Riisager. "HIE-ISOLDE." *Nucl. Instrum. Methods Phys. Res. B* 266.19 (2008). Proceedings of the XVth International Conference on Electromagnetic

Isotope Separators and Techniques Related to their Applications, pp. 4687–4691 (cit. on p. 62).

[96] ISOLDE Yield Database. 2021. URL: https://isoyields2.web.cern.ch/YieldById.aspx?Yield_Id=2537 (visited on 09/07/2021) (cit. on p. 62).

[97] J. Van de Walle, F. Aksouh, F. Ames, T. Behrens, V. Bildstein, A. Blazhev, J. Cederkäll, E. Clément, T. E. Cocolios, T. Davinson, P. Delahaye, J. Eberth, A. Ekström, D. V. Fedorov, V. N. Fedosseev, L. M. Fraile, S. Franchoo, R. Gernhauser, G. Georgiev, D. Habs, K. Heyde, G. Huber, M. Huyse, F. Ibrahim, O. Ivanov, J. Iwanicki, J. Jolie, O. Kester, U. Köster, T. Kröll, R. Krücken, M. Lauer, A. F. Lisetskiy, R. Lutter, B. A. Marsh, P. Mayet, O. Niedermaier, T. Nilsson, M. Pantea, O. Perru, R. Raabe, P. Reiter, M. Sawicka, H. Scheit, G. Schrieder, D. Schwalm, M. D. Seliverstov, T. Sieber, G. Sletten, N. Smirnova, M. Stanoiu, I. Stefanescu, J.-C. Thomas, J. J. Valiente-Dobón, P. Van Duppen, D. Verney, D. Voulot, N. Warr, D. Weisshaar, F. Wenander, B. H. Wolf and M. Zielińska. "Coulomb Excitation of Neutron-Rich Zn Isotopes: First Observation of the 2_1^+ State in ^{80}Zn." *Phys. Rev. Lett.* 99 (Oct. 2007), p. 142501 (cit. on p. 62).

[98] Y. Blumenfeld, T. Nilsson and P. Van Duppen. "Facilities and methods for radioactive ion beam production." *Phys. Scr.* T152 (2013), p. 014023 (cit. on p. 62).

[99] N. Fukuda, T. Kubo, T. Ohnishi, N. Inabe, H. Takeda, D. Kameda and H. Suzuki. "Identification and separation of radioactive isotope beams by the BigRIPS separator at the RIKEN RI Beam Factory." *Nucl. Instrum. Methods Phys. Res. B* 317 (2013). XVIth International Conference on ElectroMagnetic Isotope Separators and Techniques Related to their Applications, December 2–7, 2012 at Matsue, Japan, pp. 323–332 (cit. on p. 62).

[100] A. Gade and B. Sherrill. "NSCL and FRIB at Michigan State University: Nuclear science at the limits of stability." *Phys. Scr.* 91.5 (Apr. 2016), p. 053003 (cit. on p. 62).

[101] H. Geissel, P. Armbruster, K. Behr, A. Brünle, K. Burkard, M. Chen, H. Folger, B. Franczak, H. Keller, O. Klepper, B. Langenbeck, F. Nickel, E. Pfeng, M. Pfützner, E. Roeckl, K. Rykaczewski, I. Schall, D. Schardt, C. Scheidenberger, K.-H. Schmidt, A. Schröter, T. Schwab, K. Sümmerer, M. Weber, G. Münzenberg, T. Brohm, H.-G. Clerc, M. Fauerbach, J.-J. Gaimard, A. Grewe, E. Hanelt, B. Knödler, M. Steiner, B. Voss, J. Weckenmann, C. Ziegler, A. Magel, H. Wollnik, J. Dufour, Y. Fujita, D. Vieira and B. Sherrill. "The GSI projectile fragment separator (FRS): a versatile magnetic system for relativistic heavy ions." *Nucl. Instrum. Methods Phys. Res. B* 70.1 (1992), pp. 286–297 (cit. on p. 62).

[102] S. Gales. "SPIRAL2 at GANIL: Next Generation of ISOL Facility for Intense Secondary Radioactive Ion Beams." *Nucl. Phys. A* 834.1 (2010). The 10th International Conference on Nucleus-Nucleus Collisions (NN2009), pp. 717c–723c (cit. on p. 62).

List of figures

List of publications

Publications in refereed journals

[1] B. Fu, M. Seidlitz, A. Blazhev, M. Bouhelal, F. Haas, P. Reiter, K. Arnswald, B. Birkenbach, C. Fransen, G. Friessner, A. Hennig, H. Hess, R. Hirsch, L. Lewandowski, D. Schneiders, B. Siebeck, T. Steinbach, T. Thomas, A. Vogt, A. Wendt, K. Wolf and K. O. Zell.
γ-ray spectroscopy of ^{33}P and ^{33}S after fusion-evaporation reactions.
Phys. Rev. C 94 (Sept. 2016), p. 034318.

[2] A. Vogt, B. Birkenbach, P. Reiter, A. Blazhev, M. Siciliano, K. Hadyńska-Klęk, J. J. Valiente-Dobón, C. Wheldon, E. Teruya, N. Yoshinaga, K. Arnswald, D. Bazzacco, M. Bowry, A. Bracco, B. Bruyneel, R. S. Chakrawarthy, R. Chapman, D. Cline, L. Corradi, F. C. L. Crespi, M. Cromaz, G. de Angelis, J. Eberth, P. Fallon, E. Farnea, E. Fioretto, S. J. Freeman, B. Fu, A. Gadea, K. Geibel, W. Gelletly, A. Gengelbach, A. Giaz, A. Görgen, A. Gottardo, A. B. Hayes, H. Hess, R. Hirsch, H. Hua, P. R. John, J. Jolie, A. Jungclaus, L. Kaya, W. Korten, I. Y. Lee, S. Leoni, L. Lewandowski, X. Liang, S. Lunardi, A. O. Macchiavelli, R. Menegazzo, D. Mengoni, C. Michelagnoli, T. Mijatović, G. Montagnoli, D. Montanari, C. Müller-Gatermann, D. Napoli, C. J. Pearson, L. Pellegri, Z. Podolyák, G. Pollarolo, A. Pullia, M. Queiser, F. Radeck, F. Recchia, P. H. Regan, D. Rosiak, N. Saed-Samii, E. Şahin, F. Scarlassara, D. Schneiders, M. Seidlitz, B. Siebeck, G. Sletten, J. F. Smith, P.-A. Söderström, A. M. Stefanini, T. Steinbach, O. Stezowski, S. Szilner, B. Szpak, R. Teng, C. Ur, V. Vandone, D. D. Warner, A. Wiens, C. Y. Wu and K. O. Zell.
Isomers and high-spin structures in the N = 81 isotones ^{135}Xe and ^{137}Ba.
Phys. Rev. C 95 (Feb. 2017), p. 024316.

[3] K. Arnswald, T. Braunroth, M. Seidlitz, L. Coraggio, P. Reiter, B. Birkenbach, A. Blazhev, A. Dewald, C. Fransen, B. Fu, A. Gargano, H. Hess, R. Hirsch, N. Itaco, S. Lenzi, L. Lewandowski, J. Litzinger, C. Müller-Gatermann, M. Queiser, D. Rosiak, D. Schneiders, B. Siebeck, T. Steinbach, A. Vogt, K. Wolf and K. Zell.
Enhanced collectivity along the $N = Z$ line: Lifetime measurements in ^{44}Ti, ^{48}Cr, and ^{52}Fe.
Phys. Lett. B 772 (2017), pp. 599–606.

[4] A. Vogt, M. Siciliano, B. Birkenbach, P. Reiter, K. Hadyńska-Klęk, C. Wheldon, J. J. Valiente-Dobón, E. Teruya, N. Yoshinaga, K. Arnswald, D. Bazzacco, A. Blazhev, A. Bracco, B. Bruyneel, R. S. Chakrawarthy, R. Chapman, D. Cline, L. Corradi, F. C. L. Crespi, M. Cromaz, G. de Angelis, J. Eberth, P. Fallon, E. Farnea, E. Fioretto, C. Fransen, S. J. Freeman, B. Fu, A. Gadea, W. Gelletly, A. Giaz, A. Görgen, A. Gottardo, A. B. Hayes, H. Hess, R. Hetzenegger, R. Hirsch, H. Hua, P. R. John, J. Jolie, A. Jungclaus, V. Karayonchev, L. Kaya, W. Korten, I. Y. Lee, S. Leoni, X. Liang, S. Lunardi, A. O. Macchiavelli, R. Menegazzo, D. Mengoni, C. Michelagnoli, T. Mijatović, G. Montagnoli, D. Montanari, C. Müller-Gatermann, D. Napoli, C. J. Pearson, Z. Podolyák, G. Pollarolo, A. Pullia, M. Queiser, F. Recchia, P. H. Regan, J.-M. Régis, N. Saed-Samii, E. Şahin, F. Scarlassara, M. Seidlitz, B. Siebeck, G. Sletten, J. F. Smith, P.-A. Söderström, A. M. Stefanini, O. Stezowski, S. Szilner, B. Szpak, R. Teng, C. Ur, D. D. Warner, K. Wolf,

C. Y. Wu and K. O. Zell.
High-spin structures in ^{132}Xe and ^{133}Xe and evidence for isomers along the N = 79 isotones.
Phys. Rev. C 96 (Aug. 2017), p. 024321.

[5] M. Queiser, A. Vogt, M. Seidlitz, P. Reiter, T. Togashi, N. Shimizu, Y. Utsuno, T. Otsuka, M. Honma, P. Petkov, K. Arnswald, R. Altenkirch, B. Birkenbach, A. Blazhev, T. Braunroth, A. Dewald, J. Eberth, C. Fransen, B. Fu, H. Hess, R. Hetzenegger, R. Hirsch, J. Jolie, V. Karayonchev, L. Kaya, L. Lewandowski, C. Müller-Gatermann, J.-M. Régis, D. Rosiak, D. Schneiders, B. Siebeck, T. Steinbach, K. Wolf and K.-O. Zell.
Cross-shell excitations from the fp shell: Lifetime measurements in ^{61}Zn.
Phys. Rev. C 96 (Oct. 2017), p. 044313.

[6] L. Kaya, A. Vogt, P. Reiter, M. Siciliano, B. Birkenbach, A. Blazhev, L. Coraggio, E. Teruya, N. Yoshinaga, K. Higashiyama, K. Arnswald, D. Bazzacco, A. Bracco, B. Bruyneel, L. Corradi, F. C. L. Crespi, G. de Angelis, J. Eberth, E. Farnea, E. Fioretto, C. Fransen, B. Fu, A. Gadea, A. Gargano, A. Giaz, A. Görgen, A. Gottardo, K. Hadyńska-Klęk, H. Hess, R. Hetzenegger, R. Hirsch, N. Itaco, P. R. John, J. Jolie, A. Jungclaus, W. Korten, S. Leoni, L. Lewandowski, S. Lunardi, R. Menegazzo, D. Mengoni, C. Michelagnoli, T. Mijatović, G. Montagnoli, D. Montanari, C. Müller-Gatermann, D. Napoli, Z. Podolyák, G. Pollarolo, A. Pullia, M. Queiser, F. Recchia, D. Rosiak, N. Saed-Samii, E. Şahin, F. Scarlassara, D. Schneiders, M. Seidlitz, B. Siebeck, J. F. Smith, P.-A. Söderström, A. M. Stefanini, T. Steinbach, O. Stezowski, S. Szilner, B. Szpak, C. Ur, J. J. Valiente-Dobón, K. Wolf and K. O. Zell.
High-spin structure in the transitional nucleus ^{131}Xe: Competitive neutron and proton alignment in the vicinity of the N = 82 shell closure.
Phys. Rev. C 98 (July 2018), p. 014309.

[7] L. Kaya, A. Vogt, P. Reiter, C. Müller-Gatermann, M. Siciliano, L. Coraggio, N. Itaco, A. Gargano, K. Arnswald, D. Bazzacco, B. Birkenbach, A. Blazhev, A. Bracco, B. Bruyneel, L. Corradi, F. C. L. Crespi, G. de Angelis, M. Droste, J. Eberth, E. Farnea, E. Fioretto, C. Fransen, A. Gadea, A. Giaz, A. Görgen, A. Gottardo, K. Hadyńska-Klęk, H. Hess, R. Hetzenegger, R. Hirsch, P. R. John, J. Jolie, A. Jungclaus, W. Korten, S. Leoni, L. Lewandowski, S. Lunardi, R. Menegazzo, D. Mengoni, C. Michelagnoli, T. Mijatović, G. Montagnoli, D. Montanari, D. Napoli, Z. Podolyák, G. Pollarolo, F. Recchia, D. Rosiak, N. Saed-Samii, E. Şahin, F. Scarlassara, M. Seidlitz, P.-A. Söderström, A. M. Stefanini, O. Stezowski, S. Szilner, B. Szpak, C. Ur, J. J. Valiente-Dobón, M. Weinert, K. Wolf and K. O. Zell.
Millisecond $23/2^+$ isomers in the N = 79 isotones ^{133}Xe and ^{135}Ba.
Phys. Rev. C 98 (Nov. 2018), p. 054312.

[8] D. Rosiak, M. Seidlitz, P. Reiter, H. Naïdja, Y. Tsunoda, T. Togashi, F. Nowacki, T. Otsuka, G. Colò, K. Arnswald, T. Berry, A. Blazhev, M. J. G. Borge, J. Cederkäll, D. M. Cox, H. De Witte, L. P. Gaffney, C. Henrich, R. Hirsch, M. Huyse, A. Illana, K. Johnston, L. Kaya, T. Kröll, M. L. L. Benito, J. Ojala, J. Pakarinen, M. Queiser, G. Rainovski, J. A. Rodriguez, B. Siebeck, E. Siesling, J. Snäll, P. Van Duppen, A. Vogt, M. von Schmid, N. Warr, F. Wenander and K. O. Zell.
Enhanced Quadrupole and Octupole Strength in Doubly Magic ^{132}Sn.
Phys. Rev. Lett. 121 (Dec. 2018), p. 252501.

[9] L. Kaya, A. Vogt, P. Reiter, C. Müller-Gatermann, A. Gargano, L. Coraggio, N. Itaco, A. Blazhev, K. Arnswald, D. Bazzacco, B. Birkenbach, A. Bracco, B. Bruyneel, L. Corradi, F. C. L. Crespi, G. de Angelis, M. Droste, J. Eberth, E. Farnea, E. Fioretto, C. Fransen, A. Gadea, A. Giaz, A. Görgen, A. Gottardo, K. Hadyńska-Klęk, H. Hess, R. Hetzenegger, R. Hirsch, P. R. John, J. Jolie,

A. Jungclaus, W. Korten, S. Leoni, L. Lewandowski, S. Lunardi, R. Menegazzo, D. Mengoni, C. Michelagnoli, T. Mijatović, G. Montagnoli, D. Montanari, D. Napoli, Z. Podolyák, G. Pollarolo, F. Recchia, D. Rosiak, N. Saed-Samii, E. Şahin, M. Siciliano, F. Scarlassara, M. Seidlitz, P.-A. Söderström, A. M. Stefanini, O. Stezowski, S. Szilner, B. Szpak, C. Ur, J. J. Valiente-Dobón, M. Weinert, K. Wolf and K. O. Zell.
Identification of high-spin proton configurations in ^{136}Ba and ^{137}Ba.
Phys. Rev. C 99 (Jan. 2019), p. 014301.

[10] A. Goldkuhle, C. Fransen, A. Dewald, K. Arnswald, M. Bast, M. Beckers, A. Blazhev, T. Braunroth, G. Hackenberg, G. Häfner, J. Litzinger, J. Jolie, C. Müller-Gatermann, F. von Spee, N. Warr, D. Werner and K. O. Zell.
Lifetime measurement of excited states in ^{46}Ti.
Eur. Phys. J. A 55.4 (Apr. 2019), p. 53.

[11] L. Kaya, A. Vogt, P. Reiter, M. Siciliano, N. Shimizu, Y. Utsuno, H.-K. Wang, A. Gargano, L. Coraggio, N. Itaco, K. Arnswald, D. Bazzacco, B. Birkenbach, A. Blazhev, A. Bracco, B. Bruyneel, L. Corradi, F. C. L. Crespi, G. de Angelis, M. Droste, J. Eberth, A. Esmaylzadeh, E. Farnea, E. Fioretto, C. Fransen, A. Gadea, A. Giaz, A. Görgen, A. Gottardo, K. Hadyńska-Klęk, H. Hess, R. Hirsch, P. R. John, J. Jolie, A. Jungclaus, V. Karayonchev, L. Kornwebel, W. Korten, S. Leoni, L. Lewandowski, S. Lunardi, R. Menegazzo, D. Mengoni, C. Michelagnoli, T. Mijatović, G. Montagnoli, D. Montanari, C. Müller-Gatermann, D. Napoli, Z. Podolyák, G. Pollarolo, F. Recchia, J.-M. Régis, N. Saed-Samii, E. Şahin, F. Scarlassara, K. Schomacker, M. Seidlitz, B. Siebeck, P.-A. Söderström, A. M. Stefanini, O. Stezowski, S. Szilner, B. Szpak, E. Teruya, C. Ur, J. J. Valiente-Dobón, K. Wolf, K. Yanase, N. Yoshinaga and K. O. Zell.
Isomer spectroscopy in ^{133}Ba and high-spin structure of ^{134}Ba.
Phys. Rev. C 100 (Aug. 2019), p. 024323.

[12] K. Arnswald, P. Reiter, A. Blazhev, T. Braunroth, A. Dewald, M. Droste, C. Fransen, A. Goldkuhle, R. Hetzenegger, R. Hirsch, E. Hoemann, L. Kaya, L. Lewandowski, C. Müller-Gatermann, P. Petkov, D. Rosiak, M. Seidlitz, B. Siebeck, A. Vogt, D. Werner, K. Wolf and K.-O. Zell.
Lifetime measurements in ^{44}Ti.
Phys. Rev. C 102 (Nov. 2020), p. 054302.

[13] K. Arnswald, A. Blazhev, F. Nowacki, P. Petkov, P. Reiter, T. Braunroth, A. Dewald, M. Droste, C. Fransen, R. Hirsch, V. Karayonchev, L. Kaya, L. Lewandowski, C. Müller-Gatermann, M. Seidlitz, B. Siebeck, A. Vogt, D. Werner and K. Zell.
Enhanced quadrupole collectivity in doubly-magic ^{56}Ni: Lifetime measurements of the 4_1^+ and 6_1^+ states.
Phys. Lett. B 820 (2021), p. 136592.

[14] H. Kleis, M. Seidlitz, A. Blazhev, L. Kaya, P. Reiter, K. Arnswald, A. Dewald, M. Droste, C. Fransen, O. Möller, N. Shimizu, Y. Tsunoda, Y. Utsuno, P. von Brentano and K. O. Zell.
Lifetime measurements of excited states in ^{55}Cr.
Phys. Rev. C 104 (Sept. 2021), p. 034310.

Publications in conference proceedings

[15] C. Henrich, T. Kröll, K. Arnswald, C. Berger, T. Berry, V. Bildstein, J. Cederkäll, D. Cox, G. De Angelis, H. De Witte, G. Fernández Martínez, L. Gaffney, G. Georgiev, S. Ilieva, A. Illana Sisón, R. Lozeva, M. Matejska-Minda, P. Napiorkowski, J. Ojala, J. Pakarinen, G. Rainovski, M. Ramdhane, P. Reiter, H.-B. Rhee, D. Rosiak, M. Seidlitz, B. Siebeck, G. Simpson, J. Snäll,

V. Vaquero Soto, M. Thürauf, M. von Schmid, N. Warr, L. Werner and M. Zielińska.
Coulomb excitation of ^{142}Xe.
Acta Phys. Pol. B 49 (2018), p. 529.

[16] K. Arnswald, P. Reiter, L. Coraggio, B. Birkenbach, A. Blazhev, T. Braunroth, A. Dewald, C. Fransen, B. Fu, A. Gargano, H. Hess, R. Hirsch, N. Itaco, S. M. Lenzi, L. Lewandowski, J. Litzinger, C. Müller-Gatermann, M. Queiser, D. Rosiak, D. Schneiders, M. Seidlitz, B. Siebeck, T. Steinbach, A. Vogt, K. Wolf and K. O. Zell.
Enhanced collectivity along the $N = Z$ line: lifetime measurements in ^{44}Ti, ^{48}Cr, and ^{52}Fe.
J. Phys. Conf. Ser. 966 (Feb. 2018), p. 012029.

[17] J. Park, A. Knyazev, E. Rickert, P. Golubev, J. Cederkäll, A. N. Andreyev, G. de Angelis, K. Arnswald, L. Barber, C. Berger, C. Berner, T. Berry, M. J. G. Borge, A. Boukhari, D. Cox, J. Cubiss, D. M. Cullen, J. D. Ovejas, C. Fahlander, L. P. Gaffney, A. Gawlik, R. Gernhäuser, A. Görgen, T. Habermann, C. Henrich, A. Illana, J. Iwanicki, T. W. Johansen, J. Konki, T. Kröll, B. S. N. Singh, G. Rainovski, C. Raison, P. Reiter, D. Rosiak, S. Saha, M. Saxena, M. Schilling, M. Seidlitz, J. Snäll, C. Stahl, M. Stryjczyk, O. Tengblad, G. M. Tveten, J. J. Valiente-Dobón, P. V. Duppen, S. Viñals, N. Warr, A. Welker, L. Werner, H. D. Witte and R. Zidarova.
High-Statistics Sub-Barrier Coulomb Excitation of ^{106,108,110}Sn.
JPS Conf. Proc. 32 (2020), p. 024323.

Acknowledgements – *Danksagung*

Ich danke Herrn Prof. Dr. Peter Reiter für die Vergabe des interessanten und vielseitigen Promotionsthemas und für die Möglichkeit diese Arbeit in seiner Arbeitsgruppe am Institut für Kernphysik durchführen zu können. Ich bedanke mich sehr für die wissenschaftliche und methodische Unterstützung während der gesamten Bearbeitungsphase meiner Dissertation.

Ich danke weiterhin herzlich Herrn Prof. Dr. Jan Jolie für die Übernahme des Koreferats sowie Herrn Prof. Dr. Andreas Schadschneider für seine Bereitschaft zur Übernahme des Vorsitzes der Prüfungskommission.

I owe special thanks to Dr. Pavel Petkov from the “Horia Hulubei” National Institute for Physics and Nuclear Engineering, Bucharest-Măgurele for his advises and his instructive introduction to the subtleties of DSAM analyses!

Ich danke herzlich Herrn Dr. Andrey Blazhev für viele anregende Diskussionen und hilfreiche Erläuterungen zur Anwendung von Schalenmodell-Rechnungen.

Furthermore, I would like to thank Prof. Dr. Frédéric Nowacki as well as Dr. Luigi Coraggio, Dr. Angelina Gargano, and Dr. Nunzio Itaco for providing results from state-of-the-art shell-model calculations.

Weiterhin möchte ich mich bei Herrn Dr. Andreas Vogt und Herrn Dr. Levent Kaya für viele konstruktive und spannende Diskussionen bedanken.

Mein besonderer Dank geht an Herrn Dr. Thomas Braunroth und Herrn Dr. Michael Seidlitz, für die gemeinsame Arbeit und die vielen Diskussionen zur Interpretation der erzielten Ergebnisse.

Meiner gesamten Arbeitsgruppe gilt Dank für die zahlreichen fachlichen Gespräche, Ratschläge und Anmerkungen und für die freundliche und angenehme Arbeitsatmosphäre.

Insbesondere danke ich Herrn Dr. Herbert Hess, Herrn Dr. Jürgen Eberth, Herrn Dr. Claus Müller-Gatermann, Herrn Dr. Christoph Fransen, Frau Dr. Alina Goldkuhle, Herrn Maximilian Droste, Herrn Tim Steinbach, Herrn Rouven Hirsch und Herrn David Werner für viele anregende Diskussionen und konstruktive Hilfestellungen.

Ich bedanke mich herzlich bei meinen langjährigen Bürokollegen Herrn Michael Queiser und Herrn Dr. Dawid Rosiak für die interessante und abwechselungsreiche Zusammenarbeit in vielen Projekten.

Ein großer Dank geht an die Operateure des Tandembeschleunigers des IKP, Frank Bielau, Viktor Rehl, Otto Rudolph und Albert Wedel, die für einen reibungslosen Strahlbetrieb bei unseren zahlreichen Experimenten am IKP sorgten. Ich danke weiterhin Herrn Dr. Andrey Blazhev und Herrn Dr. Karl-

Oskar Zell für die Herstellung der Targets für die von uns durchgeführten Experimente am Tandem-Beschleuniger des IKP.

Ein ganz besonderer Dank gilt meiner Lebensgefährtin Simone Katzfuß sowie meiner Familie, die mich auf meinem Weg durch die Promotion begleitet und unterstützt haben.

Contribution to publications essential for this thesis

Publication I:
Enhanced collectivity along the $N = Z$ line: Lifetime measurements in ^{44}Ti, ^{48}Cr, and ^{52}Fe

- K. Arnswald conceived the Cologne experiments
- K. Arnswald carried out the experiments
- K. Arnswald carried out the data analysis of the three experiments
- K. Arnswald performed the GXPF1A, KB3G, and FPD6 shell-model calculations; results from the realistic effective Hamiltonian were provided by L. Coraggio, A. Gargano, and N. Itaco
- K. Arnswald wrote the paper; P. Reiter, M. Seidlitz, and L. Coraggio co-wrote the paper

Publication II:
Lifetime measurements in ^{44}Ti

- K. Arnswald conceived the Cologne experiments
- K. Arnswald carried out the experiments
- K. Arnswald carried out the data analysis of the two experiments
- K. Arnswald performed the ZBM2M, GXPF1A, KB3G, and FPD6 shell-model calculations
- K. Arnswald wrote the paper; A. Blazhev co-wrote the paper

Publication III:
Enhanced quadrupole collectivity in doubly-magic ^{56}Ni: Lifetime measurements of the 4_1^+ and 6_1^+ states

- K. Arnswald conceived the Cologne experiments
- K. Arnswald carried out the experiments
- K. Arnswald carried out the data analysis of the experiment
- K. Arnswald performed the GXPF1A shell-model calculation; results from the PFSDG-U, 2N, and 2N+3N calculations were provided by F. Nowacki
- K. Arnswald wrote the paper; F. Nowacki and P. Reiter co-wrote the paper

Erklärung zur Dissertation

Hiermit versichere ich an Eides statt, dass ich die vorliegende Dissertation selbstständig und ohne die Benutzung anderer als der angegebenen Hilfsmittel und Literatur angefertigt habe. Alle Stellen, die wörtlich oder sinngemäß aus veröffentlichten und nicht veröffentlichten Werken dem Wortlaut oder dem Sinn nach entnommen wurden, sind als solche kenntlich gemacht. Ich versichere an Eides statt, dass diese Dissertation noch keiner anderen Fakultät oder Universität zur Prüfung vorgelegen hat; dass sie – abgesehen von unten angegebenen Teilpublikationen und eingebundenen Artikeln und Manuskripten – noch nicht veröffentlicht worden ist sowie, dass ich eine Veröffentlichung der Dissertation vor Abschluss der Promotion nicht ohne Genehmigung des Promotionsausschusses vornehmen werde. Die Bestimmungen dieser Ordnung sind mir bekannt. Darüber hinaus erkläre ich hiermit, dass ich die Ordnung zur Sicherung guter wissenschaftlicher Praxis und zum Umgang mit wissenschaftlichem Fehlverhalten der Universität zu Köln gelesen und sie bei der Durchführung der Dissertation zugrundeliegenden Arbeiten und der schriftlich verfassten Dissertation beachtet habe und verpflichte mich hiermit, die dort genannten Vorgaben bei allen wissenschaftlichen Tätigkeiten zu beachten und umzusetzen. Ich versichere, dass die eingereichte elektronische Fassung der eingereichten Druckfassung vollständig entspricht.

Köln, den 1. Oktober 2021

(Konrad Arnswald)

Die Dissertation beinhaltet die Gewinnung von Primärdaten sowie die Analyse dieser Daten, die auf den Servern[ii] des Instituts für Kernphysik der Universität zu Köln gesichert und zugänglich sind.

Teilpublikationen

- K. Arnswald *et al.* „Enhanced collectivity along the $N = Z$ line: Lifetime measurements in ^{44}Ti, ^{48}Cr, and ^{52}Fe“. *Phys. Lett. B* 772 (2017) 599–606
- K. Arnswald *et al.* „Enhanced collectivity along the $N = Z$ line: lifetime measurements in ^{44}Ti, ^{48}Cr, and ^{52}Fe“. *J. Phys. Conf. Ser.* 966 (2018) 012029
- K. Arnswald *et al.* „Lifetime measurements in ^{44}Ti“. *Phys. Rev. C* 102, 054302 (2020)
- K. Arnswald *et al.* „Enhanced quadrupole collectivity in doubly-magic ^{56}Ni: Lifetime measurements of the 4_1^+ and 6_1^+ states“. *Phys. Lett. B* 820 (2021) 136592

[ii] unter: /data/karnswald/experiments/dissertation/
/data/karnswald/nushellx/linux/BE2/
/data/karnswald/src/kshell-1.2g/